ADOLPHO EMANUEL QUINTELA DA ROCHA

PARTITIONING EVAPOTRANSPIRATION AND CARBON FLUX IN A TALLGRASS PRAIRIE: EFFECTS OF RAINFALL VARIABILITY AND GRAZING

Thesis submitted to the Applied Meteorology Graduate Program of the Universidade Federal de Viçosa in partial fulfillment of the requirements for the degree of *Doctor Scientiae*.

Adviser: Eduardo Alvarez Santos

VIÇOSA – MINAS GERAIS
2022

Ficha catalográfica elaborada pela Biblioteca Central da Universidade Federal de Viçosa - Campus Viçosa

T
R672p
2022

Rocha, Adolpho Emanuel Quintela da, 1990-
Partitioning evapotranspiration and carbon flux in a tallgrass prairie: effects of rainfall variability and grazing / Adolpho Emanuel Quintela da Rocha. – Viçosa, MG, 2022.
1 tese eletrônica (108 f.): il. (algumas color.).

Texto em inglês.
Orientador: Eduardo Alvarez Santos.
Tese (doutorado) - Universidade Federal de Viçosa, Departamento de Engenharia Agrícola, 2022.
Inclui bibliografia.
DOI: https://doi.org/10.47328/ufvbbt.2022.168
Modo de acesso: World Wide Web.

1. Evapotranspiração. 2. Análise de covariância. 3. Pastagens. 4. Plantas - Transpiração. 5. Uso eficiente da água . I. Santos, Eduardo Alvarez, 1981-. II. Universidade Federal de Viçosa. Departamento de Engenharia Agrícola. Programa de Pós-Graduação em Meteorologia Aplicada. III. Título.

CDD 22. ed. 551.572

Bibliotecário(a) responsável: Alice Regina Pinto CRB6 2523

ADOLPHO EMANUEL QUINTELA DA ROCHA

PARTITIONING EVAPOTRANSPIRATION AND CARBON FLUX IN A TALLGRASS PRAIRIE: EFFECTS OF RAINFALL VARIABILITY AND GRAZING

Thesis submitted to the Applied Meteorology Graduate Program of the Universidade Federal de Viçosa in partial fulfillment of the requirements for the degree of *Doctor Scientiae*.

APPROVED: February 04, 2022.

Assent:

Adolpho Emanuel Quintela da Rocha
Author

Eduardo A. Santos
Eduardo Alvarez Santos
Adviser

To my wife, Luana

To my parents, Manoel and Edla

To my uncle, Rinaldo (In memorian)

To my grandmother, Iracema (In memorian)

To my brother, Álvaro

ACKNOWLEDGEMENTS

To God!

I would like to express my sincere appreciation to my adviser, Dr. Eduardo Santos, for his guidance, encouragement words, opportunities and support. I will be forever grateful.

I would like to thank Dr. Clenton Owensby for providing the Rannells Flint Hills Prairie Preserve data and suggestion in the manuscript.

I would also like to thank Dr. Andres Patrignani for providing the soil evaporation measurements and suggestions to the manuscript.

I would like to thank to the members of my committee, Dr. Fábio Marin, Dra. Gabrielle Pires, Dr. Gustavo Lyra and Dra. Hewlley Acioli for their suggestions.

I am deeply grateful to the Universidade Federal de Viçosa for the opportunities.

To Kansas State University to all support during my doctoral internship.

To the National Ecological Observatory Network (NEON) for providing micrometeorological data.

To NEON researchers, especially Chris Florian, Becky Eaves and Hongyan Luo, for their clarification and availability to always help.

To the PHENOCAM network for providing image data.

To the Kansas MESONET for providing meteorological data.

I am grateful to Graça Freitas for her help during this journey.

I am grateful to my friends, Alian Cássio, Claudio Soriano, Chinthaka Weerasekara, Gabriel Peterle, Guilherme Mapa, Hugo Santos, José Darlon, Mariana Reis, Mario Véras and Marshall Santos, for exchanging knowledge and relaxing moments along this journey.

I would like to thank Emma McElhaney for her grammatical suggestions in the manuscript.

To the Coordenação de Aperfeiçoamento de Pessoal de Nível Superior – Brasil (CAPES), to granting the scholarship.

This study was financed in part by the Coordenação de Aperfeiçoamento de Pessoal de Nível Superior – Brasil (CAPES) – Finance Code 88882.437129/2019-01.

ABSTRACT

ROCHA, Adolpho Emanuel Quintela da, D.Sc., Universidade Federal de Viçosa, February, 2022. **Partitioning evapotranspiration and carbon flux in a tallgrass prairie: effects of rainfall variability and grazing**. Adviser: Eduardo Alvarez Santos.

Partitioning evapotranspiration (*ET*) and carbon flux is key to understanding ecosystem responses to rainfall variability and management practices. In this study, we evaluated the effects of rainfall variability and grazing on carbon and water vapor fluxes in tallgrass prairies. In addition, a footprint model was used to assess the spatial representativeness of eddy covariance (*EC*) measurement and the influence of surface heterogeneity on energy balance closure (*EBC*). The research was conducted in two tallgrass prairie sites located in Kansas, U.S. The effects of rainfall variability on fluxes were evaluated during the 2017, 2018 and 2019 growing seasons. The impacts of grazing on fluxes were assessed during the 2003, 2004 and 2005 growing seasons. Carbon and water vapor fluxes were measured using the *EC* technique. Net ecosystem CO_2 exchange (*NEE*) partitioning into gross primary productivity (*GPP*) and ecosystem respiration (R_{eco}) was performed using the relationship between the air temperature and nighttime *NEE* data. *ET* partitioning into transpiration (*T*) and evaporation (*E*) was obtained using the concept of underlying water use efficiency (*uWUE*). To evaluate the *uWUE* approach, we compared daily *E* estimates obtained from the *uWUE* with *E* observations provided by microlysimeters (*ML*) during the 2018 growing season. *EBC* was poor during nighttime and stable atmospheric conditions, but was not affected by surface heterogeneity. The correlations between vertical wind velocity and scalars indicated that low-frequency processes affected *EBC*. The contribution of *T* to *ET* (*T/ET*) was lowest during the dry growing season (0.50) and higher during wet growing seasons (0.63 and 0.65). The relationship between *uWUE* approach and *ML E* measurements showed a Pearson correlation coefficient (*r*) of 0.42 and a root mean square error (*RMSE*) of 0.58 mm d^{-1}. Air temperature was the main environmental driver of *T/ET* during the wet growing seasons, while the subsurface soil moisture (0.45 m) was the main driver of *T/ET* during the dry growing season. Grazing did not affect *GPP*, but increased R_{eco} (9.4%) and reduced *NEE* (11.9%). *T/ET* was reduced by grazing (7.0%), while *ET* increased by 3.3% due to the increase in *E* (26.6%). Our findings demonstrate that the precipitation variability not only has a direct impact on

the *ET* components but also modulates the response of those components to other environmental drivers. In turn, grazing regime adopted in this tallgrass prairie impacts the carbon cycle more strongly than the water cycle.

Keywords: Eddy covariance. Grasslands. Transpiration. Evaporation. Underlying water use efficiency.

RESUMO

ROCHA, Adolpho Emanuel Quintela da, D.Sc., Universidade Federal de Viçosa, fevereiro de 2022. **Particionamento da evapotranspiração e fluxo de carbono em uma pradaria de grama alta: efeitos da variabilidade da chuva e pastejo**. Orientador: Eduardo Alvarez Santos.

A partição da evapotranspiração e fluxo de carbono é fundamental para entender as respostas dos ecossistemas à variabilidade da precipitação e práticas de manejo. Neste estudo, foram avaliados os efeitos da variabilidade da chuva e do pastejo sobre os componentes do fluxo de carbono e água em pradarias. Além disso, um modelo de footprint foi utilizado para avaliar a representatividade espacial das medidas de covariância de vórtices turbulentos (*EC*) e o efeito da heterogeneidade da superfície sobre o fechamento do balanço de energia (*EBC*). A pesquisa foi conduzida em duas pradarias de grama alta localizadas no Kansas, EUA. Os efeitos da variabilidade da precipitação sobre os fluxos foram avaliados durantes as estações de crescimento de 2017, 2018 e 2019. Os impactos do pastejo sobre os fluxos foram avaliados durante as estações de crescimento de 2003, 2004 e 2005. Fluxos de carbono e água foram medidos utilizada a técnica *EC*. O particionamento da troca líquida de CO_2 do ecossistema (*NEE*) entre produtividade primária bruta (*GPP*) e respiração do ecossistema (R_{eco}) foi realizada usando a relação entre os dados noturnos de temperatura do ar e *NEE*. A partição da *ET* entre evaporação (*E*) e transpiração (*T*) foi obtida usando o conceito de eficiência no uso da água subjacente (*uWUE*). Para avaliar a abordagem *uWUE*, foram comparadas as estimativas diárias de *E* obtidas através de *uWUE* com observações de *E* fornecidas por microlisímetros (*ML*). *EBC* foi menor durante à noite e condições atmosféricas estáveis, mas não foi afetado pela heterogeneidade da superfície. As correlações entre a velocidade vertical do vento e os escalares indicou que processos de baixa frequência afetaram o *EBC*. A contribuição de *T* para *ET* (*T/ET*) foi menor durante a estação de crescimento seca (0.50) e maior durante estações de crescimento úmidas (0.63 e 0.65). A relação entre a abordagem *uWUE* e *E* obtida por *ML* mostrou um coeficiente de correlação de Pearson (*r*) de 0.42 e raiz do erro quadrático médio (*RMSE*) de 0.58 mm d^{-1}. A temperatura do ar foi a principal variável ambiental governando a dinâmica de *T/ET* durante as estações de crescimento úmidas, enquanto a umidade do solo na

subsuperfície (0.45 m) foi a principal variável ambiental governando *T/ET* durante a estação de crescimento seca. O pastejo não afetou o *GPP*, mas aumentou *Reco* (9.4%) e reduziu *NEE* (11.9%). *T/ET* foi reduzida pelo pastejo (7.0%), enquanto a *ET* aumentou em 3.3% devido ao acréscimo de *E* (26.6%). Os resultados deste estudo demonstram que a variabilidade da precipitação não apenas tem um impacto direto nos componentes de *ET,* mas também modula as respostas destes componentes aos outros impulsionadores ambientais. Por sua vez, o regime de pastejo adotado nesta pradaria impacta mais fortemente o ciclo do carbono do que o ciclo da água.

Palavras-chave: Covariância de vórtices turbulentos. Pastagens naturais. Transpiração. Evaporação. Eficiência no uso da água subjacente.

LIST OF FIGURES

LIST OF TABLES

LIST OF ACRONYMS AND ABBREVIATIONS

AGB	Aboveground biomass
C_d	Heat capacity of dry soil
C_s	Volumetric heat capacity of the soil
C_w	Heat capacity of water
d	Zero-plane displacement
E	Evaporation
EBC	Energy budget closure
EBR	Energy balance ratio
EC	Eddy covariance
ET	Evapotranspiration
G	Soil heat flux
GCC	Green chromatic coordinate
GLAI	Green leaf area index
GPP	Gross primary productivity
GR	Grazed
H	Sensible heat flux
h	Planetary boundary layer height
h_c	Canopy height
KPBS	Konza prairie biological station
L	Obukhov length
LAI	Leaf area index
LE	Latent heat flux
ML	Microlysimeters
NEE	Net ecosystem exchange
NEON	National ecological observatory network
P	Precipitation
θ	Soil water content
q	Water vapor mixing ratio
θ_{15}	Soil water content at depth of 0.15 m
θ_{45}	Soil water content at depth of 0.45 m
r	Pearson correlation coefficient

ρ_b	Soil bulk density
R_{eco}	Ecosystem respiration
Res	Residual of the energy balance closure
Rg	Incoming solar radiation
RH	Relative humidity
RMSE	Root mean square error
Rn	Net radiation
ρ_w	Density of water
R_{wq}	Correlation coefficients for vertical wind velocity and water vapor
R_{wt}	Correlation coefficients for vertical wind velocity and temperature
S_g	Soil heat storage
σ_v	Standard deviation of lateral velocity fluctuations
T	Transpiration
T	Sonic temperature
T_{air}	Air temperature
TKE	Turbulent kinetic energy
u*	Friction velocity
UG	Ungrazed
uWUE	Underlying water use efficiency
$uWUE_a$	Apparent underlying water use efficiency
$uWUE_p$	Potential underlying water use efficiency
VPD	Vapor pressure deficit
WD	Wind direction
WS	Horizontal wind speed
WUE	Water use efficiency
z	Measurement height
z_m	Measurement height

SUMMARY

1 GENERAL INTRODUCTION

Grasslands play an important role in the water and carbon cycles (Rajan et al., 2015; Song et al., 2018). In the U.S. Great Plains region, carbon and water vapor fluxes in tallgrass prairie are affected by high rainfall variability, cattle grazing and prescribed burning (Fischer et al., 2012; Owensby et al., 2006). Quantifying water vapor and carbon fluxes can provide insights into how tallgrass prairie will respond to increased rainfall variability helping to improve fire and grazing management.

The U.S. Great Plains climate is characterized by extremely variable weather conditions. According to Rosenberg (1986), this high variability of weather conditions is a consequence of the distance from the main water bodies and the alternation of air masses with different characteristics in the region. As a result, the region experiences high interannual precipitation variability with occurrence of drought and flood years (Dong et al., 2011; Hoerling et al., 2012). For instance, the year 2006 was characterized by an extreme drought, associated with the movement of dry air from Canada northward into the central United States, which prevented the transport of moist air from the Gulf of Mexico (Dong et al., 2011). On the other hand, 2007 was marked by an extreme flood, linked to rising motion that favored the development of thunderstorms (Dong et al., 2011). Furthermore, droughts have been recurrent in recent years, with the 2012 drought being the most severe in the last 117 years (Gerken et al., 2018; Hoerling et al., 2012).

The rainfall variability in the U.S. Great Plains can affect the functioning and structure of the tallgrass prairies, impacting the carbon dioxide (CO_2) uptake, evapotranspiration (*ET*), aboveground biomass productivity and plant species richness (Fischer et al., 2012; Fay et al., 2003; Jones et al., 2016). The tallgrass prairie growing season occurs between April and September (Fig. 1.1), when about 72% of the total annual rainfall occurs. The dormant season between October and March is characterized by low air temperatures and snow events (Brunsell et al., 2014). Since that about 98% of the CO_2 assimilation by vegetation occurs during the growing season (Petrie et al., 2016), the distribution of precipitation in this period has a strong influence on carbon sequestration in this ecosystem.

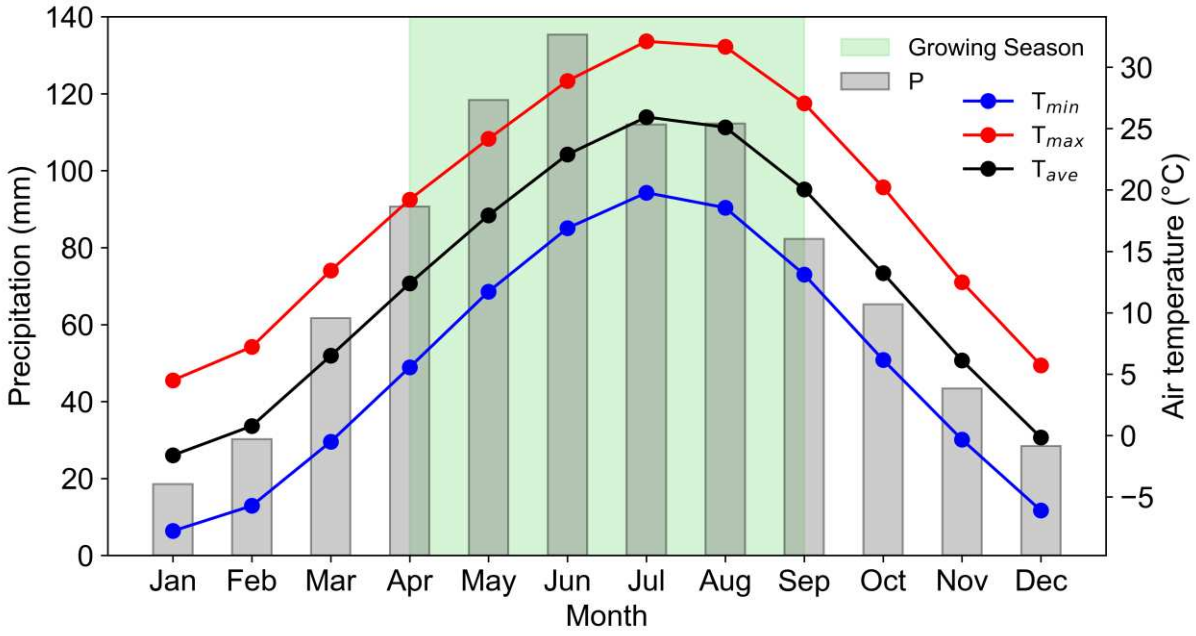

Figure 1.1 – Monthly precipitation (P), minimum (T_{min}), maximum (T_{max}) and average air temperature (T_{ave}) from 1981 – 2010 climate normals in the U. S. Great Plains, Manhattan, Kansas, U.S. (Adapted from www.noaa.gov/).

In addition to precipitation variability, prescribed burning and grazing also impact structure and functioning of tallgrass prairies. Prescribed burning is a common management practice adopted in tallgrass prairies, aiming to reduce woody plant encroachment and improve forage quality (Brunsell et al., 2017; Veach et al., 2014; Towne and Craine, 2014). Burned tallgrass prairie have shown greater CO_2 assimilation, green leaf area index (*LAI*), green aboveground biomass and increase in the grass cover (Fischer et al., 2012; Bremer and Han, 2010; Gibson and Hulbert, 1987). On the other hand, fire exclusion leads to an increase in forbs and woody plant species (Gibson and Hulbert, 1987). In addition, litter accumulation and standing dead on unburned tallgrass prairies decreases available energy and increase shading, affecting the emergence of new shoots and photosynthetic rates and reducing grassland productivity (Knapp, 1984; Knapp and Seastedt, 1986; Fischer et al, 2012).

Grazing, often combined with prescribed burning, is a common management practice used in tallgrass prairies (Briggs et al., 2016). The preference of animals for recently burned patch has been demonstrated in previous studies and linked to forage quality (Allred et al., 2011; Vermeire et al., 2014; Coppedge and Shaw, 1998). The reduction in grass cover by grazing contributes to the maintenance of grassland

heterogeneity, increasing species richness and diversity (Elson and Hartnett, 2017; Collins and Calabrese, 2012). These alterations promoted by fire and grazing, combined with rainfall variability, can lead to changes in carbon and water cycles in tallgrass prairies (O' Keefe and Nippert, 2016; Fischer et al., 2012).

Eddy covariance (*EC*) technique has been widely used for continuously monitoring of carbon and water vapor fluxes in several ecosystems (Baldocchi et al., 2020; Runkle et al., 2017). However, one of main limitation of *EC* is that it only providing net ecosystem CO_2 exchange (*NEE*) and total evapotranspiration (*ET*) (Palatella et al., 2014). Partitioning *NEE* into gross primary productivity (*GPP*) and ecosystem respiration (R_{eco}) and *ET* into evaporation (*E*) and transpiration (*T*) is key to understand how biotic and abiotic processes affect carbon and water cycles (Unger et al., 2009, Scott et al., 2021) and how grasslands will be impacted by climate change (Han et al., 2018).

The separation of *NEE* into its primary components is commonly based on the relationship between nighttime *NEE* and air temperature data (Wutzler et al., 2018; Reichstein et al., 2005). On the other hand, *ET* partitioning obtained from *EC* data remains challenging and had led to the development of various approaches (Kool et al., 2014). *ET* partitioning approaches based on the relationship between *GPP* and *ET* have grown in recent years (Zhou et al., 2016; Berkelhammer et al., 2016; Scott and Biederman, 2017; Skaggs et al., 2018). The approach developed by Zhou et al. (2016), based on the concept of underlying water use efficiency (*uWUE*), has been widely used in recent studies due to its simplicity and because it allows separating *E* and *T* at different time scales (Zhou et al., 2016).

1.1 Outline and objectives

Ecosystem scale *ET* and *NEE* partitioning studies are still scarce. In this study, we used data obtained from eddy covariance flux towers to investigate how the rainfall variability and cattle grazing affect *ET*, *NEE* and their components in tallgrass prairies. In addition, due to the different management practices around the measuring tower, a footprint model was used to assess the spatial representativeness of *EC* measurement and the influence of surface heterogeneity on energy balance closure (*EBC*).

This thesis is divided into three studies. In the first one, we used a footprint model to investigate the spatial representativeness of eddy covariance measurements

and the reasons that lead to the lack of the energy balance closure in a tallgrass prairie. In the second manuscript, the response of *T/ET* to environmental variables was evaluated in a tallgrass prairie under contrasting rainfall regimes. In the third manuscript, we used *ET* and *NEE* flux partitioning approaches to evaluate the effect of cattle grazing on tallgrass prairie CO_2 and H_2O exchanges.

References

Allred, B. W., Fuhlendorf, S. D., Engle, D. M., Elmore, R. D., 2011. Ungulate preference for burned patches reveals strength of fire–grazing interaction. Ecology and Evolution, 1(2), 132-144. https://doi.org/10.1002/ece3.12

Baldocchi, D. D., 2020. How eddy covariance flux measurements have contributed to our understanding of Global Change Biology. Global Change Biology, 26(1), 242-260. https://doi.org/10.1111/gcb.14807

Bremer, D. J., Ham, J. M., 2010. Net carbon fluxes over burned and unburned native tallgrass prairie. Rangeland Ecology & Management, 63(1), 72-81. https://doi.org/10.2111/REM-D-09-00010.1

Briggs, J. M., Blair, J. M., Horne, E. A., 2016. Ecohydrological and climate change studies at the Konza Prairie Biological Station. Transactions of the Kansas Academy of Science (1903-), 119(1), 5-11.

Brunsell, N. A., Nippert, J. B., Buck, T. L., 2014. Impacts of seasonality and surface heterogeneity on water-use efficiency in mesic grasslands. Ecohydrology, *7*(4), 1223-1233. https://doi.org/10.1002/eco.1455

Brunsell, N. A., Van Vleck, E. S., Nosshi, M., Ratajczak, Z., Nippert, J. B., 2017. Assessing the roles of fire frequency and precipitation in determining woody plant expansion in central US grasslands. Journal of Geophysical Research: Biogeosciences, 122(10), 2683-2698. https://doi.org/10.1002/2017JG004046

Collins, S. L., Calabrese, L. B., 2012. Effects of fire, grazing and topographic variation on vegetation structure in tallgrass prairie. Journal of Vegetation Science, 23(3), 563-575. https://doi.org/10.1111/j.1654-1103.2011.01369.x

Coppedge, B. R., Shaw, J. H.,1998. Bison grazing patterns on seasonally burned tallgrass prairie. Rangeland Ecology & Management/Journal of Range Management Archives, 51(3), 258-264.

Dong, X., et al., 2011. Investigation of the 2006 drought and 2007 flood extremes at the Southern Great Plains through an integrative analysis of observations. Journal of Geophysical Research: Atmospheres, 116(D3). https://doi.org/10.1029/2010JD014776

Elson, A., Hartnett, D. C., 2017). Bison increase the growth and reproduction of forbs in tallgrass prairie. The American Midland Naturalist, 178(2), 245-259. https://doi.org/10.1674/0003-0031-178.2.245

Fay, P. A., Carlisle, J. D., Knapp, A. K., Blair, J. M., Collins, S. L., 2003. Productivity responses to altered rainfall patterns in a C4-dominated grassland. Oecologia, 137(2), 245-251. https://doi.org/10.1007/s00442-003-1331-3

Fischer, M. L., Torn, M. S., Billesbach, D. P., Doyle, G., Northup, B., Biraud, S. C., 2012. Carbon, water, and heat flux responses to experimental burning and drought in a tallgrass prairie. Agricultural and Forest Meteorology, 166, 169-174. https://doi.org/10.1016/j.agrformet.2012.07.011

Gerken, T., Bromley, G. T., Ruddell, B. L., Williams, S., Stoy, P. C., 2018. Convective suppression before and during the United States Northern Great Plains flash drought of 2017. Hydrology and Earth System Sciences, 22(8), 4155-4163. https://doi.org/10.5194/hess-22-4155-2018

Gibson, D. J., Hulbert, L. C., 1987. Effects of fire, topography and year-to-year climatic variation on species composition in tallgrass prairie. Vegetatio, 72(3), 175-185. https://doi.org/10.1007/BF00039839

Han, D., Wang, G., Liu, T., Xue, B. L., Kuczera, G., Xu, X., 2018. Hydroclimatic response of evapotranspiration partitioning to prolonged droughts in semiarid grassland. Journal of Hydrology, 563, 766-777. https://doi.org/10.1016/j.jhydrol.2018.06.048

Hoerling, M., Eischeid, J., Kumar, A., Leung, R., Mariotti, A., Mo, K., Schubert, S., Seager, R., 2014. Causes and predictability of the 2012 Great Plains drought. Bulletin of the American Meteorological Society, 95(2), 269-282. https://doi.org/10.1175/BAMS-D-13-00055.1

Jones, S. K., Collins, S. L., Blair, J. M., Smith, M. D., Knapp, A. K., 2016. Altered rainfall patterns increase forb abundance and richness in native tallgrass prairie. Scientific Reports, 6(1), 1-10. https://doi.org/10.1038/srep20120

Knapp, A. K., 1984. Post-burn differences in solar radiation, leaf temperature and water stress influencing production in a lowland tallgrass prairie. American Journal of Botany, 71(2), 220-227. https://doi.org/10.1002/j.1537-2197.1984.tb12507.x

Knapp, A. K., Seastedt, T. R., 1986. Detritus accumulation limits productivity of tallgrass prairie. BioScience, 36(10), 662-668. https://doi.org/10.2307/1310387

Lasslop, G. et al., 2012. On the choice of the driving temperature for eddy-covariance carbon dioxide flux partitioning. Biogeosciences, 9(12), 5243-5259. https://doi.org/10.5194/bg-9-5243-2012

O'Keefe, K., Nippert, J. B., 2017. Grazing by bison is a stronger driver of plant ecohydrology in tallgrass prairie than fire history. Plant and Soil, 411(1), 423-436. https://doi.org/10.1007/s11104-016-3048-1

Owensby, C. E., Ham, J. M., Auen, L. M., 2006. Fluxes of CO_2 from grazed and ungrazed tallgrass prairie. Rangeland Ecology & Management, 59(2), 111-127. https://doi.org/10.2111/05-116R2.1

Palatella, L., Rana, G., Vitale, D., 2014. Towards a flux-partitioning procedure based on the direct use of high-frequency eddy-covariance data. Boundary-layer Meteorology, 153(2), 327-337. https://doi.org/10.1007/s10546-014-9947-x

Petrie, M. D., Brunsell, N. A., Vargas, R., Collins, S. L., Flanagan, L. B., Hanan, N. P., Litvak, M. E., Suyker, A. E., 2016. The sensitivity of carbon exchanges in Great Plains grasslands to precipitation variability. Journal of Geophysical Research: Biogeosciences, 121(2), 280-294. https://doi.org/10.1002/2015JG003205

Rajan, N., Maas, S. J., Cui, S., 2015. Extreme drought effects on summer evapotranspiration and energy balance of a grassland in the Southern Great Plains. Ecohydrology, 8(7), 1194-1204. https://doi.org/10.1002/eco.1574

Reichstein, M. et al.., 2005. On the separation of net ecosystem exchange into assimilation and ecosystem respiration: review and improved algorithm. Global Change Biology, 11(9), 1424-1439. https://doi.org/10.1111/j.1365-2486.2005.001002.x

Rosenberg, N. J., 1986. Climate of the Great Plains region of the United States. Great Plains Quarterly, 22-32.

Runkle, B. R., 2017. Delta-Flux: An Eddy Covariance Network for a Climate-Smart Lower Mississippi Basin. Agricultural & Environmental Letters, 2(1), ael2017-01. https://doi.org/10.2134/ael2017.01.0003

Scott, R. L., Biederman, J. A., 2017. Partitioning evapotranspiration using long-term carbon dioxide and water vapor fluxes. Geophysical Research Letters, 44(13), 6833-6840. https://doi.org/10.1002/2017GL074324

Scott, R. L., Knowles, J. F., Nelson, J. A., Gentine, P., Li, X., Barron-Gafford, G., Bryant, R., Biederman, J. A., 2021. Water availability impacts on evapotranspiration partitioning. Agricultural and Forest Meteorology, 297, 108251. https://doi.org/10.1016/j.agrformet.2020.108251

Skaggs, T. H., Anderson, R. G., Alfieri, J. G., Scanlon, T. M., & Kustas, W. P., 2018. Fluxpart: Open source software for partitioning carbon dioxide and water vapor fluxes. Agricultural and Forest Meteorology, 253, 218-224. https://doi.org/10.1016/j.agrformet.2018.02.019

Song, J. et al., 2018. The carbon sequestration potential of China's grasslands. Ecosphere, 9(10), e02452. https://doi.org/10.1002/ecs2.2452

Stoy, P. C., et al., 2019. Reviews and syntheses: Turning the challenges of partitioning ecosystem evaporation and transpiration into

opportunities. Biogeosciences, 16(19), 3747-3775. https://doi.org/10.5194/bg-16-3747-2019

Towne, E. G., Craine, J. M., 2014. Ecological consequences of shifting the timing of burning tallgrass prairie. PLoS One, 9(7), e103423. https://doi.org/10.1371/journal.pone.0103423

Unger, S., Maguas, C., Pereira, J. S., Aires, L. M., David, T. S., Werner, C., 2009. Partitioning carbon fluxes in a Mediterranean oak forest to disentangle changes in ecosystem sink strength during drought. agricultural and forest meteorology, 149(6-7), 949-961. https://doi.org/10.1016/j.agrformet.2008.11.013

Vermeire, L. T., Mitchell, R. B., Fuhlendorf, S. D., Gillen, R. L., 2004. Patch burning effects on grazing distribution. Rangeland Ecology and Management, 57(3), 248-252. https://doi.org/10.2111/1551-5028(2004)057[0248:PBEOGD]2.0.CO;2

Veach, A. M., Dodds, W. K., Skibbe, A., 2014. Fire and grazing influences on rates of riparian woody plant expansion along grassland streams. PloS One, 9(9), e106922. https://doi.org/10.1371/journal.pone.0106922

Wutzler, T., Lucas-Moffat, A., Migliavacca, M., Knauer, J., Sickel, K., Šigut, L., Menzer, O., Reichstein, M., 2018. Basic and extensible post-processing of eddy covariance flux data with REddyProc. Biogeosciences, 15(16), 5015-5030. https://doi.org/10.5194/bg-15-5015-2018

Zhou, S., Yu, B., Zhang, Y., Huang, Y., Wang, G., 2016. Partitioning evapotranspiration based on the concept of underlying water use efficiency. Water Resources Research, 52(2), 1160-1175. https://doi.org/10.1002/2015WR017766

2 ENERGY BALANCE CLOSURE AND SPATIAL REPRESENTATIVENESS OF EDDY COVARIANCE MEASUREMENTS IN TALLGRASS PRAIRIE

Abstract

Eddy covariance (*EC*) approach is a micrometeorological technique widely used to study the exchanges of energy, water and carbon between ecosystems and the atmosphere. However, the lack of the energy balance closure (*EBC*) remains unsolved. In this study, we used a flux footprint model to assess the spatial representativeness of eddy covariance measurements and to investigate whether the heterogeneity of the surface affects *EBC* in a tallgrass prairie. In addition, we evaluated the *EBC* as a function of atmospheric conditions, turbulence and phase differences between vertical wind velocity and scalars. The research was conducted at the National Ecological Observatory Network (NEON) KONZ site in Kansas, U.S, during three growing seasons (2017 – 2019). *EBC* was evaluated using three approaches: bulk method or energy balance ratio (*EBR*), regression slope and residual (*Res*). The footprint analysis revealed that 84.9% of the flux originated from the watershed of interest, but the contribution from other watersheds did not affect the *EBC*. The regression slopes and *EBR* indicated a lack of *EBC* of 31% and 23%, respectively, and the inclusion of soil heat storage (S_g) enhanced the slopes (5.1%) more than *EBR* (1.2%). Stable atmospheric conditions reduced the *EBC*, while neutral and unstable conditions increased. On the other hand, *Res* was higher during unstable conditions. The correlation between vertical wind velocity and scalars indicated that low-frequency processes affect the *EBC* at KONZ site.

Keywords: Energy balance; Footprint model; Soil heat storage; Heterogeneity

2.1 Introduction

Eddy covariance (*EC*) approach is a micrometeorological technique widely used to study the exchanges of energy, water and carbon between ecosystems and the atmosphere. The use of the *EC* technique has improved the understanding of ecosystem responses to climate change (Baldocchi, 2020), management practices and the rational use of water in croplands (Gong et al., 2017; Guo et al., 2020).

However, although the *EC* approach is a well-established and to provide standard measurements to validate evapotranspiration (*ET*) estimates from remote sensing and models (Li et al., 2018; Li et al., 2016), some problems remain unsolved, such as lack of the energy balance closure (*EBC*) (Mauder et al., 2020).

The non-closure of the energy balance occurs when there is a discrepancy between the sum of latent (*LE*) and sensible heat fluxes (*H*) obtained by the *EC* technique and the available surface energy, represented by the difference between the net radiation (*Rn*) and soil heat flux (*G*) and measured using independent sensors (Foken, 2008). Previous research carried out in different ecosystems have usually reported that (*Rn-G)* exceeds (*LE+H*) (Stoy et al., 2013; Xu et al., 2017; Zhou and Li, 2019; Eshonkulov et al., 2019).

The reasons for the lack of *EBC* include the occurrence of large eddies, atmospheric conditions, neglect of storage terms, surface heterogeneity, among others (Leuning et al., 2012; Kim et al., 2014; McGloin et al., 2018; Eshonkulov et al., 2019; Campos et al., 2019). Large eddies affect *EBC* by increasing the phase differences between the vertical wind velocity and scalars, which results in *EC* flux underestimation (Gao et al., 2017). Poor *EBC* values have also been associated with low turbulence, observed during neutral atmospheric stability conditions, low friction velocity (u^*) and turbulent kinetic energy (*TKE*) (McGloin et al., 2018, Zhou and Li, 2019; Campos et al., 2019). The inclusion of storage terms in flux calculations has improved *EBC* between 3% and 10% (Wang and Zhang, 2011; Kutikoff et al, 2019; Meyers and Hollinger, 2004). However, in short canopies, the soil heat storage (S_g) has been generally the only storage term used in *EBC* calculations, since other storage components are small (Liu et al., 2017; Xin et al., 2018). Nevertheless, *Sg* estimates, as well as *Rn* and *G* measurements, have a much smaller spatial representativeness compared to *EC* and may contribute to the lack of *EBC*, especially in heterogeneous sites (Shao et al., 2014).

The reduction of *EBC* in heterogeneous ecosystems has been associated with the differences between the footprint of *Rn* measurements and turbulent fluxes derived from *EC* (Kim et al., 2014; Zhou and Li, 2019). While 100% of the cumulative footprint of the net radiometer is reached a few meters from the tower (Marcola and Cescatti, 2018), the *EC* flux source area extends for several meters and varies according to the sensor height, wind direction and speed and atmospheric stability conditions (Chen et al., 2009). Previous studies have reported spatial variation of *Rn* in heterogeneous

ecosystems (Shao et al., 2014; Anthoni et al., 2000). However, the use of multiples net radiometer sensors to capture the heterogeneity of the underlying surface contributing to the *EC* fluxes is cost prohibitive. Thus, the use of footprint models in sites surrounded by different surfaces or management practices is an alternative to investigate the effect of landscape heterogeneity on *EBC* and the spatial representativeness of *EC* measurements (Masseroni et al., 2014; Zhao et al., 2014; Chu et al., 2021).

In this study, we used a flux footprint model to assess the spatial representativeness of *EC* measurements and to investigate whether the heterogeneity of the surface, resulting from the grazing and prescribed burning around the measurement site, affects the *EBC* in a tallgrass prairie. In addition, we evaluated the *EBC* as a function of atmospheric conditions, turbulence and phase differences between vertical velocity and scalars.

2.2 Material and methods

2.2.1 Site description

The study was conducted during the 2017-2019 growing seasons (May to October) at the National Ecological Observatory Network (NEON) KONZ site (Fig. 2.1) within the Konza Prairie Biological Station (KPBS). The KPBS is a C_4-dominated native tallgrass prairie, situated in Kansas, U.S. (39°05’55’’N, 96°34’02’’W, elevation 415 m a.s.l.). The region has a mid-continental climate with an average air temperature of 13˚C and average annual precipitation of 806.9 mm (1982-2017), with 73% concentrated between April and September during the growing season (O’Connor et al., 2020).

The KPBS is divided into 55 watersheds managed with different treatments of fire frequency combined with grazed and ungrazed regimes (Briggs et al., 2016). The KONZ site is located on K2A, an ungrazed watershed that experiences prescribed burning every 2 years. Table 2.1 shows the watersheds surrounding the measurement tower on K2A (66.1 ha).

Figure 2.1 –Tallgrass prairie at the KONZ site (NEON, 2020).

Table 2.1. Watersheds and management practices on the Konza Prairie Biological Station (Blair and O'neal, 2021).

Watershed	Grazing regime	Fire Frequency (years)	Prescribed burning (Date)		
			2017	2018	2019
K1B	Ungrazed	1	04/11	03/21	03/22
K2A	Ungrazed	2	-	03/21	-
K20A	Ungrazed	20	03/16	-	-
C3SA	Grazed	3		-	03/18
C3SB	Grazed	3	03/10	-	-

2.2.2 Eddy covariance and complementary measurements

Fluxes of CO_2 and energy were measured using the *EC* technique. The *EC* system at the KONZ site is installed at a height of 7.9 m and consists of a 3D sonic anemometer (CSAT3, Campbell Scientific, Inc., Logan, UT, USA) to measure the sonic temperature and wind velocity orthogonal components fluctuations, combined with an enclosed-path CO_2/H_2O infrared gas analyzer (LI-7200, LI-COR, USA) to measure carbon dioxide and water vapor mixing ratios. All EC sensors were scanned at 20 Hz. Latent (*LE*) and sensible heat fluxes (*H*) were calculated at 30 min intervals using the EddyPro software (Version 6.2.1, LI-COR). Data processing included the following steps: high-frequency data spike removal (Vickers and Mahrt, 1997), double coordination rotation (Kaimal and Finnigan, 1994), block average detrending, time lag compensation using covariance maximization (Fan et al., 1990) and spectral corrections for high (Moncrieff et al., 1997) and low frequency losses (Moncrieff et al., 2004). Post-processing included the removal of low-quality fluxes based on the steady state test (Mauden and Foken, 2004).

2.2.2 Flux footprint analysis

The contribution of each watershed surrounding the KONZ site to the measured *EC* fluxes was evaluated using a two-dimensional flux footprint parameterization (Kljun et al., 2015). The input micrometeorological variables used in footprint model included: measurement height (z_m), zero-plane displacement (d), friction velocity (u^*), Monin-Obukhov length (L), standard deviation of lateral velocity fluctuations (σ_v), wind direction (wd), mean wind velocity at measurement height ($\bar{u}$) and planetary boundary layer height (h). All other input micrometeorological variables were calculated using the EddyPro software (Version 6.2.1, LI-COR). To quantify the contribution of each watershed to the 30-min *EC* fluxes, polygons representing each watershed were overlaid with the estimated 30-min flux footprints (Neftel et al., 2008; Prajapati and Santos, 2018).

2.2.3 Complementary measurements

Net radiation (*Rn*) was measured by a four-component net radiometer (NR01, Hukseflux, Netherlands) installed at 8.4 m above the ground. Soil temperature was measured by three probes thermocouples (RTD100, Thermometrics, USA) at depths of 0.01 and 0.05 m. Volumetric soil water content (θ) was measured at depth of 0.05 m using five capacitance probes (EnviroSCAN TriSCAN, Sentek Technologies, Australia). Soil heat flux (*G*) was measured using three heat flux plates (HFP01SC, Hukseflux) at a depth of 0.08 m. The soil heat storage (S_g) above the heat plates was estimated as follows (Oliphant et al., 2004; Moderow et al., 2009):

$$S_g = C_s \frac{\Delta T_{soil}}{\Delta t} \Delta z \quad (1)$$

where: C_s is the volumetric heat capacity of the soil (J m^{-3} K^{-1}), ΔT_{soil} is the change in soil temperature (K) above the heat flux plate, Δt is the time averaging interval (1800 s) and Δz is the height above the soil heat flux plate (0.08 m). C_s depends on soil moisture and was determined as follows (Oliphant et al., 2004; Moderow et al., 2009):

$$C_s = \rho_b C_d + \theta \rho_w C_w \quad (2)$$

where ρ_b is the soil bulk density (682.6 kg m^{-3}), θ is the volumetric soil moisture (m^3 m^{-3}), ρ_w is the density of water (1000 kg m^{-3}), C_w is the heat capacity of water (4190 J kg^{-1} K^{-1}) and C_d is the heat capacity of dry soil, adopted equal to 840 J kg^{-1} K^{-1} (Hanks and Ashcroft, 1980). Half-hourly meteorological and soil variables were obtained from the NEON portal (NEON, 2020).

2.2.4 Energy balance closure

The surface energy balance can be written by the following equation (Cui and Chui, 2019):

$$Rn - G - S = LE + H \quad (3)$$

where *Rn* is the net radiation, *G* is the soil heat flux, *H* is the sensible heat flux, *LE* is the latent heat flux, and *S* represents the storage term related to photosynthesis, air, biomass and soil (Eshonkulov et al., 2019). In this study, except for S_g, which was estimated when T_{soil} and θ data were available, the other *S* components were not considered (Cui and Chui, 2019). *EBC* was evaluated considering three approaches: in the first one, the bulk method or energy balance ratio (*EBR*), *EBC* is calculated using the ratio between the cumulative values of turbulent fluxes (*LE+H*) and available energy (*Rn-G*) over the growing season. In this approach, *EBC* is reached when *EBR* is one (Stoy et al., 2013):

$$EBR = \frac{\sum(LE + H)}{\sum(Rn - G - S)} \quad (4)$$

In the second approach, *EBC* was derived using a linear regression analysis between available energy (*Rn-G*) and turbulent fluxes (*LE+H*). In this approach, the *EBC* is achieved when the slope is one and the intercept is zero. In the third approach, *EBC* was evaluated by the residual (*Res*) of the energy balance equation, with the *EBC* occurring when *Res* is zero (Nelli et al., 2020):

$$Res = Rn - G - LE - H - S \quad (5)$$

The evaluation of *EBC*, based on the previous three approaches, was performed as a function of atmospheric conditions, turbulence and during daytime (morning and afternoon) and nighttime when the four main half-hourly components (*Rn*, *G*, *LE* and *H*) were available. Incoming solar radiation above to 20 W m^{-2} was adopted to define the daytime period. Due to the lower availability of T_{soil} and θ data compared to the other energy balance components, S_g was used only to evaluate its influence on *EBC*.

The atmospheric conditions were characterized by the stability parameter, which can be expressed as (Franssen et al., 2010):

$$\zeta = \left(\frac{z - d}{L}\right) \quad (6)$$

where z is the measurement height (m), d is the zero-plane displacement (m), calculated as $0.67h_c$, in which h_c is the canopy height, and L is the Monin-Obukhov length (m). We adopted the following classification for atmospheric conditions: unstable ($\zeta \leq -0.1$), neutral ($-0.1 < \zeta < 0.1$) and stable ($\zeta \geq 0.1$) (Franssen et al., 2010). The effect of turbulence on *EBC* was evaluated using the friction velocity (u^*) and turbulent kinetic energy (*TKE*), calculated as follows (Zhou and Li, 2019):

$$u^* = \left(\overline{u'w'}^2 + \overline{v'w'}^2\right)^{0.25} \quad (7)$$

$$TKE = 0.5\left(\overline{u'}^2 + \overline{v'}^2 + \overline{w'}^2\right) \quad (8)$$

where u', v' and w' are fluctuations of horizontal, lateral and vertical wind velocities (m s^{-1}), respectively.

2.2.5 Correlation coefficients for water vapor and temperature

The influence of large eddies on phase differences between vertical velocity and scalars on *EBC* was evaluated by the correlation coefficients for vertical wind velocity and water vapor (R_{wq}) and sonic temperature (R_{wt}) (Kaimal and Finningan, 1994):

$$R_{wq} = \frac{\overline{w'q'}}{\sigma_w \sigma_q} \quad (9)$$

$$R_{wt} = \frac{\overline{w'T'}}{\sigma_w \sigma_T} \quad (10)$$

where w'(m s^{-1}), q'(mmol mol^{-1}) and T' (K) are the turbulent components of vertical wind velocity, water vapor mixing ratio and sonic temperature; σ_w, σ_q and σ_T are the standard deviations of vertical wind velocity (m s^{-1}), water vapor mixing ratio (mmol mol^{-1}) and sonic temperature (K). R_{wq} and R_{wt} calculations were restricted to unstable atmospheric conditions and above u^* thresholds, since the atmospheric stability conditions and u^* affect the correlation coefficients and *EBC* (McGloin et al., 2008). The ReddyProc tool was used for estimating the u^* thresholds in each growing season (Wutzler et al., 2018), which were 0.21, 0.24 and 0.24 m s^{-1} for the 2017, 2018 and 2019 growing seasons, respectively. The relationships between the R_{wq} and R_{wt} and

EBR were evaluated by separating the correlation coefficients in ten percentiles (McGloin et al., 2008).

2.3 Results and discussion

2.3.1 Wind direction (WD), horizontal wind speed (WS) and flux footprint

During the three growing seasons, most of the *WD* values were observed between SW and SE sectors, which concentrated 49.2% (2017), 48.8% (2018) and 58.0% (2019) of the records (Fig. 2.2). In contrast, winds were less frequent between W and N, with 7.4 (2017), 7.5 (2018) and 11.2% (2019) of the values.

The highest *WS* values were observed in the sectors where winds were more frequent (Fig. 2.2). Most of the *WS* values were between 4.0 and 8.0 m s^{-1} (average of 44.2 %), but 84.2 (2017), 84.0% (2018) and 82.0% (2019) occurred from 0.0 to 8.0 m s^{-1} (Fig. 2.2). The highest *WS* was observed during 2017 (19.3 m s^{-1}), while the maximum *WS* values in 2017 and 2019 were 15.0 and 15.2 m s^{-1}, respectively.

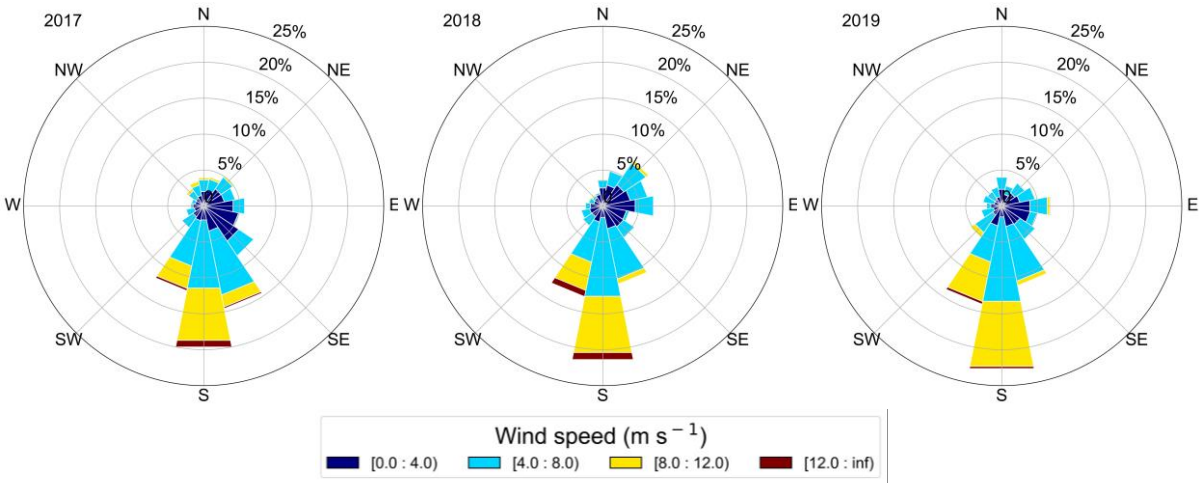

Figure 2.2 - Distribution of wind direction and wind speed for the 2017, 2018 and 2019 growing seasons.

The aggregated flux footprints at the site for the 2017, 2018 and 2019 growing seasons is shown in the Fig. 2.3. The aggregated flux footprint was similar during the three growing seasons, with 90% of the contributions to the measured fluxes

originating from 800 m from the flux tower in the prevailing south *WD* and approximately 350 and 500 m in W and E directions, respectively.

The average contribution of K2A to the measured fluxes was 84.9%, followed by C3SA (11.8%) and K20A (2.3%), while the contribution from other watersheds was below 1% (Table 2.2). According to the criteria established by Chu et al. (2021), the *EC* measurements at KONZ has a high representativeness, since more than 80% of the measured flux originating from the K2A watershed. However, the contribution from the different watersheds to the measured fluxes was dependent on *WD* and atmospheric stability conditions (Fig. 2.4).

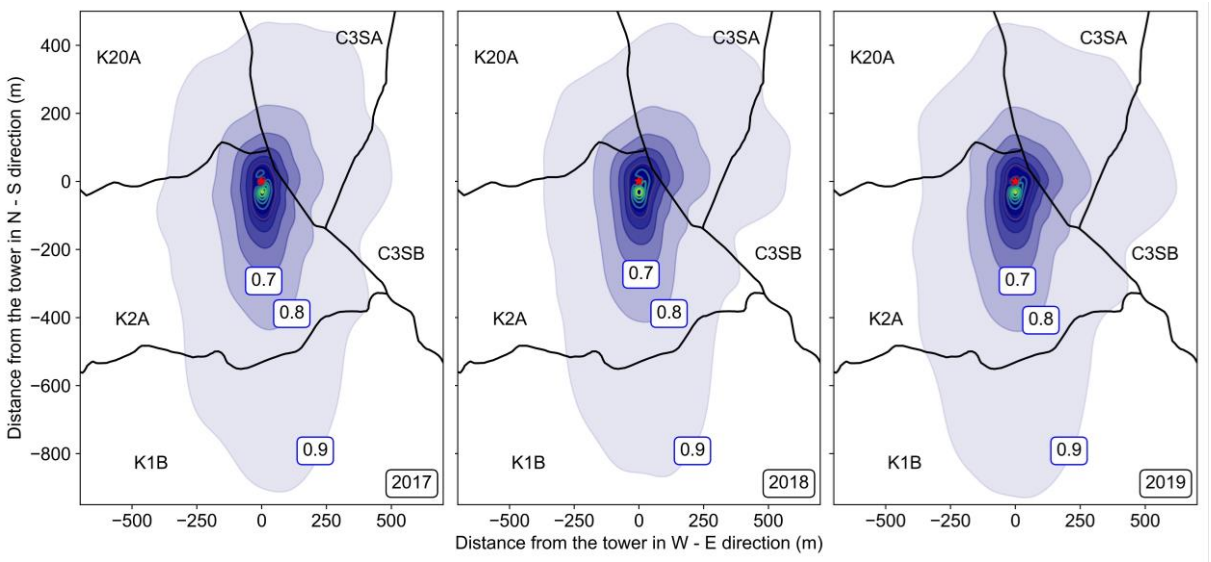

Figure 2.3 - Footprint climatology estimated for the 2017, 2018 and 2019 growing seasons and overlaid on the watershed map (C3SA, C3SB, K1B, K2A and K20A). The contour lines are the cumulative footprint every 10%. The red asterisk represents the measurement tower.

Table 2.2 - Relative contribution from watersheds to the measured eddy covariance fluxes during the 2017, 2018 and 2019 growing seasons.

Watershed	Year of growing season			
	2017	2018	2019	Average 2017 - 2019
	Contribution to the measured flux (%)			
K1B	0.3	0.0	0.3	0.2
K2A	85.6	83.6	85.5	84.9
K20A	2.6	1.7	2.6	2.3
C3SA	10.7	13.7	10.9	11.8
C3SB	0.8	0.8	0.7	0.8
Others	0.0	0.2	0.0	0.0

[1]Calculations were based on the source area contributing to 80% of the measured flux.

Under unstable and neutral atmospheric stability conditions, the contributions from K2A were 82.5% and 89.9%, respectively (Fig. 2.4a-f). On the other hand, under stable conditions, the contribution from K2A was reduced to 72.8%, while that from C3SA increased to 19.2% (Fig. 2.4g-i). The contribution from K1B was lower than 0.1% under unstable and neutral conditions, but increased to 1.2% under stable conditions (Fig. 2.4g-i).

The higher contribution from K2A under neutral and unstable conditions is associated to the higher restriction of the flux source area during these conditions (Nelli et al., 2020). Under unstable conditions, the higher restriction of the flux source is favored by intensification of the convection and turbulent diffusion (Arriga et al., 2017). Conversely, the decrease in contribution from K2A in stable conditions occur because the flux source area becomes less restricted (Griebel et al., 2017), increasing the contribution from watersheds located further away from the measurement point. The flux source from the south decreased more under unstable than in neutral conditions, which explains the higher contribution from K2A under neutral conditions.

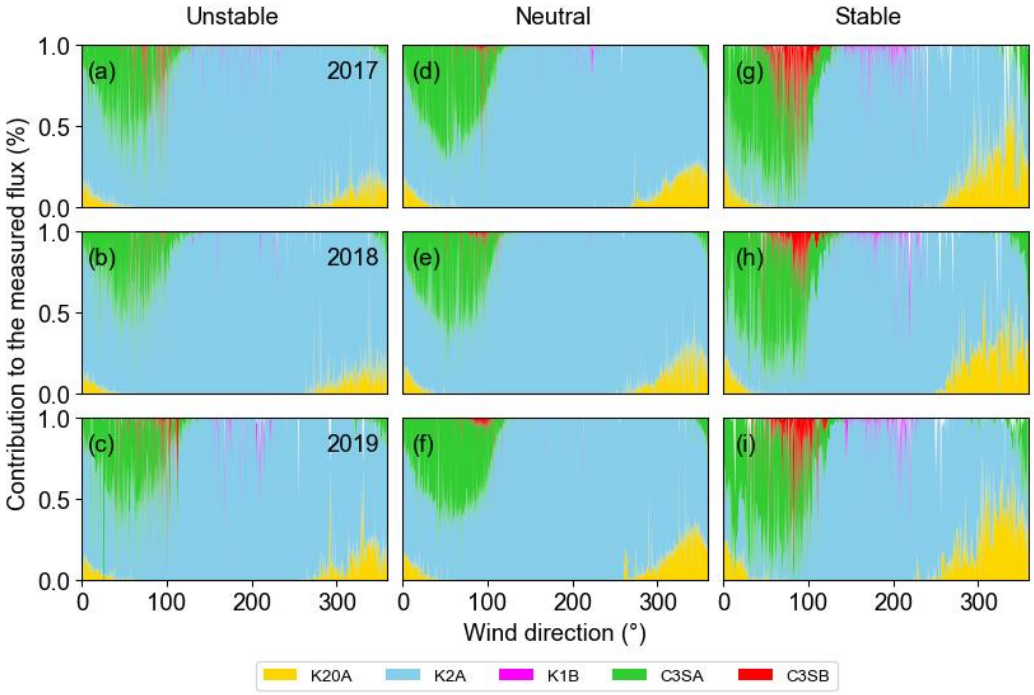

Figure 2.4 - Relationship between the wind direction and the watersheds flux contribution during unstable, neutral and stable atmospheric conditions for the 2017 (a, d and g), 2018 (b, e and h) and 2019 (c, f and i) growing seasons.

2.3.2 Energy balance closure

The *EBR* ranged from 0.69 (2018) to 0.82 (2017), resulting in *Res* averages of 48.50 and 26.89 W m^{-2}, respectively (Fig. 2.5). The slopes were lower than *EBR*, but followed the same pattern among the years, ranging from 0.64 (2018) to 0.73 (2017). The intercepts values were all positives, being lower in 2018 (9.25 W m^{-2}) and higher in 2019 (15.02 W m^{-2}). The coefficients of determination (R^2) were highest in the years with higher *EBR* and slopes, ranging from 0.84 (2018) to 0.91 (2017 and 2019).

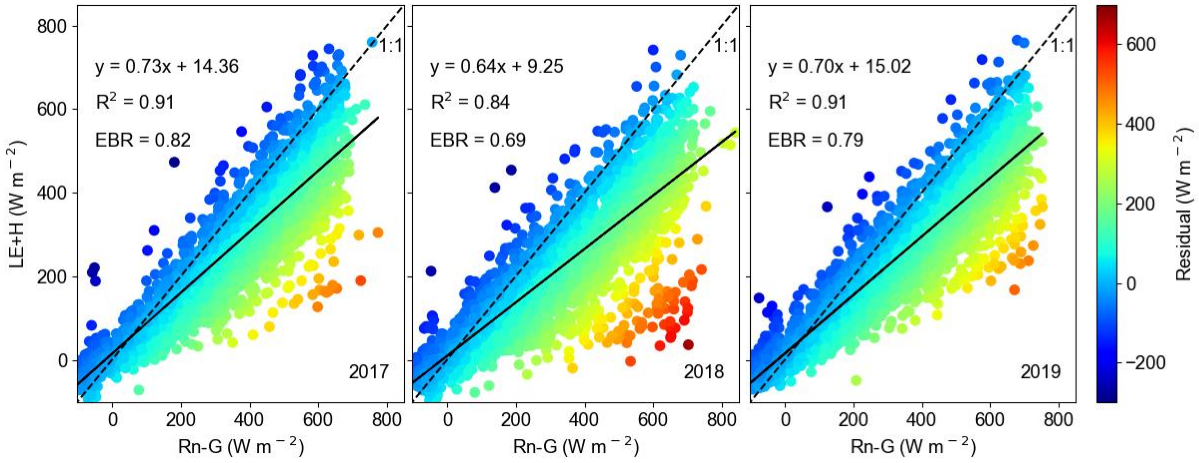

Figure 2.5 - Relationship between the available energy (*Rn-G*) and turbulent fluxes (*LE+H*) and energy balance ratio (*EBR*) for the 2017, 2018 and 2019 growing seasons.

The *EBR* values found in our study are within the range found for 62 grasslands (0.86 ± 0.20) at FLUXNET sites (Stoy et al., 2013). The differences between *EBR* and slopes found in our study ranged from 5.0% (2018) and 9.0% (2017 and 2019). Sanchez et al. (2010) found that *EBR* overcame the slopes between 9.0% and 12.0% in a boreal forest in Finland. Highest differences with *EBR* overcoming the slopes from 5.0 to 25.0% were reported for several ecosystems at ChinaFlux sites (Li et al., 2005). The highest *EBC* reached using *EBR* instead the slopes occur because large differences between *(Rn-G)* and *(LE+H)* and the contribution of storage terms are smoothed by accumulating fluxes throughout the day (Blanken et al., 1998).

The reduction in the contribution of storage terms and large fluctuations when using *EBR* was evidenced by separating the fluxes in the morning, afternoon and nighttime (Table 2.3). The largest slope values and *EBR* were observed in daytime, while nighttime was characterized by poor *EBC*, likely due to the weak turbulence mixing (Soltani et al., 2018). However, while similar slope values were observed in the morning and afternoon, the *EBR* in the afternoon increased from 14.0% (2017) to 19.0% (2018) compared to those in the morning.

Table 2.3 - Linear regression parameters, energy balance ratio (*EBR*), average residual of the energy balance closure (*Res*) and number of observations (*N*) during the nighttime, morning and afternoon for the 2017, 2018 and 2019 growing seasons.

		Year of growing season		
Time	**Parameters**	**2017**	**2018**	**2019**
Nighttime	Slope	0.53	0.39	0.36
	Intercept (W m^{-2})	7.94	-0.41	0.12
	R^2	0.25	0.23	0.24
	EBR	0.38	0.40	0.36
	Residual (W m^{-2})	-33.26	-26.85	-32.44
	N	2009	1907	1734
Morning	Slope	0.75	0.63	0.71
	Intercept (W m^{-2})	-20.83	-22.46	-20.42
	R^2	0.85	0.71	0.88
	EBR	0.68	0.55	0.64
	Residual (W m^{-2})	92.05	129.90	109.04
	N	1070	1119	1001
Afternoon	Slope	0.75	0.64	0.71
	Intercept (W m^{-2})	20.42	28.41	32.07
	R^2	0.82	0.73	0.84
	EBR	0.82	0.74	0.81
	Residual (W m^{-2})	59.32	81.13	60.99
	N	1577	1613	1418

Highest *EBR* in the afternoon has been reported in several studies and related to storage terms, which are higher during the morning (Wilson et al., 2002; Xu et al., 2017; Soltani et al., 2018; Kutikoff et al., 2019). On the other hand, the heat stored in soil, biomass and air in the morning can be lost throughout the afternoon, decreasing the discrepancy between *(Rn-G)* and *(LE-H)* (Leuning et al., 2012; Grachev et al., 2020). Furthermore, the hysteresis between *Rn* and the others energy balance components, especially in the morning, has been related to the lack of surface energy balance (Liu et al., 2017).

The inclusion of S_g enhanced the slopes from 4.6% (2017) to 5.4% (2018) and *EBR* between 1.0% (2017) and 1.3% (2018), while the *Res* was reduced between 6.0 (2018) and 7.4% (2017 and 2019) (Table 2.4). The lower increase in *EBR* even after the inclusion of S_g also suggests that the contribution of storage terms is reduced by accumulating fluxes throughout the day. The contributions of S_g found in our study are consistent with those reported for other grassland ecosystems. For instance, Zuo et al. (2011) evaluated the *EBC* in a semi-arid grassland in the Loess Plateau, China, and observed that S_g improved the slopes between 6.0% and 7.0%. For a subalpine meadow grassland in Northwest China, Wang and Zang (2011) found that S_g was the main storage component, being equivalent to 1.6% of the available energy. In a study conducted on the Mongolian Plateau in a desert steppe grassland, the contribution of S_g ranged between 1.8 and 2.7% of the available energy (Shao et al., 2017).

Table 2.4 - Changes (%) in the slopes, energy balance ratio (*EBR*) and average residual of the energy balance closure (*Res*) by accounting for soil heat storage (S_g) for the 2017, 2018 and 2019 growing seasons.

Parameters	Year of growing season		
	2017	**2018**	**2019**
	Change after adding of S_g		
Slope	4.6	5.4	5.2
EBR	1.0	1.3	1.2
Residual	-7.4	-6.0	-7.4

The values of *EBR* considering only 30-min data in which 100% of the measured fluxes originated from the K2A were similar to those considering all data, 0.80 (2017), 0.68 (2018) and 0.77 (2019). The slopes were slightly improved during 2017 (0.74) and 2018 (0.65), but not changed in 2019. These results show that the surface heterogeneity resulting from the different management practices has a low influence on *EBC* at KONZ site, since most of the fluxes originate from the K2A watershed.

2.3.3 Effect turbulence, atmospheric conditions (ζ) and correlation coefficients (R_{wq} and R_{wt}) on *EBC*

The daily courses of the average ζ, *u** and *TKE* for the three growing seasons are shown in Fig. 2.6. The daytime period was characterized by unstable conditions, while stable conditions were more frequent in nighttime (Fig. 2.6a). Times close to sunrise and sunset were characterized by neutral conditions, although these conditions were also frequent throughout the daytime. The *u** and *TKE* increased since sunrise, as the atmosphere become unstable, reaching their peak around noon, and decreased in the afternoon and nighttime, as the atmosphere became more stable (Fig. 2.6b and 2.6c).

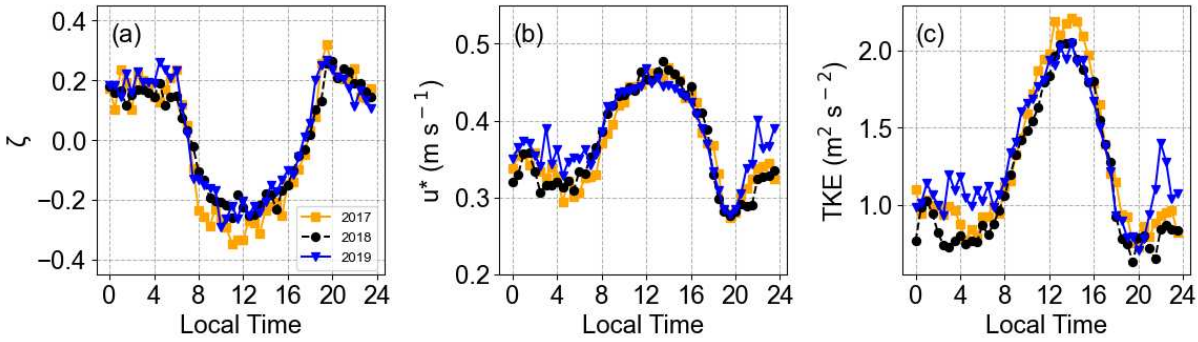

Figure 2.6 - Average daily courses of a) stability parameter (ζ), b) friction velocity (*u**) and c) turbulent kinetic energy (*TKE*) for the 2017, 2018 and 2019 growing seasons.

Most fluxes measurements were conducted in neutral atmospheric stability conditions during the 2017 (51.4%), 2018 (56.5%) and 2019 (60.8%) growing seasons (Table 2.5). Unstable atmospheric conditions were more frequent in 2017 (29.4%) and 2018 (24.4%) and less frequent in 2019 (20.4%). Fluxes measurements under stable conditions were less frequent in all growing seasons, occurring in 19.2% (2017), 19.1% (2018) and 18.8% (2019) of the measured intervals.

Table 2.5 - Linear regression parameters, energy balance ratio (*EBR*), average residual of the energy balance closure (*Res*) and number of observations (*N*) during the unstable, neutral and stable atmospheric stability conditions for the 2017, 2018 and 2019 growing seasons.

		Year of growing season		
Atmospheric conditions	**Parameters**	**2017**	**2018**	**2019**
Unstable	Slope	0.77	0.64	0.72
	Intercept (W m^{-2})	3.87	7.00	8.98
	R^2	0.78	0.64	0.78
	EBR	0.78	0.65	0.74
	Residual (W m^{-2})	84.67	134.69	110.29
	N	1366	1133	848
Neutral	Slope	0.71	0.65	0.71
	Intercept	11.15	6.38	11.19
	R^2	0.90	0.84	0.90
	EBR	0.82	0.70	0.79
	Residual (W m^{-2})	17.37	38.55	29.76
	N	2393	2622	2526
Stable	Slope	0.40	0.29	0.47
	Intercept (W m^{-2})	6.14	-1.33	13.19
	R^2	0.28	0.13	0.47
	EBR	0.27	0.32	0.19
	Residual (W m^{-2})	-35.69	-32.23	-37.64
	N	895	884	779

The slopes and *EBR* were improved during unstable and neutral atmospheric conditions, while poor slopes and *EBR* were observed under stable conditions (Table 2.5). The available energy explained between 64% and 90% of the variability of turbulent fluxes under neutral and unstable conditions, while in stable conditions the (*Rn-G)* explained between 13% of 47% of *(LE+H)* (Table 2.5). The slopes were higher in unstable conditions (ranging from 0.64 to 0.77), while the higher *EBR* values were

observed in neutral conditions (ranging from 0.70 to 0.82) (Table 2.5). It is important to note that despite the lower slopes and *EBR* under stable conditions, the higher absolute *Res* were observed in unstable conditions, related to the greater magnitude of *Rn* (Table 2.5). Therefore, despite the increase in *EBR* and slopes during unstable conditions, the higher absolute *Res* indicate that the lack of *EBC* has a higher impact during daytime, affecting, for example, evapotranspiration studies (Franssen et al., 2010).

The *EBR* was improved as ζ decreased, while positive values of ζ resulted in *EBR* values generally less than one (Fig. 2.7). Interestingly, a large fluctuation in *EBR*, with values ranging from about minus five to plus five, was observed in the transition between neutral and stable conditions, especially at sunrise and sunset, when the magnitudes of the fluxes are small. Similar fluctuations in *EBR* under neutral and stable atmospheric conditions were also reported by Eshonkulov et al. (2019) and Cui and Chui (2019).

Large fluctuations in *EBR* were observed under low values of *u** and *TKE* (Fig. 2.7). *EBR* became closer to one as *TKE* increased, while a scattered relationship between high values of *u** and *EBR* was still observed, indicating that *u** should be used with caution to filter *EC* fluxes. According to Acevedo et al. (2009), *u** can be influenced by mesoscale flux, and depending on the time scale considered, non-turbulent periods may have high *u** values and vice versa. Furthermore, while *u** indicates only the mechanical/shear production, *TKE* includes the effects of mechanical/shear production, buoyant production/destruction, turbulent transport and dissipation (Zhou and Li, 2019). For this reason, *TKE* and other parameters such as vertical velocity fluctuations (σ_w), have been proposed instead of *u** to filter *EC* fluxes (Acevedo et al., 2009; del Castillo et al., 2018; Zhou and Li, 2019).

The increase of *EBR* as a function of *TKE* and under neutral and unstable atmospheric conditions has been reported in previous studies (Campos et al. 2019; Eshonkulov et al. 2019; Zhou and Li, 2019). The poor *EBR* and slopes observed under low *TKE* are associated with low turbulence intensity, which results in an underestimation of turbulent fluxes, especially in nighttime (Sánchez et al., 2010).

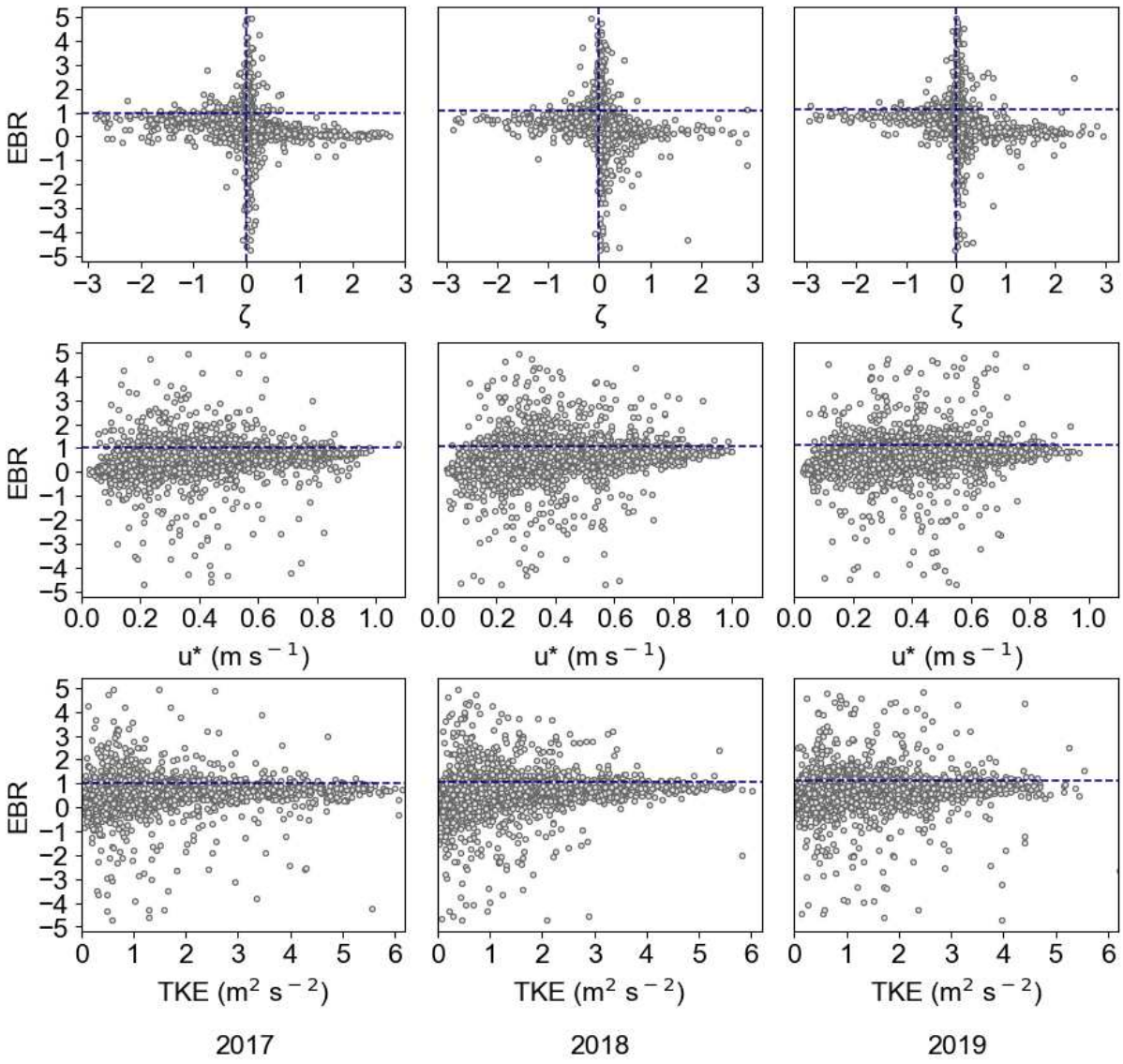

Figure 2.7 - Relationship between stability parameter (ζ), friction velocity (u^*) and turbulent kinetic energy (*TKE*) and EBR for the 2017, 2018 and 2019 growing seasons.

Smaller values of R_{wq} and R_{wt} are associated with low-frequency processes (i.e., large eddies), which in turn cause phase differences between *w* and *T* and *w* and *q*, decreasing the magnitude of turbulent fluxes and increasing the lack of surface energy balance (Gao et al., 2017; von Randow et al., 2006). In this study, the *EBR* was clearly improved with increasing of R_{wq} and R_{wt} (Fig. 2.8). The average of *EBR* increased from 0.49 to 0.88 as a function of R_{wq}, but a maximum *EBR* of 0.90 was reached in 2017 and 2019 (Fig. 2.8a). Considering R_{wt}, average *EBR* increased from 0.54 to 0.88 reaching a peak of 0.91 in 2017 (Fig. 2.8b). The increase of *EBR* as a function of R_{wq} and R_{wt} was observed in several studies, although *EBR* has not been influenced by

these correlation coefficients in some ecosystems (McGloin et al., 2018; Zhou and Li; Campos et al., 2019).

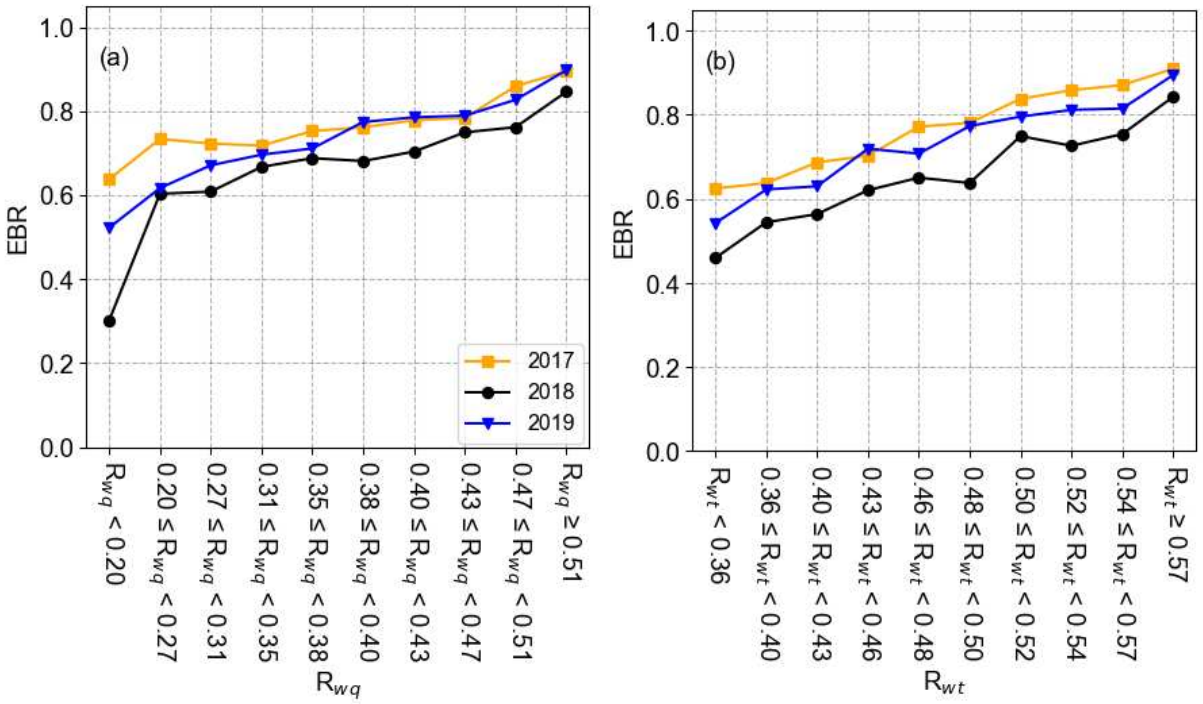

Figure 2.8 - Relationship between the correlation coefficients for (a) vertical wind velocity and water vapor vertical (R_{wq}) and (b) wind velocity and sonic temperature (R_{wt}) and energy balance ratio (*EBR*) for 2017, 2018 and 2019 growing seasons.

2.4 Conclusions

The contribution from the different watersheds to the measured fluxes was dependent on wind direction and atmospheric stability conditions. Stable atmospheric conditions resulted in lower flux source area from the area of interest. However, although the flux tower is surrounded by watersheds under different management practices, most of the fluxes originated from a single watershed (K2A), so the *EBC* was not affected by surface heterogeneity. The slopes of linear regression and *EBR* indicated a lack of *EBC* of 31% and 23%, respectively. The inclusion of S_g in the *EBC* calculations enhanced *EBR* and regression slopes by 1.2% and 5.1%, respectively. Stable atmospheric conditions resulted in poor *EBC*, but unstable conditions revealed higher energy residual. *EBR* improved with the increase of *TKE*, while the increase in

*u** did not result in an improvement in *EBR*. The relationship between the correlation coefficients (R_{wq} and R_{wt}) and *EBR* indicated that low-frequency processes affect the *EBC* at KONZ site.

Our findings reveal that the use of *EBR* in the *EBC* studies decreases the effects of neglecting storage components. Further studies are still needed to investigate the influence of other storage terms on *EBC* in tallgrass prairie. In addition, the use of *TKE* for *EC* data filtering could be useful in future studies.

References

Acevedo, O. C., Moraes, O. L., Degrazia, G. A., Fitzjarrald, D. R., Manzi, A. O., Campos, J. G., 2009. Is friction velocity the most appropriate scale for correcting nocturnal carbon dioxide fluxes? Agricultural and Forest Meteorology, 149(1), 1-10. https://doi.org/10.1016/j.agrformet.2008.06.014

Anthoni, P. M., Law, B. E., Unsworth, M. H., Vong, R. J., 2000. Variation of net radiation over heterogeneous surfaces: measurements and simulation in a juniper–sagebrush ecosystem. Agricultural and Forest Meteorology, 102(4), 275-286. https://doi.org/10.1016/S0168-1923(00)00104-0

Arriga, N., Rannik, Ü., Aubinet, M., Carrara, A., Vesala, T., Papale, D., 2017. Experimental validation of footprint models for eddy covariance CO_2 flux measurements above grassland by means of natural and artificial tracers. Agricultural and Forest Meteorology, 242, 75-84. https://doi.org/10.1016/j.agrformet.2017.04.006

Baldocchi, D. D., 2020. How eddy covariance flux measurements have contributed to our understanding of Global Change Biology. Global Change Biology, 26(1), 242-260. https://doi.org/10.1111/gcb.14807

Blair, J. M., O'neal, P. R. 2021. KFH01 Konza prairie fire history. Environmental Data Initiative. http://dx.doi.org/10.6073/pasta/213f54ba6ce198ee51f5931fe66faad1

Blanken, P. D., Black, T. A., Neumann, H. H., Den Hartog, G., Yang, P. C., Nesic, Z., Staebler, R., Chen, W., Novak, M. D., 1998. Turbulent flux measurements above and below the overstory of a boreal aspen forest. Boundary-Layer Meteorology, 89(1), 109-140. https://doi.org/10.1023/A:1001557022310

Briggs, J. M., Blair, J. M., Horne, E. A., 2016. Ecohydrological and climate change studies at the Konza Prairie Biological Station. Transactions of the Kansas Academy of Science (1903-), 119(1), 5-11.

Campos, S. et al., 2019. Closure and partitioning of the energy balance in a preserved area of a Brazilian seasonally dry tropical forest. Agricultural and Forest Meteorology, 271, 398-412. https://doi.org/10.1016/j.agrformet.2019.03.018

Chen, B., Black, T. A., Coops, N. C., Hilker, T., Trofymow, J. T., & Morgenstern, K., 2009. Assessing tower flux footprint climatology and scaling between remotely sensed and eddy covariance measurements. Boundary-Layer Meteorology, 130(2), 137-167. https://doi.org/10.1007/s10546-008-9339-1

Chu, H. et al., 2021. Representativeness of Eddy-Covariance flux footprints for areas surrounding AmeriFlux sites. Agricultural and Forest Meteorology, 301, 108350. https://doi.org/10.1016/j.agrformet.2021.108350

Cui, W., Chui, T. F. M., 2019. Temporal and spatial variations of energy balance closure across FLUXNET research sites. Agricultural and Forest Meteorology, 271, 12-21. https://doi.org/10.1016/j.agrformet.2019.02.026

del Castillo, E. G., Sánchez-Azofeifa, A., 2018. Turbulence scales for eddy covariance quality control over a tropical dry forest in complex terrain. Agricultural and Forest Meteorology, 249, 390-406. https://doi.org/10.1016/j.agrformet.2017.11.014

Eshonkulov, R. et al., 2019. Evaluating multi-year, multi-site data on the energy balance closure of eddy-covariance flux measurements at cropland sites in southwestern Germany. Biogeosciences, 16(2), 521-540. https://doi.org/10.5194/bg-16-521-2019

Eshonkulov, R., Poyda, A., Ingwersen, J., Pulatov, A., Streck, T., 2019. Improving the energy balance closure over a winter wheat field by accounting for minor storage terms. Agricultural and Forest Meteorology, 264, 283-296. https://doi.org/10.1016/j.agrformet.2018.10.012

Franssen, H. H., Stöckli, R., Lehner, I., Rotenberg, E., Seneviratne, S. I., 2010. Energy balance closure of eddy-covariance data: A multisite analysis for European FLUXNET stations. Agricultural and Forest Meteorology, 150(12), 1553-1567. https://doi.org/10.1016/j.agrformet.2010.08.005

Foken, T., 2008. The energy balance closure problem: an overview. Ecological Applications, 18(6), 1351-1367. https://doi.org/10.1890/06-0922.1

Gao, Z., Liu, H., Katul, G. G., Foken, T., 2017. Non-closure of the surface energy balance explained by phase difference between vertical velocity and scalars of large atmospheric eddies. Environmental Research Letters, 12(3), 034025. https://doi.org/10.1088/1748-9326/aa625b

Grachev, A. A. et al., 2020. On the surface energy balance closure at different temporal scales. Agricultural and Forest Meteorology, 281, 107823. https://doi.org/10.1016/j.agrformet.2019.107823

Griebel, A., Bennett, L. T., Metzen, D., Cleverly, J., Burba, G., Arndt, S. K., 2016. Effects of inhomogeneities within the flux footprint on the interpretation of seasonal, annual, and interannual ecosystem carbon exchange. Agricultural and Forest Meteorology, 221, 50-60. https://doi.org/10.1016/j.agrformet.2016.02.002

Gong, D., Mei, X., Hao, W., Wang, H., Caylor, K. K., 2017. Comparison of ET partitioning and crop coefficients between partial plastic mulched and non-mulched maize fields. Agricultural Water Management, 181, 23-34. https://doi.org/10.1016/j.agwat.2016.11.016

Guo, H., Li, S., Kang, S., Du, T., Tong, L., Hao, X., Ding, R., 2020. Crop coefficient for spring maize under plastic mulch based on 12-year eddy covariance observation in the arid region of Northwest China. Journal of Hydrology, 588, 125108. https://doi.org/10.1016/j.jhydrol.2020.125108

Hanks, R. J., & Ashcroft, G. L., 1980. Water potentials. In Applied Soil Physics (pp. 20-61). Springer, New York, NY.

Kaimal, J. C., Finnigan, J. J., 1994. Atmospheric boundary layer flows: their structure and measurement. Oxford university press.

Kim, S., Lee, Y. H., Kim, K. R., Park, Y. S., 2014. Analysis of surface energy balance closure over heterogeneous surfaces. Asia-Pacific Journal of Atmospheric Sciences, 50(1), 553-565. https://doi.org/10.1007/s13143-014-0045-2

Kljun, N., Calanca, P., Rotach, M. W., Schmid, H. P., 2015. A simple two-dimensional parameterisation for Flux Footprint Prediction (FFP). Geoscientific Model Development, 8(11), 3695-3713. https://doi.org/10.5194/gmd-8-3695-2015

Kutikoff, S., Lin, X., Evett, S., Gowda, P., Moorhead, J., Marek, G., ... & Brauer, D. (2019). Heat storage and its effect on the surface energy balance closure under advective conditions. Agricultural and Forest Meteorology, 265, 56-69. https://doi.org/10.1016/j.agrformet.2018.10.018

Leuning, R., Van Gorsel, E., Massman, W. J., Isaac, P. R., 2012. Reflections on the surface energy imbalance problem. Agricultural and Forest Meteorology, 156, 65-74. https://doi.org/10.1016/j.agrformet.2011.12.002

Li, S. et al., 2018. Assessment of multi-source evapotranspiration products over china using eddy covariance observations. Remote Sensing, 10(11), 1692. https://doi.org/10.3390/rs10111692

Li, S., Kang, S., Zhang, L., Zhang, J., Du, T., Tong, L., Ding, R., 2016. Evaluation of six potential evapotranspiration models for estimating crop potential and actual evapotranspiration in arid regions. Journal of Hydrology, 543, 450-461. https://doi.org/10.1016/j.jhydrol.2016.10.022

Liu, X., Yang, S., Xu, J., Zhang, J., Liu, J., 2017. Effects of soil heat storage and phase shift correction on energy balance closure of paddy fields. Atmósfera, 30(1), 39-52. https://doi.org/10.20937/ATM.2017.30.01.04

Marcolla, B., Cescatti, A., 2018. Geometry of the hemispherical radiometric footprint over plant canopies. Theoretical and Applied Climatology, 134(3), 981-990. https://doi.org/10.1007/s00704-017-2326-z

Masseroni, D., Corbari, C., Mancini, M., 2014. Limitations and improvements of the energy balance closure with reference to experimental data measured over a maize field. Atmósfera, 27(4), 335-352. https://doi.org/10.1016/S0187-6236(14)70033-5

Mauder, M., Foken, T., Cuxart, J., 2020. Surface-energy-balance closure over land: a review. Boundary-Layer Meteorology, 177, 395-426. https://doi.org/10.1007/s10546-020-00529-6

McGloin, R., Šigut, L., Havránková, K., Dušek, J., Pavelka, M., & Sedlák, P., 2018. Energy balance closure at a variety of ecosystems in Central Europe with contrasting topographies. Agricultural and forest meteorology, 248, 418-431. https://doi.org/10.1016/j.agrformet.2017.10.003

Meyers, T. P., Hollinger, S. E., 2004. An assessment of storage terms in the surface energy balance of maize and soybean. Agricultural and Forest Meteorology, 125(1-2), 105-115. https://doi.org/10.1016/j.agrformet.2004.03.001

Moderow, U. et al., 2009. Available energy and energy balance closure at four coniferous forest sites across Europe. Theoretical and Applied Climatology, 98(3), 397-412. https://doi.org/10.1007/s00704-009-0175-0

Moncrieff, J. B., Massheder, J. M., De Bruin, H., Elbers, J., Friborg, T., Heusinkveld, B., Kabat, P., Scott, S., Soeggard, H., Verhoef, A., 1997. A system to measure surface fluxes of momentum, sensible heat, water vapour and carbon dioxide. Journal of Hydrology, 188, 589-611. https://doi.org/10.1016/S0022-1694(96)03194-0

Moncrieff, J., Clement, R., Finnigan, J., Meyers, T., 2004. Averaging, detrending, and filtering of eddy covariance time series. In Handbook of Micrometeorology (pp. 7-31). Springer, Dordrecht.

Neftel, A., Spirig, C., Ammann, C., 2008. Application and test of a simple tool for operational footprint evaluations. Environmental Pollution, 152(3), 644-652. https://doi.org/10.1016/j.envpol.2007.06.062

Nelli, N. R. et al., 2020. Micrometeorological measurements in an arid environment: Diurnal characteristics and surface energy balance closure. Atmospheric Research, 234, 104745. https://doi.org/10.1016/j.atmosres.2019.104745

NEON - National Ecological Observatory Network., 2020. Data Products NEON.DP1.00023.001, NEON.DP1.00033.001, NEON.DP1.00040.001, NEON.DP1.00094.001, NEON.DP1.00096.001, NEON.DP1.00098.001, NEON.IP0.00200.001, DP1.00033.001. Provisional data downloaded from http://data.neonscience.org on February 10, 2020. Battelle, Boulder, CO, USA.

O'Connor, R. C., Taylor, J. H., & Nippert, J. B., 2020. Browsing and fire decreases dominance of a resprouting shrub in woody encroached grassland. Ecology, 101(2), e02935. https://doi.org/10.1002/ecy.2935

Oliphant, A. J. et al., 2004. Heat storage and energy balance fluxes for a temperate deciduous forest. Agricultural and Forest Meteorology, 126(3-4), 185-201. https://doi.org/10.1016/j.agrformet.2004.07.003

Prajapati, P., Santos, E. A., 2018. Estimating methane emissions from beef cattle in a feedlot using the eddy covariance technique and footprint analysis. Agricultural and Forest Meteorology, 258, 18-28. https://doi.org/10.1016/j.agrformet.2017.08.004

Sánchez, J. M., Caselles, V., Rubio, E. M., 2010. Analysis of the energy balance closure over a FLUXNET boreal forest in Finland. Hydrology and Earth System Sciences, 14(8), 1487-1497. https://doi.org/10.5194/hess-14-1487-2010

Shao, C., Chen, J., Li, L., Dong, G., Han, J., Abraha, M., John, R., 2017. Grazing effects on surface energy fluxes in a desert steppe on the Mongolian Plateau. Ecological Applications, 27(2), 485-502. https://doi.org/10.1002/eap.1459

Shao, C., Li, L., Dong, G., Chen, J., 2014. Spatial variation of net radiation and its contribution to energy balance closures in grassland ecosystems. Ecological Processes, 3(1), 1-11. https://doi.org/10.1186/2192-1709-3-7

Soltani, M., Mauder, M., Laux, P., & Kunstmann, H., 2018. Turbulent flux variability and energy balance closure in the TERENO prealpine observatory: a hydrometeorological data analysis. Theoretical and Applied Climatology, 133(3), 937-956. https://doi.org/10.1007/s00704-017-2235-1

Stoy, P. C., Mauder, M., Foken, T., Marcolla, B., Boegh, E., Ibrom, A., ... & Varlagin, A., 2013. A data-driven analysis of energy balance closure across FLUXNET research sites: The role of landscape scale heterogeneity. Agricultural and Forest Meteorology, 171, 137-152. https://doi.org/10.1016/j.agrformet.2012.11.004

Wang, R., Zhang, Q., 2011. An assessment of storage terms in the surface energy balance of a subalpine meadow in Northwest China. Advances in Atmospheric Sciences, 28(3), 691-698. https://doi.org/10.1007/s00376-010-9152-x

Wilson, K. et al., 2002. Energy balance closure at FLUXNET sites. Agricultural and Forest Meteorology, 113(1-4), 223-243. https://doi.org/10.1016/S0168-1923(02)00109-0

Wutzler, T., 2018. Basic and extensible post-processing of eddy covariance flux data with REddyProc. Biogeosciences, 15(16), 5015-5030. https://doi.org/10.5194/bg-15-5015-2018

Xin, Y. F. et al., 2018. Surface energy balance closure at ten sites over the Tibetan plateau. Agricultural and Forest Meteorology, 259, 317-328. https://doi.org/10.1016/j.agrformet.2018.05.007

Xu, Z., Ma, Y., Liu, S., Shi, W., Wang, J., 2017. Assessment of the energy balance closure under advective conditions and its impact using remote sensing data. Journal of Applied Meteorology and Climatology, 56(1), 127-140. DOI: https://doi.org/10.1175/JAMC-D-16-0096.1

Li, Z.Q.,Yu, G.R.,Wen,X.F., Zhang, L.M.,Ren, C.Y., Fu,Y.L., 2005. Energy balance closure at ChinaFLUX sites. Science in China Earth Sci, 48, 51–62. https://doi.org/10.1360/05zd0005

Vickers, D., Mahrt, L., 1997. Quality control and flux sampling problems for tower and aircraft data. Journal of Atmospheric and Oceanic Technology, 14(3), 512-526. https://doi.org/10.1175/1520-0426(1997)014%3C0512:QCAFSP%3E2.0.CO;2

von Randow, C., Kruijt, B., Holtslag, A. A., 2006. Low-frequency modulation of the atmospheric surface layer over Amazonian rain forest and its implication for similarity relationships. Agricultural and Forest Meteorology, 141(2-4), 192-207. https://doi.org/10.1016/j.agrformet.2006.10.005

Zhao, J., Chen, X., Bao, A. M., 2014. Spatial representativeness of eddy covariance measurements using footprint analysis in arid areas. Environmental Earth Sciences, 71(4), 1691-1697. https://doi.org/10.1007/s12665-013-2573-y

Zhou, Y., Li, X., 2019. Energy balance closures in diverse ecosystems of an endorheic river basin. Agricultural and Forest Meteorology, 274, 118-131. https://doi.org/10.1016/j.agrformet.2019.04.019

Li, C., Huang, J., Ding, L., Liu, X., Yu, H., Huang, J. (2020). Increasing escape of oxygen from oceans under climate change. Geophysical Research Letters, 47(11), e2019GL086345. https://doi.org/10.3724/SP.J.1226.2011.00041

3 PARTITIONING EVAPOTRANSPIRATION IN A TALLGRASS PRAIRIE USING MICROMETEOROLOGICAL AND WATER USE EFFICIENCY APPROACHES UNDER CONTRASNTING RAINFALL REGIMES

Abstract

Partitioning evapotranspiration (*ET*) into evaporation (*E*) and plant transpiration (*T*) is key to understanding ecosystem responses to rainfall variability resulting from climate change. The goal of this study was to quantify *T* and *E* using eddy covariance (*EC*) flux measurements in a tallgrass prairie in consecutive growing seasons with contrasting rainfall regimes. The field measurements were conducted at the National Ecological Observatory Network (NEON) KONZ site, in Kansas, U.S., during the growing seasons of 2017, 2018 and 2019. The *ET* partitioning was performed using an approach based on the concept of the underlying water use efficiency (*uWUE*). To evaluate the *uWUE* approach, we compared daily *E* estimates obtained from the *uWUE* with *E* observations provided by microlysimeters (*ML*). Green chromatic coordinate (*GCC*) was used to monitor the vegetation dynamics. In the 2017 growing season, the total rainfall was 23.1% below the site's long-term average cumulative precipitation. On the other hand, in 2018 and 2019 the accumulated growing season precipitations were 7.2% and 40.2%, respectively, above the long-term precipitation average. The relationship between *uWUE* approach and *ML E* measurements showed a Pearson correlation coefficient (*r*) of 0.42 and a root mean square error (*RMSE*) of 0.58 mm d^{-1}. The lowest *T/ET* average value (0.50) was observed in the 2017 growing season, while the largest *T/ET* average (0.65) was observed in 2018. The correlations *GCC* and *T/ET* were reduced during the growing seasons that experienced drought periods. Air temperature was the main environmental driver of *T/ET* during the wet growing seasons (r = 0.49 and 0.72). The subsurface soil moisture (0.45 m) was the main environmental driver of *T/ET* during a dry growing season (r = 0.41). These results demonstrate that the precipitation variability not only has a direct impact on the *ET* components but also modulates the response of those components to other environmental drivers. Since *ET* partitioning studies at the ecosystem scale are still scarce, our results can improve *T/ET* and water use efficiency estimates in long-term modelling studies. This will help to better understand how *ET* in ecosystems will

respond to global warming and increased CO_2 concentration during wet and dry growing seasons.

Keywords: Evapotranspiration partitioning; Rainfall variability; Underlying water use efficiency; Eddy covariance; Grasslands

3.1 Introduction

The grasslands in the U.S. Great Plains are subject to highly variable precipitation (Jones et al., 2016; O'Connor et al., 2020). Recent studies report an increase in the frequency of large rainfall events (> 25.4 mm) for the period of 1979-2009 over the Central U.S. (Groisman et al., 2012) and forecast an increase in frequency and intensity of extreme precipitation events due to climate change (Kirchmeier-Young and Zhang, 2020). Since rainfall variability has been identified as the main environmental driver of water and carbon fluxes in grasslands (Chen et al., 2019; Zhang et al., 2019), predicted changes in the rainfall regime will likely lead to significant changes in grassland structure and function, especially during dry years (Felton et al., 2020).

Evapotranspiration (*ET*) is a key variable linking the carbon, water and energy cycles in ecosystems (Fisher et al., 2017), as well as a leading indicator of ecosystem responses to rainfall variability and flash droughts (Rajan et al., 2015; Yue et al., 2019; Anderson et al., 2013). However, the magnitude of *ET* primary components, abiotic evaporation (*E*) and leaf transpiration (*T*), has distinct responses to biophysical variables (Berg and Sheffield, 2019). For instance, *E* is inversely proportional to canopy cover, which reduces surface wind speed and attenuates the incoming solar radiation reaching the soil surface (Song et al., 2018). Conversely, the contribution of *T* to *ET* (*T/ET*) tends to increase with canopy cover and is also governed by plant phenology (Wang et al., 2014; Rigden et al., 2018; Scott et al., 2021). Furthermore, the responses of the *ET* components to rainfall are dependent on the frequency and magnitude of rain events. For example, small and frequent rain events that increase soil surface moisture favors *E* losses, while large rainfall events usually increase *T/ET* (Sun et al., 2020; Zou et al., 2015; Cavanaugh et al., 2011).

In the long term, climate change is expected to affect the contributions of *E* and *T* to the total *ET* differently (Niu et al., 2019). Model simulations performed by Zhang

et al. (2016) indicate that the global *ET* trended upwards in the period from 1981 to 2012. The researchers also reported a positive trend in *T* and a negative trend in *E,* which they attribute to an increase of vegetation leaf area index (*LAI*) credited to the effect of CO_2 fertilization in their simulations. In addition, CMIP5 model simulations for the 2071 to 2100 period predict an increase in *T/ET* in middle and high latitudes due to the increase in air temperature, and reduction in *T/ET* in humid tropical regions due to plant responses to higher CO_2 atmospheric levels (Berg and Sheffield, 2019). Despite the importance, long-term global scale *ET* predictions still contain major uncertainties (Lian et al., 2018). Field-scale *ET* partitioning studies are needed to improve global scale *ET* modeling and to provide insights into the effect of climate change on global water and carbon cycles.

Ecosystem-level *ET* partitioning remains challenging given the limitations inherent to the various methods (Kool et al., 2014). For example, the sap flow method has been commonly used to measure *T* at the plant level (Nelson et al., 2020), but this method is impractical in ecosystems with large plant diversity and herbaceous plants (Williams et al., 2004). Microlysimeters (*ML*) have been used as a standard approach to validate *E* estimates from other methods or models (Moran et al., 2009; Florentin and Agam, 2017). This method has the advantage of directly measuring changes in soil mass due to evaporation, but *ML* measurements represent a small area (< 1 m^2) and are labor-intensive, limiting their use in ecosystem studies. Partitioning *ET* using micrometeorological measurements has the advantage of allowing continuous flux monitoring at scales relevant for ecosystem studies.

Micrometeorological approaches based on the coupling between carbon and water fluxes have been used as an alternative for partitioning *ET* (Sun et al., 2019; Stoy et al., 2019). These methods are often based on the water use efficiency (*WUE = GPP/ET*), often determined as the ratio of gross primary productivity (*GPP*) to *ET*. Scott and Biederman (2017) proposed a statistical approach to partition monthly *ET* using multi-year CO_2 and water fluxes derived from eddy covariance (*EC*) measurements. Likewise, Skaggs et al. (2018) developed the Fluxpart model to partition *ET* and carbon fluxes simultaneously using high-frequency *EC* data. However, the Fluxpart model requires *a priori* knowledge of *WUE* at the leaf scale, which is challenging to obtain in ecosystems with mixed C_3 and C_4 vegetation such as grasslands.

Zhou et al. (2016) developed an *ET* partitioning approach using *EC* data based on the concept of underlying *WUE* (*uWUE*). The *uWUE* concept emerged as a modification of the inherent *WUE* approach, which considers the non-linear effect of vapor pressure deficit (*VPD*) on *ET* for the daily *WUE* calculation (Beer et al., 2009). Although the correlation between *GPP* and *ET* is improved by introducing *VPD* in daily *WUE* calculations, Zhou et al. (2014) still observed a time lag between *ET* and *GPP,* especially at sub-daily time scales. To correct this time lag, Zhou et al. (2014) developed the *uWUE* model ($uWUE = GPP \cdot VPD^{0.5}/ET$), in which *VPD* is corrected by an exponent. From the concept of *uWUE*, Zhou et al. (2016) distinguished an apparent *uWUE* ($uWUE_a$) and a potential *uWUE* ($uWUE_p$), which differ by the presence and absence of *E*, respectively. Hence, *T/ET* can be estimated by the $uWUE_a/uWUE_p$ ratio. This relatively simple approach has the advantage of allowing the *ET* partitioning at different temporal scales (half-hourly to annual) and has shown satisfactory results when compared to microlysimeters, stable isotopes and sap flow (Zhou et al., 2018; Bai et al., 2019; Nelson et al., 2020; Xu et al., 2021).

In this study, we use a unique flux dataset in three consecutive growing seasons with distinct precipitation totals and distributions to investigate the response of *T/ET* to environmental drivers in a tallgrass prairie. We hypothesize that grassland *T/ET* responses to environmental drivers will vary during wet and dry years. To test this hypothesis, *EC* fluxes and the *uWUE* approach were used for partitioning *ET* into *E* and *T*. The performance of the *uWUE* approach was evaluated by comparing its *E* estimates with the ones provided by *ML*.

3.2 Material and methods

3.2.1 Site description

The field measurements were conducted at the National Ecological Observatory Network (NEON) KONZ site (Loescher et al., 2014) located at the Konza Prairie Biological Station (KPBS) during the growing seasons (May to October) of years 2017, 2018 and 2019. The KPBS is a 3,487-ha native tallgrass prairie located in the Flint Hills region in Kansas, U.S. (39°05’55’’N, 96°34’02’’W, elevation 415 m a.s.l.). The region is characterized by a mid-continental climate (O’Connor et al., 2020), with mean annual air temperature of 13°C and monthly average air temperature ranging from -3°C in

January to 27°C in July. The mean annual rainfall is 845 mm, with about 73% of total annual precipitation occurring between April and September during the growing season (Towne and Craine, 2014). The predominant vegetation across the KPBS consists of warm-season C_4 grasses such as *Andropogon gerardii*, *Sorghastrum nutans* and *Schizachyrium scoparium*. However, forbs represent more than 75% of the species richness (Towne, 2002). The soil at the KONZ site is classified as fine, smectitic, mesic Pachic Udertic Argiustolls, consisting of 39.0% clay and 4.4% sand and a bulk density of 1.0 g cm^{-3} at the 0 to 66 cm depth (NEON, 2020).

The KPBS is divided into 55 plots or watersheds that include different fire and grazing regimes (Briggs et al., 2016) (Fig. 3.1). Table 3.1 shows the management practices in the watersheds surrounding the measurement tower on K2A (66.1 ha).

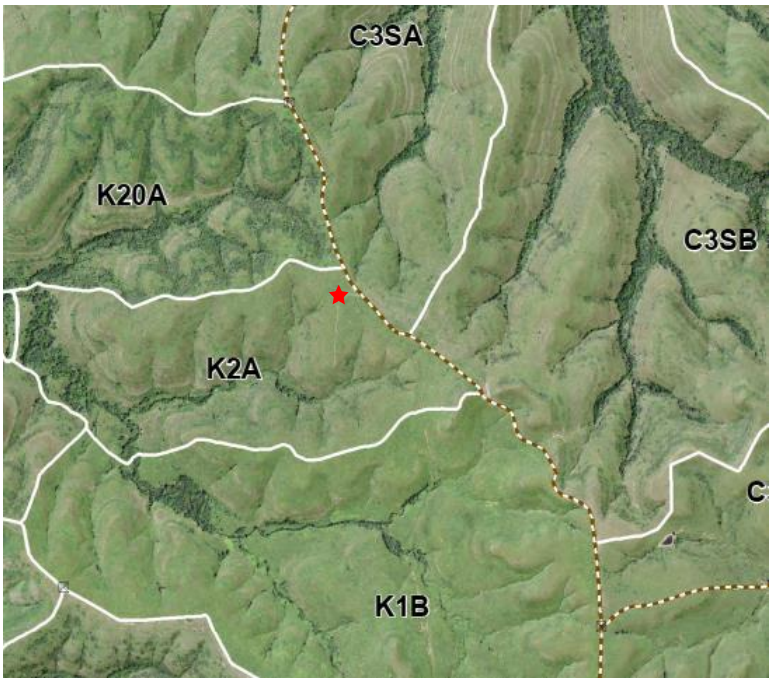

Figure 3.1 - Aerial image showing the watersheds C3SA, C3SB, K1B, K2A and K20A, surrounding the measurement tower at the KONZ site. The red asterisk represents the measurement tower.

Table 3.1 - Watersheds and management practices on the Konza Prairie Biological Station (Blair and O'neal, 2021).

Watershed	Grazing regime	Fire Frequency (years)	Prescribed burning (Date)		
			2017	2018	2019
K1B	Ungrazed	1	04/11	03/21	03/22
K2A	Ungrazed	2	-	03/21	-
K20A	Ungrazed	20	03/16	-	-
C3SA	Grazed	3		-	03/18
C3SB	Grazed	3	03/10	-	-

3.2.2 Flux measurements

Fluxes of CO_2 and energy were measured using the *EC* technique. The *EC* system was mounted on a tower at 7.9 m above the ground. Wind velocity orthogonal components and sonic temperature fluctuations were measured using a 3D sonic anemometer (CSAT3, Campbell Scientific, Inc., Logan, UT, USA). An enclosed-path CO_2/H_2O infrared gas analyzer (LI-7200, LI-COR, USA) was used to measure carbon dioxide and water vapor mixing ratios. All *EC* system variables were acquired at a rate of 20 Hz. Half-hourly net ecosystem CO_2 exchange (*NEE*), latent (*LE*) and sensible heat fluxes (*H*) were calculated using the EddyPro software (Version 6.2.1, LI-COR). The data processing steps included high-frequency data spike removal (Vickers and Mahrt, 1997), double coordination rotation (Kaimal and Finnigan, 1994), block average detrending, time lag compensation using covariance maximization (Fan et al., 1990) and spectral corrections for high (Moncrieff et al., 1997) and low (Moncrieff et al., 2004) frequency losses.

The flux data were screened using quality flags based on the steady state test proposed by Mauder and Foken (2004) with flag values of 0, 1, and 2 corresponding to high, moderate, and low-quality data, respectively. In this study, flux data associated with flag values equal to 2 were discarded. In addition, friction velocity (u^*) thresholds were calculated for each growing season to identity and remove carbon flux measured under low turbulence conditions (Papale et al., 2006). The values of u^* thresholds were 0.21 ms^{-1} for 2017 and 0.24 m s^{-1} for 2018 and 2019. The quality of the *EC* data was

also assessed by the energy budget closure (*EBC*), determined using a linear regression analysis between available energy and turbulent energy fluxes (*LE + H*). The slopes of the *EBC* linear regression ranged between 0.64 (2018) and 0.73 (2017) (Fig. 3.2).

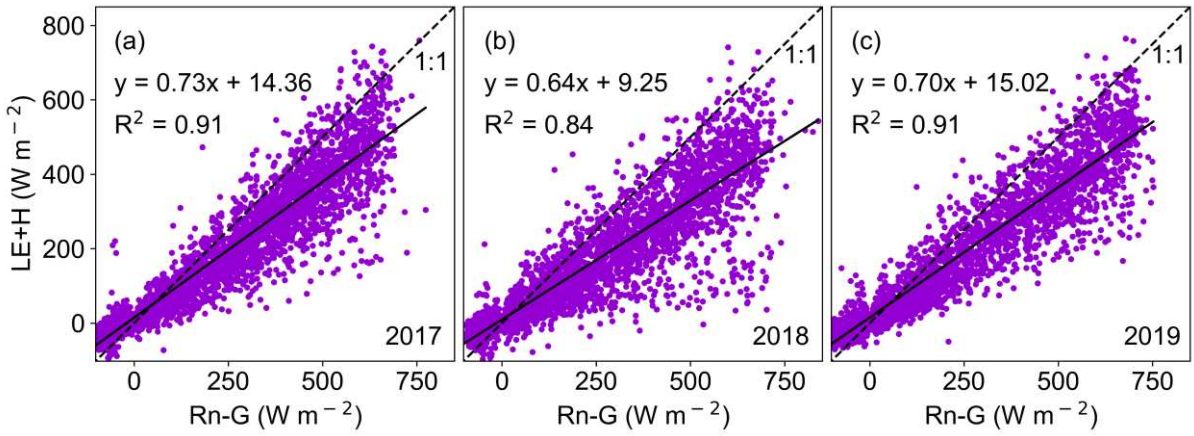

Figure 3.2 - Relationship between the available energy (*Rn-G*) and turbulent fluxes (*LE+H*) for the 2017, 2018 and 2019 growing seasons.

The flux gap filling and *NEE* partitioning into gross primary productivity (*GPP*) and ecosystem respiration (R_{eco}) were performed using the ReddyProc tool, developed by the Max Planck Institute for Biogeochemistry (Wutzler et al., 2018). Nighttime *NEE* and air temperature measurements were used to parameterize an exponential regression model and extrapolate the R_{eco} values to daytime air temperature (Reichstein et al., 2005), so that *GPP* was calculated by subtracting R_{eco} from *NEE*.

3.2.3 Flux footprint calculations

At the KONZ site, surrounding watersheds under different fire and grazing management practices likely contribute to the observed fluxes. Fire frequency and grazing can lead to differences in C_3 and C_4 plant composition in the tallgrass prairie (Collins and Calabrese, 2012), and consequently on ecosystem *uWUE*. To investigate the influence of each watershed surrounding the tower on the measured fluxes, a two-dimensional flux footprint parameterization (Kljun et al., 2015) was used to compute the contribution of different watersheds to the measured *EC* fluxes. Then, the relative

contribution of each watershed to the 30-min *EC* fluxes was estimated by overlaying half-hourly flux footprints with polygons representing each watershed (Neftel et al., 2008; Prajapati and Santos, 2018).

3.2.4 Complementary measurements

Complementary measurements included: incoming solar radiation (*Rg*) and net radiation (*Rn*), which were measured by a four-component net radiometer (NR01, Hukseflux, Netherlands) at 8.4 m above the ground; air temperature (T_{air}) and relative humidity (*RH*), measured by a thermo-hygrometer (HMP155, Vaisala, Finland) at 7.9 m above the ground; soil heat flux (*G*), obtained by three heat flux plates (HFP01SC, Hukseflux) at a depth of 0.08 m; volumetric soil water content (θ), determined by five capacitance probes (EnviroSCAN TriSCAN, Sentek Technologies, Australia) with sensors at depths of 0.15 (θ_{15}) and 0.45 m (θ_{45}). Soil instruments were distributed on the K2A watershed considering the dominant soil type and spatial variation of soil temperature and moisture (Loescher et al., 2014). Half-hourly meteorological variables were obtained from the NEON portal (NEON, 2020). Detailed information on the instrumentation at NEON sites is given by Metzger et al. (2019). Daily precipitation (*P*) data were obtained from the Ashland Bottoms station of the Kansas Mesonet (Patrignani et al., 2020).

3.2.5 Evapotranspiration partitioning

ET was partitioned using the approach developed by Zhou et al. (2016) which is based on the *uWUE* concept. Based on this approach, the potential *uWUE* ($uWUE_p$) and the apparent *uWUE* ($uWUE_a$) were calculated as follows (Zhou et al. (2016):

$$uWUE_p = \frac{GPP\ VPD^{0.5}}{T} \quad (1)$$

$$uWUE_a = \frac{GPP\ VPD^{0.5}}{ET} \quad (2)$$

where *VPD* is the vapor pressure deficit, *ET* is the evapotranspiration and *T* is the transpiration. In an ecosystem with uniform vegetation, $uWUE_p$ is identical to the *uWUE*

at the leaf scale and assumed to be almost constant under steady state conditions (Zhou et al., 2016). On the other hand, $uWUE_a$ represents the *uWUE* affected by *E*. Thus, when *E* is negligible, *T* approximates *ET* (*T/ET* ≅ 1), and $uWUE_a$ is equal to $uWUE_p$. Under field conditions, values of *T/ET* are close to unity when the ecosystem vegetation has a high *LAI* and the soil water content in the upper soil layer is low (Zhou et al., 2016; Zhou et al., 2018). Based on the $uWUE_p$ and $uWUE_a$ concepts, *T/ET* and *T* at the ecosystem level were determined as follows (Zhou et al., 2016):

$$\frac{T}{ET} = \frac{uWUE_a}{uWUE_p} \tag{3}$$

$$T = \left(\frac{uWUE_a}{uWUE_p}\right) ET \tag{4}$$

Following Zhou et al. (2016), the long-term average $uWUE_p$ was estimated by the 95th quantile regression between half-hourly *ET* and $GPP \cdot VPD^{0.5}$ data collected during this study. In addition, individual $uWUE_p$ values were estimated for each growing season to test the assumption that $uWUE_p$ is relatively constant over the years.

Values of $uWUE_a$ at different timescales (daily, monthly and seasonal) were determined by the linear regression analysis slope between *ET* and $GPP \cdot VPD^{0.5}$. To ensure that *GPP* is equal to zero when the stomata are closed, all regression analysis were performed forcing the regression line through origin.

In this study, values of $uWUE_a$ and $uWUE_p$ were determined under daytime conditions (incoming solar radiation >20 W m^{-2}). To identify the main environmental elements that drive *T/ET*, a partial correlation analysis was used to remove the interactions between variables. The significance of the partial correlation coefficients was verified by a Student's t-test at a significance level of 5% (Li et al., 2016).

3.2.6 Soil evaporation measurements

To evaluate the *uWUE* method, daily *E* was measured using *ML* during the 2018 growing season. The *ML* were built from polyvinyl chloride (PVC) pipe with an internal diameter of 10.2 cm and cut at 20 cm in length. The bottom edge of the *ML* was beveled to facilitate insertion into the soil profile. A total of 21 *ML* were inserted in advance between grassland plants to the south of the tower (prevailing wind direction) with the

aid of a rubber mallet. To minimize the impact of minor soil disturbances generated during the installation process of the *ML* in our *E* measurements, the *ML* were left inserted in the soil for about two weeks that included couple rainfall events. Rainfall events help restoring the soil surface conditions that may have been disturbed as a consequence of vibrations during the installation process. Rainfall also helps sealing small gaps between the wall of the *ML* and the surrounding soil. Three measurement campaigns were carried out on days without rainfall during August, September, and October of 2018. At the beginning of each sampling campaign, a total of seven *ML* were carefully excavated using a shovel to minimize disturbances to the soil column inside the *ML*. The *ML* bottoms were sealed with a plastic film to eliminate drainage losses and to retain the soil column inside the *ML* for daily weighting. Seven *ML* were monitored during each campaign for a period no longer than five days per campaign to maintain soil moisture conditions within the *ML* similar to its surroundings (Evett et al., 1995). The August 2018 campaign was shortened due the occurrence of rainfall during the seven-day sampling period. The *ML* were weighed daily using a digital scale with resolution of ±1 g (V11P6, Ohau, USA), which translates to an *E* resolution of 0.13 mm d^{-1}. Soil evaporation (*E,* mm d^{-1}) was calculated as follows (Wang and Wang, 2017):

$$E = 10\frac{\Delta W/\rho}{\pi\left(\frac{D}{2}\right)^2} \tag{5}$$

where ΔW (g) is the change in mass of the *ML* between two measurements, ρ is the density of water (1.0 g cm^{-3}), and *D* is the diameter of the *ML* (cm). The relationship between *E* measured by *ML* and derived from the *uWUE* approach was evaluated using the root mean square error (*RMSE*) and Pearson's correlation coefficient (*r*).

3.2.7 Vegetation dynamics

The vegetation dynamics was monitored using the green chromatic coordinate (*GCC*) obtained from the Phenocam Dataset 2.0 (Seyednasrollah et al., 2019). The vegetation images were acquired every 15 min using a digital camera (CAM-SEC5IR, StarDot, USA) and converted to a three-layer *RGB* array, corresponding to red (*R*),

green (*G*) and blue (*B*) channels. During the image processing, a digital number (*DN*) associated to each color channel was extracted from a region of interest (*ROI*), that excludes portions of road and sky (Richardson, 2019). The *GCC* values for each image was determined from the following equation (Richardson et al., 2007):

$$GCC = \frac{G_{DN}}{R_{DN} + G_{DN} + B_{DN}} \quad (6)$$

where R_{DN}, G_{DN} and B_{DN} are the average red, green and blue *DN* extracted from *ROI*. To minimize noise due to the effects of clouds, aerosols and fog in scene illumination, only 90th percentile values of *GCC* were used to calculate a 3-day moving average in this study, with the daily *GCC* value attributed to the center of the 3-day moving window (Sonnentag et al., 2012).

3.3 Results

3.3.1 Weather conditions

Over the growing seasons evaluated, the highest average T_{air} was observed in 2018 (22.1°C), followed by 2017 (21.7 °C) and 2019 (20.8 °C) (Fig. 3.3a-c). The mean *VPD* values were higher in 2017 (10.7 hPa) and 2018 (10.2 hPa) compared to the average *VPD* (8.4 hPa) for 2019 (Fig. 3.3a-c).

The long-term (1994-2013) average accumulated precipitation at KPBS during the growing season (May to October) is 612 mm (Nippert, 2020). In 2017, the total rainfall (470.4 mm) was 23.1% below the long-term average precipitation and four dry periods with length ranging from 11 to 21 days were recorded (Fig. 3.3d). The dry conditions during the 2017 growing season maintained θ_{15} and θ_{45} close to 0.10 and 0.20 $m^3\ m^{-3}$ (Fig. 3.3d), respectively, despite the occurrence of two rainfall events above 50 mm d^{-1} at end of June (Day of year 180) and early August (Day of year 217). During 2018, the accumulated growing season precipitation (656.3 mm) was 7.2% above the long-term average rainfall and the 2018 longest dry period (11 days) occurred at the end of growing season (Fig. 3.3e). The 2018 growing season was marked by smaller rainfall events from May to mid-August, resulting in θ_{15} and θ_{45} close to 0.10 $m^3\ m^{-3}$ during this period (Fig. 3.3e). From mid-August 2018 (Day of year 231),

large rainfall events higher than 70 mm raised θ_{15} and θ_{45} to about 0.40 m^3 m^{-3}. In contrast, the accumulated growing season precipitation in 2019 (858.3 mm) was 40.2% above the long-term average and the frequent large rainfall events (>25.4 mm) resulted in θ_{15} and θ_{45} above or close to 0.40 m^3 m^{-3} throughout the entire growing season (Fig. 3.3f).

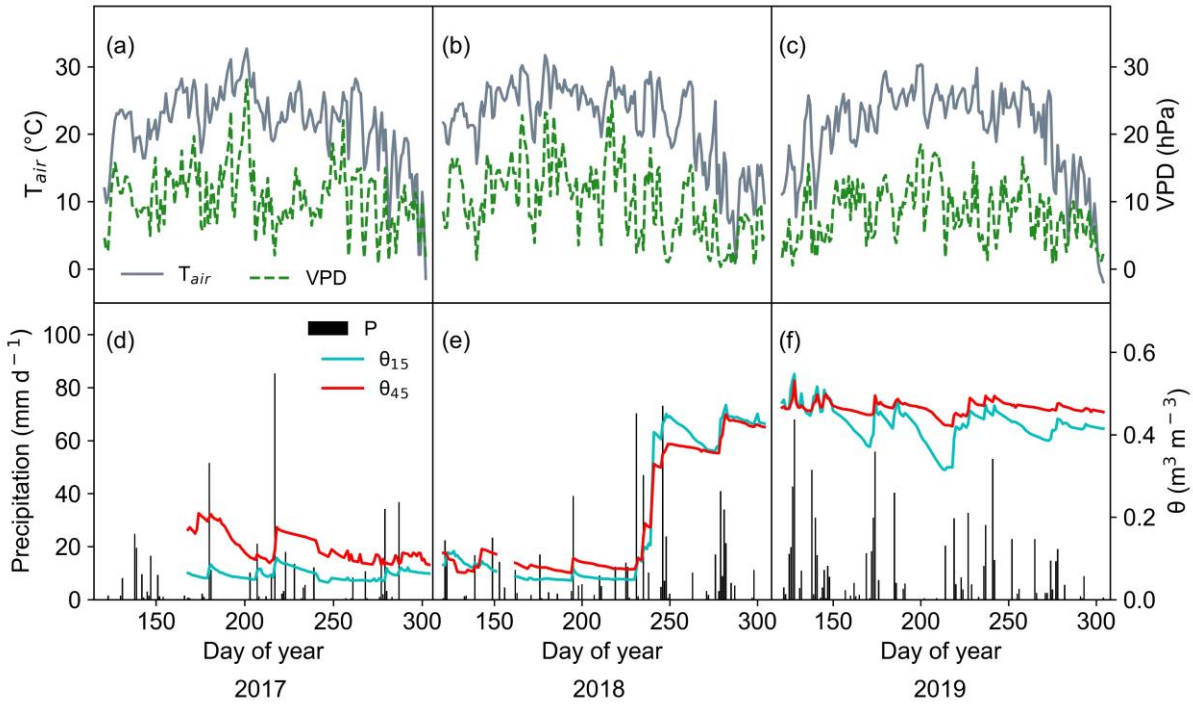

Figure 3.3 - Daily averages of a, b and c) air temperature (T_{air}) and vapor pressure deficit (*VPD*); d, e and f) precipitation (*P*) and volumetric soil water content at 0.15 (θ_{15}) and 0.45 m (θ_{45}) depths during the 2017, 2018 and 2019 growing seasons.

3.3.2 Flux footprint and potential ($uWUE_p$) and apparent ($uWUE_a$) underlying water use efficiencies

The footprint climatology or aggregated flux footprint, estimated for the three growing seasons, was overlaid on the watershed map (Fig. 3.4). Most of the measured 30-min fluxes (82.7%) originated from the K2A watershed, followed by the C3SA (12.5%), K20A (2.8%) and C3SB (1.1%) and K1B (0.5%), with a total contribution of 99.6% to the *EC* fluxes (Table 3.2).

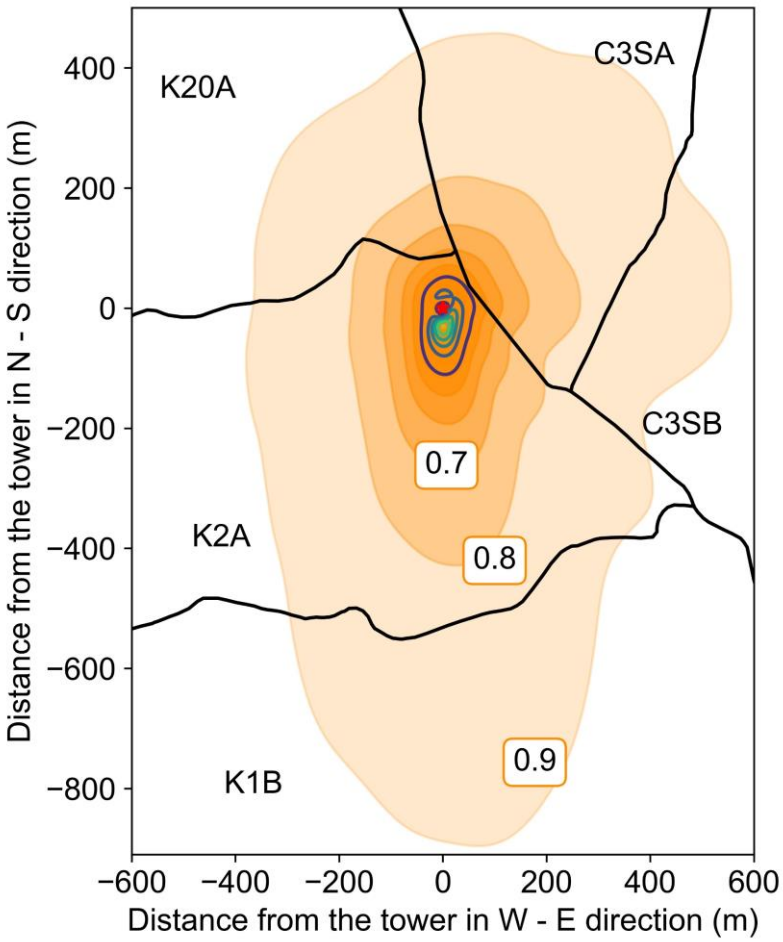

Figure 3.4 - Footprint climatology estimated for the three growing seasons (2017-2019) and overlaid on the watershed map (C3SA, C3SB, K1B, K2A and K20A). The contour lines are the cumulative footprint every 10%. The red asterisk represents the measurement tower.

Table 3.2 - Relative contribution from watersheds to the measured *EC* fluxes during the 2017, 2018 and 2019 growing seasons.

Watershed	Contribution to the measured fluxes (%)[1]			
	2017	2018	2019	2017-2019 Average
K1B	0.6	0.4	0.6	0.5
K2A	83.4	82.7	82.1	82.7
K20A	3.0	2.4	3.0	2.8
C3SA	11.4	13.4	12.7	12.5
C3SB	1.1	0.9	1.3	1.1
Others plots	0.5	0.2	0.3	0.4

[1]Calculations were based on the source area contributing to 80% of the measured flux.

The overall $uWUE_p$ throughout all growing seasons was 14.31 g C $hPa^{0.5}$ kg H_2O^{-1}. Considering individual growing seasons, the largest $uWUE_p$ was observed in 2018 (16.30 g C $hPa^{0.5}$ kg H_2O^{-1}) followed by 2019 (13.81 g C $hPa^{0.5}$ kg H_2O^{-1}), and the lowest $uWUE_p$ was recorded in 2017 (11.36 g C $hPa^{0.5}$ kg H_2O^{-1}). The mean $uWUE_a$ showed a similar pattern as $uWUE_p$ with yearly values of 7.10 (2017), 9.33 (2018) and 8.86 g C $hPa^{0.5}$ kg H_2O^{-1} (2019). To investigate the effect of the surround watersheds to the estimated *uWUE*, the mean $uWUE_p$ and yearly $uWUE_a$ were estimated using only 30-min data in which 100% of the measured fluxes originated from the K2A watershed. The mean $uWUE_p$ was 14.57 g C $hPa^{0.5}$ kg $H2O^{-1}$ and $uWUE_a$ values were 7.56, 9.55 and 9.37 g C $hPa^{0.5}$ kg $H2O^{-1}$ for 2017, 2018 and 2019, respectively. The *uWUE* estimates using only K2A data were similar to the ones obtained using the full *EC* flux dataset, indicating that differences in source area had minor impact on $uWUE_p$ and $uWUE_a$. Therefore, in this study the *ET* partitioning was performed using the entire flux dataset.

The seasonal dynamics of $uWUE_a$ was distinct among the growing seasons evaluated (Fig. 3.5). In 2018, $uWUE_a$ decreased from the beginning of the growing season until the month of August. On the other hand, in 2017 and 2019 an opposite trend was observed with an increase of monthly $uWUE_a$ values from May to July. The $uWUE_a$ for the month of August was similar for all years. The end of growing season

(September and October) $uWUE_a$ values were higher for 2018 in comparison to 2017 and 2019 values.

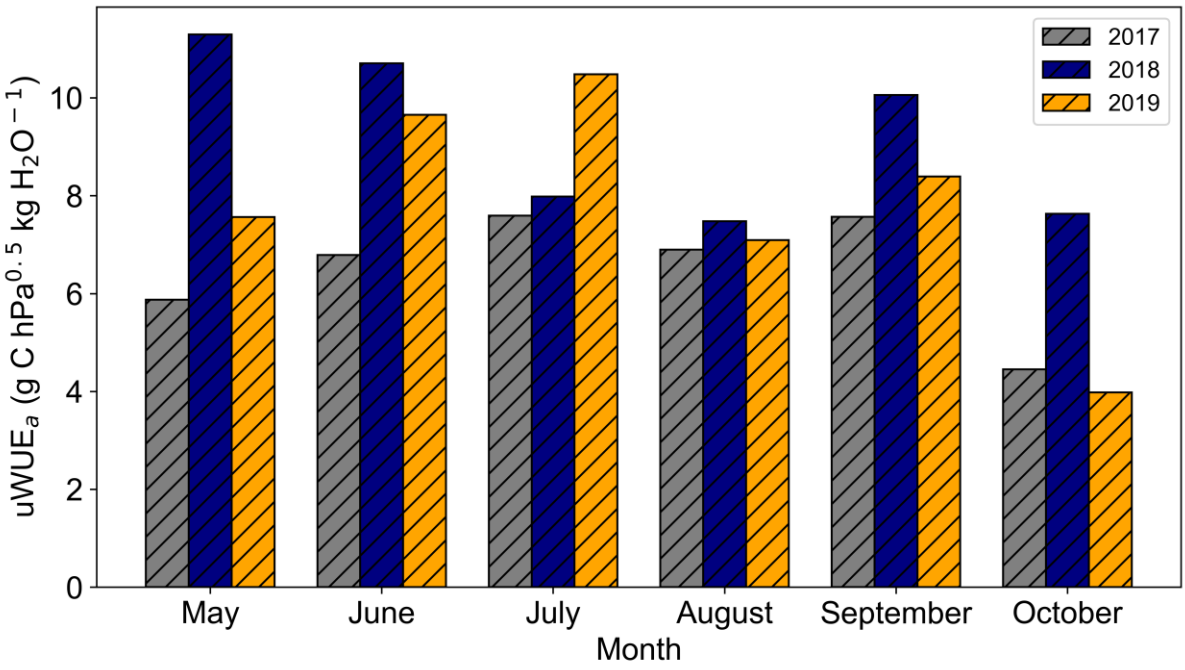

Figure 3.5 - Monthly apparent underlying water use efficiency ($uWUE_a$) for the 2017, 2018 and 2019 growing seasons.

3.3.3 Comparison between *uWUE* and microlysimeter soil evaporation estimates

The comparison of daily *E* values derived from the *uWUE* method and measured by *ML* is shown in Fig. 3.6. The overall average *E* (± standard deviation) estimated by *uWUE* was 0.73 ± 0.18 mm d^{-1}, while measured *E* using *ML* resulted in 1.21 ± 0.36 mm d^{-1}. The relationship between *uWUE* and *ML* estimates showed a Pearson correlation coefficient of 0.42 and *RMSE* of 0.58 mm d^{-1}. In general, the *uWUE* method underestimated *E* rate compared to *ML* estimates.

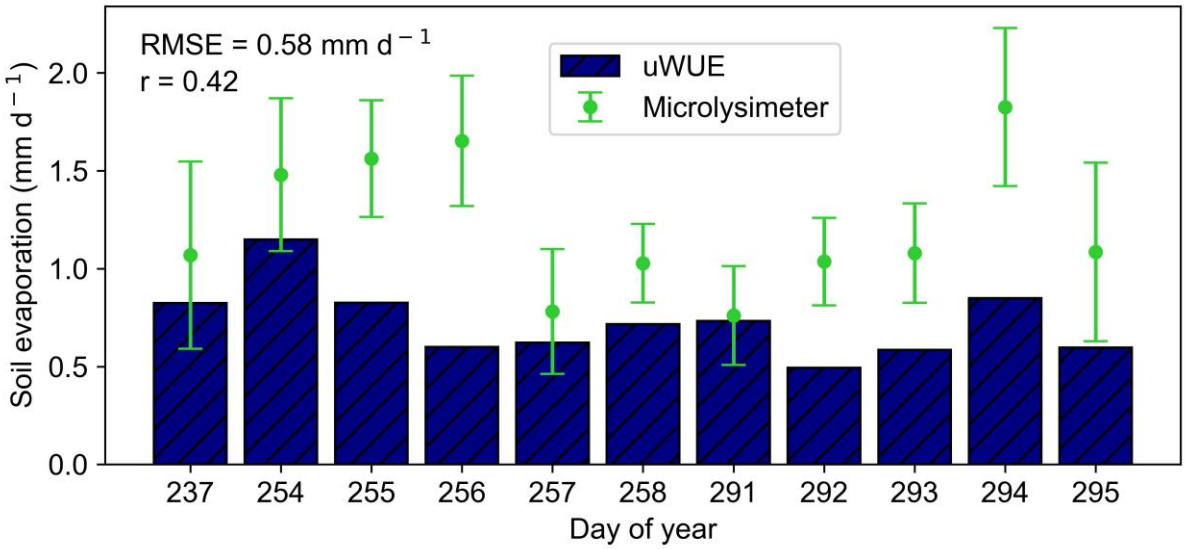

Figure 3.6 - Daily values of soil evaporation derived from the underlying water use efficiency method (*uWUE*) and measured by microlysimeters during the 2018 growing season. Error bars represent the standard deviation of microlysimeters.

3.3.4 Seasonal variations of carbon and water fluxes and *T/ET*

The seasonal variation of carbon and water vapor fluxes was driven by the vegetation phenology and soil moisture conditions. At the beginning of the 2017 growing season, *T* and *GPP* varied widely and reached values close to zero (Fig. 3.7a and 3.7d). Due to the low rainfall amounts during the 2017 early growing season, the grassland alternated from being a carbon source (*NEE* > 0) and a carbon sink (*NEE* < 0). At the end of June 2017, days after two large consecutives rainfall events totaling 62.7 mm, *T*, *GPP* and R_{eco} peaked at 3.28 mm d^{-1}, -10.61 g C m^{-2} d^{-1} and 7.38 g C m^{-2} d^{-1}, respectively.

In 2018, *T*, *GPP* and R_{eco} were very low during the early growing season, but increased rapidly by the end of May (Fig. 3.7b and 3.7e), reaching the maximum values of 4.40 mm d^{-1}, -13.80 g C m^{-2} d^{-1} and 9.02 g C m^{-2} d^{-1}, respectively. The ecosystem was a carbon sink until the end of June. After that, *T*, *GPP* and R_{eco} decreased, and the ecosystem alternated from being a carbon sink and a carbon source due to the dry conditions. In mid-August, the ecosystem became a carbon sink after large rainfall events.

In contrast to 2017 and 2018 growing seasons, water and carbon fluxes were closely coupled with the vegetation phenology in 2019. *T*, *GPP* and R_{eco} increased from May to mid-July, showing maximum values of 4.74 mm d^{-1}, -17.01 and 13.18 g C m^{-2} d^{-1}, respectively (Fig. 3.7c and 3.7f), and decreased from mid-July until the end of the growing season. During 2019, the grassland was mostly a carbon sink from early May until the first half of September.

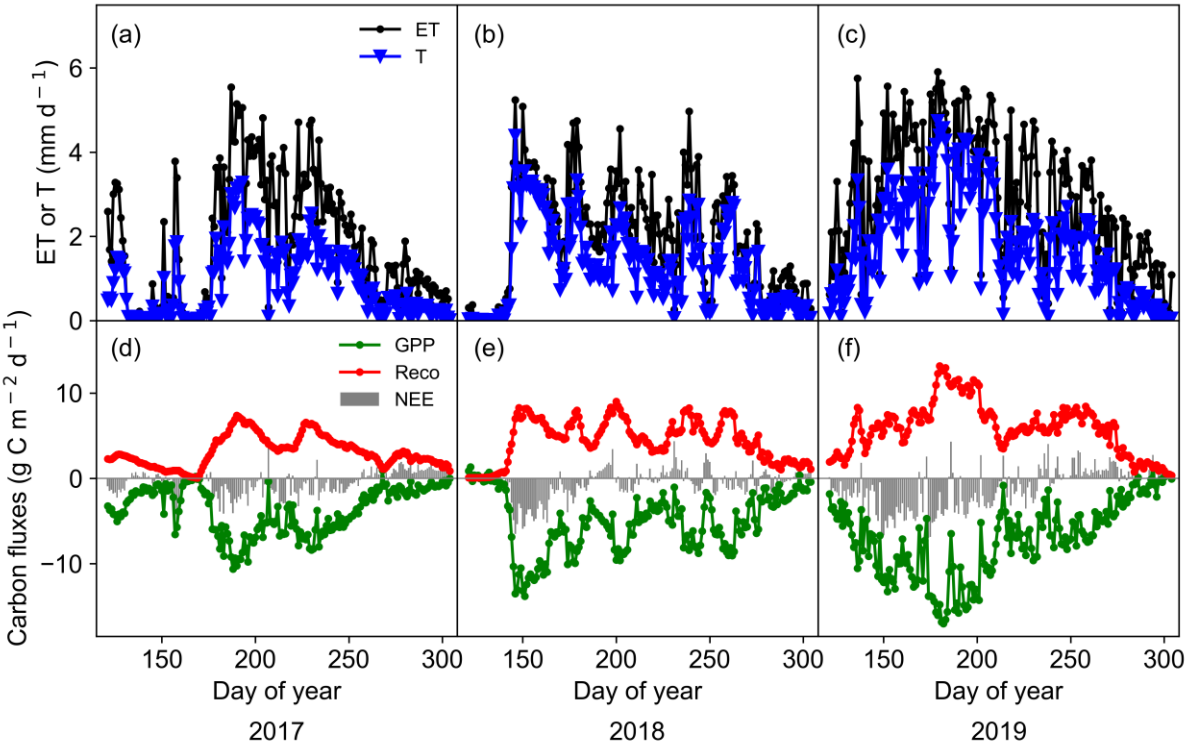

Figure 3.7 - a-c) Daily evapotranspiration (*ET*) and transpiration (*T*); and d-f) gross primary productivity (*GPP*), ecosystem respiration (R_{eco}) and net ecosystem exchange (*NEE*) over the 2017, 2018 and 2019 growing seasons.

The cumulative water vapor and carbon fluxes increased as a function of total rainfall during growing seasons (Table 3.3). The grassland acted as a carbon sink during the three years evaluated, despite the 2017 growing season drought. The lowest and highest cumulative *GPP*, R_{eco}, *NEE*, *ET* and *T* occurred during 2017 and 2019, respectively, while the lowest *E* was recorded during 2018.

Table 3.3 - Cumulative rainfall (*P*), gross primary productivity (*GPP*), ecosystem respiration (R_{eco}), net ecosystem exchange (*NEE*), evapotranspiration (*ET*), transpiration (*T*) and evaporation (*E*) over the 2017, 2018 and 2019 growing seasons (May – October).

Variables	Year of Growing Season		
	2017	**2018**	**2019**
P (mm)	470.4	656.3	858.3
GPP (g C m^{-2})	-669.42	-931.07	-1309.04
R_{eco} (g C m^{-2})	577.68	827.14	1096.12
NEE (g C m^{-2})	-91.74	-103.92	-212.92
ET (mm)	333.82	361.26	532.92
T (mm)	168.68	237.72	326.34
E (mm)	165.14	123.54	206.57
T/ET	0.50	0.65	0.62

The seasonal variation of *T/ET* followed the *GCC* dynamics, increasing from early to mid-growing seasons and decreasing at the end of growing seasons, despite oscillations due to rainfall variability (Fig. 3.8a-c). In the 2017 growing season, the *GCC* showed the lower values (Fig. 3.8a), ranging from 0.33 to 0.39, which resulted in the lowest *T/ET* average (0.50) among the years evaluated (Fig. 3.8a and Table 3.3). The highest *T/ET* average (0.65) among the years evaluated occurred in 2018 (Fig. 3.8b), which exhibited *GCC* values (Fig. 3.8b) between 0.33 and 0.44. The *GCC* values during 2019 (Fig. 3.8c) were similar to the ones observed in 2018, ranging from 0.32 to 0.44, however, the 2019 *T/ET* average (0.62) was slightly lower than that observed in 2018. The *T/ET* peaks were recorded in May 2017 (0.95), July 2018 (0.97) and July 2019 (0.95), while the *GCC* peaks were observed in May for the three growing seasons (Figure 3.8a-c).

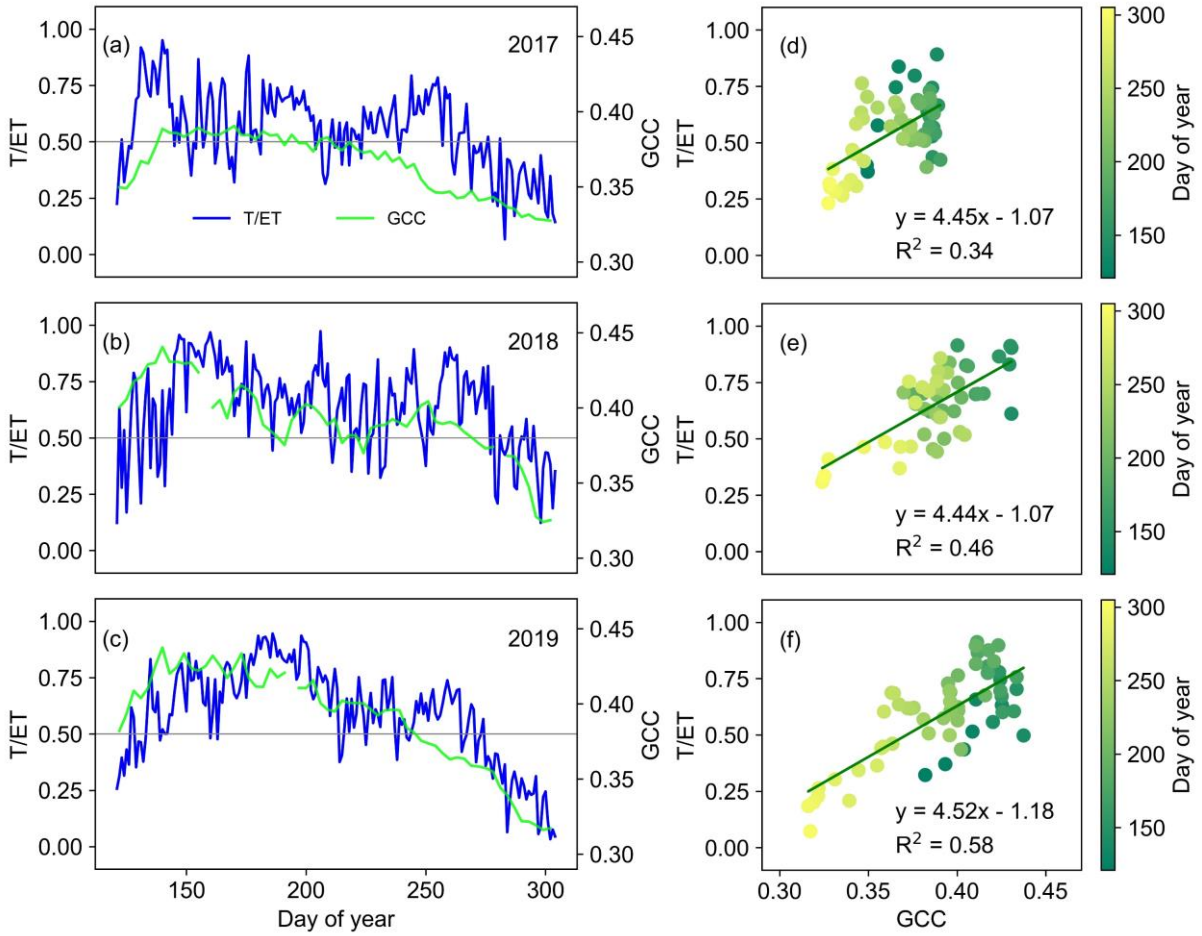

Figure 3.8 - a-c) Time series of daily transpiration/evapotranspiration fraction (*T/ET*) and green chromatic coordinate (*GCC*); and d-f) linear relationship between 3-day *GCC* and *T/ET* during the 2017, 2018 and 2019 growing seasons.

The linear regressions analysis between 3-day moving averages of *GCC* and *T/ET* indicated that *GCC* explained between 34.0% (2017) and 58.0% (2019) of the *T/ET* variability (Fig. 3.8d-f). The partial correlation coefficients between *T/ET* and several environmental variables are shown in Fig. 3.9. In general, *T/ET* showed higher positive correlations with T_{air}. Correlation coefficients between *T/ET* and T_{air} were all statistically significant ($P < 0.01$) and equal to 0.35 (2017), 0.49 (2018) and 0.72 (2019). *T/ET* was negatively correlated with θ_{15} during the 2017 (-0.32) and 2018 (-0.20) growing seasons, and positively correlated with θ_{45}, with statistically significant ($P<0.01$) correlation coefficients of 0.41 (2017) and 0.25 (2018). On the other hand, there were no significant correlations between *T/ET* and θ_{15} and θ_{45} during the 2019

growing season. *Rn* and *VPD* did not show significant correlation with *T/ET* during the growing seasons evaluated.

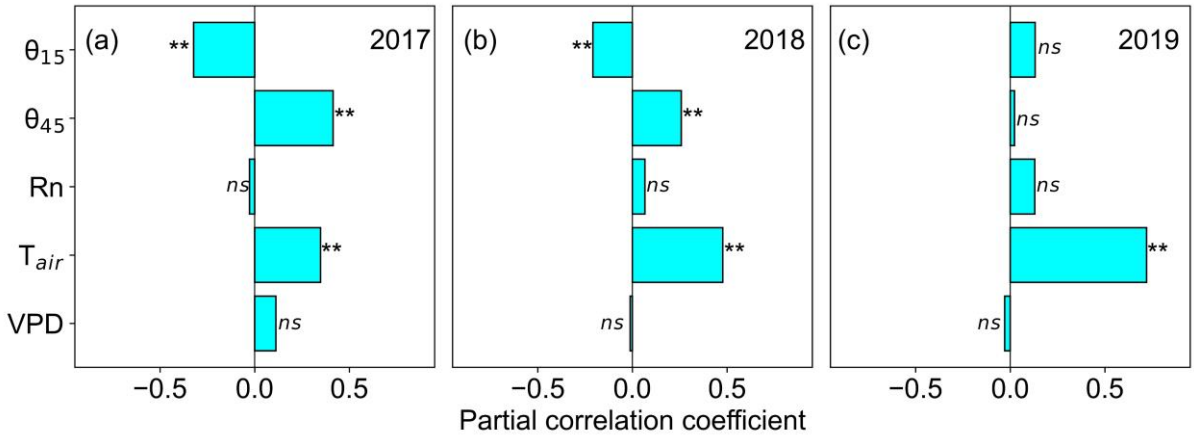

Figure 3.9 - Partial correlation coefficients between transpiration/evapotranspiration fraction (T/ET) and volumetric soil water content at 0.15 (θ_{15}) and 0.45 m (θ_{45}) depths, net radiation (*Rn*), air temperature (T_{air}) and vapor pressure deficit (*VPD*) during the 2017, 2018 and 2019 growing seasons. **Significant; and ^{ns} not significant by the Student's t-test ($P < 0.01$).

3.4 Discussion

3.4.1 Annual $uWUE_p$ and $uWUE_a$ variation

The long-term average $uWUE_p$ value and inter-annual $uWUE_p$ variations found in our study were within the range of values reported for other grassland ecosystems (Han et al., 2018; Hu et al., 2018; Zhou et al., 2016). Han et al. (2018) observed a 10-year $uWUE_p$ of 14.70 g C $hPa^{0.5}$ kg H_2O^{-1}, with an inter-annual maximum difference of 10.1% in relation to mean $uWUE_p$ for a grassland in Inner Mongolia, China. Hu et al. (2018) evaluated $uWUE_p$ during three years in a grassland in Northern China. They found an average $uWUE_p$ equal to 12.34 g C $hPa^{0.5}$ kg H_2O^{-1} and an inter-annual maximum difference with respect to the mean of 13.5%. Zhou et al. (2016) estimated $uWUE_p$ for five grassland types using flux datasets ranging from two and six years in different regions of USA. They observed that the long-term average $uWUE_p$ ranged between 11.57 and 14.28 g C $hPa^{0.5}$ kg H_2O^{-1} with an inter-annual maximum difference

close to 20.0%. In our study, the relative differences between the annual $uWUE_p$ and the three-year $uWUE_p$ ranged between 3.5% (2019) and 20.6% (2017), indicating that except for 2017, which was a dry year, $uWUE_p$ was relatively constant. In addition, the long-term average $uWUE_p$ estimated excluding the 2017 data (15.10 g C $hPa^{0.5}$ kg H_2O^{-1}) was slightly higher than that estimated using the entire dataset (14.31 C $hPa^{0.5}$ kg H_2O^{-1}), showing that the 2017 data had a small influence on long-term average $uWUE_p$.

Previous studies in grasslands showed that $uWUE_a$ increases during wetter years (Han et al., 2018) and decreases under severe drought (Hu et al., 2018). However, a direct relationship between $uWUE_a$ and drought is not observed for all grassland ecosystems. For instance, Yang et al. (2016) showed that in arid ecosystems where *WUE* is controlled by *E*, *WUE* generally increases under drought conditions. Conversely, in semiarid/sub-humid ecosystems, *WUE* increases as function of water availability due to its greater sensitivity of *GPP*. In our study, the accumulated *GPP* during the 2018 and 2019 growing seasons were respectively 39.1% and 95.5% higher than the accumulated *GPP* observed in 2017. On the other hand, the accumulated *ET* values during 2018 and 2019 were 8.2% and 59.6% higher than the one recorded in 2017, respectively. These results show that *WUE* at the KONZ site is mainly controlled by *GPP*.

However, despite *GPP* in 2019 being the largest among the years evaluated, $uWUE_a$ was higher in 2018. Two peculiarities of the 2018 growing season should be considered when interpreting these results: the uneven rainfall distribution and spring prescribed burn (03/21/2018). In 2018, lower rainfall values were observed from May to mid-August and larger precipitation was recorded after the second half of August (Fig. 3.3e). This distribution of rainfall resulted in a slight increase in *GCC* (Fig. 3.8b), *T* (Fig. 3.7b), *GPP* (Fig. 3.7e) and $uWUE_a$ (Fig. 3.5) close to the end of growing season. Conversely, *GCC*, *T*, *GPP* and $uWUE_a$ had already declined in 2017 and 2019 at that point of the growing season. These results show that not only the rainfall amount but also the timing of the rainfall is important to explain inter-annual variability of $uWUE_a$ in grasslands.

In addition, previous research conducted at KPBS (Bremer and Ham, 2010; Knapp, 1985; Johnson and Matchett, 2001) and other grasslands (Feldman et al., 2004; Fischer et al., 2012; Wagle et al., 2019) showed that fire increases the green *LAI*, green biomass accumulation and photosynthesis rates. These changes are more

apparent at the beginning of the growing season. In this study, *uWUE*$_a$, *GPP*, and *GCC* at the beginning of 2018 (Fig. 3.5, 2.7e, and 2.8b, prescribed burning year) were higher than the ones observed in 2019 (Fig. 3.5, 3.7f and 3.8c), even though the soil water content was much higher in 2019 (Fig. 3.3f) than in the spring of 2018 (Fig. 3.3e). This occurs due to the reduction in shading and the greater solar radiation reaching the soil surface, favoring a fast emergence of new shoots (Knapp and Seastedt, 1986). Moreover, prescribed fires result in an increase in the C_4 grasses abundance (Collins and Calabrese, 2012), which in turn have higher photosynthetic rates and *WUE* (Nippert et al., 2007).

3.4.2 Comparison between *uWUE* and microlysimeter soil evaporation estimates

Previous comparisons between *E* estimates obtained using the *uWUE* approach and *ML* conducted in Northwest China showed that both methods are capable of capturing *E* seasonal variability in croplands (Zhou et al., 2018; Bai et al., 2019; Tong et al., 2019). However, better agreement between these two methods was observed at the peak of the growing season, while large differences at the beginning and end of the growing season were observed (Zhou et al., 2018; Bai et al., 2019; Tong et al., 2019). According to Hirschi et al. (2017), there are large differences between daily *ET* estimated using *ML* and *EC* measurements, yet these methods tend to show greater agreement at the annual scale. The *RMSE* of 0.58 mm d^{-1} for the relationship between *E* using *ML* and *uWUE* found in our study is similar to that reported by Nelson et al. (2020), who estimated *T* using the *uWUE* approach for several forest ecosystems and obtained *RMSE* ranging from 0.28 to 0.67 mm d^{-1} for the relationship between *uWUE* estimates and sap flow measurements.

Our results show that the *E* values measured by *ML* were usually higher than the *uWUE* approach *E* estimates (Fig. 3.6). One explanation for these discrepancies was the fact that we did not consider the plant basal area in our *ML E* estimates. The adjustment for the basal area would reduce the *ML* daily *E* values since the effective area undergoing evaporation would be lower than the cross-section area of the *ML*. However, we estimated the plant basal to be approximately 1% because the plant stems measure around 0.5 to 1 mm in diameter at the site. Furthermore, the *ML* have a small diameter (10.2 cm) and were installed between plants, minimizing the number

of steams inside the *ML*. Therefore, using plant basal area to scale *ML E* estimates would not lead to a significant change in our results.

Another explanation for the discrepancies between the two methods is the spatial variability of *E* in this ecosystem. Differences between *E* estimates from the two methods are expected due to discrepancies in spatial scales of *ML* and the *EC* approach (Kool et al., 2014). Furthermore, variations in the flux footprint size and location over the day may also contribute to differences between *E* estimated by the two methods (Evett et al., 2012; Moorhead et al., 2017). The spatial variability of *E* in complex ecosystem such as the KPBS is difficult to capture using *ML*. Nevertheless, we believe to be important to report the discrepancies between the two methods since validation studies of *ET* partitioning methods are scarce.

The *E* values estimated from the *uWUE* approach can also be influenced by the uncertainty in *GPP* estimates (Wohlfahrt and Galvano, 2017). Previous study conducted with stable isotopes measurements showed that daytime R_{eco} and *GPP* extrapolated from nighttime measurements are overestimated by 10% and 13%, respectively (Oikawa et al., 2017). These overestimations occur because daytime R_{eco} is lower than nighttime R_{eco} at the same temperature, since light inhibits the foliar mitochondrial respiration (Kok effect) (Heskel et al., 2013). Values of $uWUE_a$ and $uWUE_p$ are both proportional to *GPP* (Eqs. 1 and 2) so they are both affected by biases in *GPP*. Therefore, *T/ET* (Eq. 3) is not expected to be very sensitive to biases in *GPP*.

3.4.3 Effect of the rainfall and fire on fluxes and *T/ET*

Despite the dry conditions in 2017 and part of the 2018 growing season, the tallgrass prairie was still a carbon sink during these years (Table 3.3). According to Fay et al. (2000), the reduction in aboveground net primary productivity at KPBS is not associated with a reduction in rainfall amounts, but with the increase in the interval between rainfall events. In addition, during dry years the ecosystem functioning can be affected by the increase in rainfall variability and the occurrence of large rainfall events, reducing the rain use efficiency (*RUE*), while during wetter years these impacts are reduced (Felton et al., 2020).

The *RUE*, expressed as the ratio of monthly accumulated *GPP* and rainfall, was 2.31 g C m^{-2} mm^{-1} in 2017. On the other hand, the average *RUE* values were 1.87 and 2.26 g C m^{-2} mm^{-1} for the 2018 and 2019 growing seasons, respectively. The small

rainfall events recorded during 2017 in comparison to the 2018 and 2019 growing seasons may have contributed to the larger *RUE* for that year and to net CO_2 uptake by the ecosystem (Table 3.3). Conversely, the occurrence of large rainfall events from mid-August 2018 and throughout 2019 likely increased water losses to deep soil layers (Knapp et al., 2008) reducing *RUE*.

Our *T/ET* values (ranging from 0.50 to 0.65) are within the range of values (0.57 ± 0.19) reported by Schlesinger and Jasechko (2014) for various temperate grasslands worldwide. The highest *T/ET* observed during 2018 is related to the higher $uWUE_a$ resulting likely from the rainfall distribution and prescribed burning (Section 3.4.1). The removal of vegetation biomass and litter can increase *E*, especially at the beginning of the growing season (Fig. 3.8b). However, prescribed burning also reduces the rainfall interception by litter and biomass, which may enable greater soil water storage. At KPBS, it was demonstrated that the average rainfall interception by canopy is 19.0% and 38.0% for burned and unburned plots, respectively (Gilliam et al., 1987). Likewise, rainfall interception ranging between 20.0% and 60.0% over the growing season was reported for an unburned tallgrass prairie in Oklahoma (Zou et al., 2015).

Conversely, during growing seasons without prescribed burning, the higher litter accumulated can result in higher soil water availability (Craine and Nippert, 2014). Yet, the water from small rainfall events is more likely to be intercepted by canopy and dead biomass preventing it from reaching the soil surface (Wang et al., 2016; Zou et al., 2015). Thus, the predominance of small rainfall events in 2017 and greater above ground biomass may have contributed to increase water losses from *E*, reducing $uWUE_a$ and *T/ET*. In addition to the increase in *E* of intercepted water from canopy and litter, the reduction in *T/ET* during 2019 compared to 2018 was probably related to the high near surface soil moisture over 2019 (Fig. 3.3f), which can increase *E* and reduce *T/ET* (Wagle et al., 2020; Wei et al., 2018).

3.4.4 Effect of vegetation growth and environment variables on *T/ET*

Previous studies show that the weekly variation in *T/ET* derived from *uWUE* approach is strongly correlated with vegetation indexes, such as the Normalized Difference Vegetation Index (*NDVI*) and Enhanced Vegetation Index (*EVI*) (Zhou et al., 2016; Hu et al., 2018). In our study, the relationship between *GCC* and *T/ET* evaluated using 3-day time moving averages increased as a function of water availability (Fig.

3.8d-f). Our results show that the *T/ET* temporal dynamics is better explained by *GCC* when the physiological variables *GPP* and *T* are mainly driven by phenology (Migliavacca et al., 2011). On the other hand, *T/ET* variability is not completely captured by *GCC* for short time intervals under drought conditions. This decoupling between *GCC* and *T/ET* can be explained by the lag between variations in soil moisture and vegetation responses to soil water deficits. Moreover, *ET* and *GPP* variability is larger in response to environment conditions compared to *GCC* (Yan et al., 2019). Positive correlations between vegetation indexes and *T/ET* in grasslands are expected due the strong influence of *LAI* on *T/ET* (Scott et al., 2021; Xu et al., 2021).

Previous studies show that T_{air} (Tong et al., 2019) and θ (Cui et al., 2020) are important drivers of *T/ET*. At the seasonal time scale, the highest partial correlation between T_{air} and *T/ET* can be explained by T_{air} influence on *LAI* and photosynthesis (Wagle et al., 2014; Sun et al., 2020). On the other hand, the negative correlations between *T/ET* and θ_{15} observed in 2017 and 2018 might be related to the higher *E* contribution from soil upper layers, especially right after rainfalls (Sun et al., 2020; Wagle et al., 2020). In 2017 and 2018, the positive correlations between *T/ET* and θ_{45} is related to the water uptake by plant roots from subsurface soil layers, especially during drought conditions (Nippert et al., 2012; Maxwell and Condon, 2016; Sun et al., 2021). In 2019, the lack of correlation between θ and *T/ET* can be explained by the high θ values during all growing season compared to previous years. Our results agree with those observed by Scott et al. (2021) for a grassland in Arizona, U.S., in which *T/ET* was positively correlated with the subsurface soil moisture and T_{air}. Likewise, negative correlation between *T/ET* and upper layer soil moisture was observed by Xu et al. (2021) for an Alpine Meadow in northwest China.

3.4.5 Impact of precipitation variability on *ET* components and research needs

Previous studies have reported trends of wet regions becoming wetter and dry regions becoming drier in response to global warming (Chou et al., 2013; Liu and Allan, 2013). These changes in precipitation patterns will intensity with the increase in extreme precipitation events (Donat et al., 2016). Our dataset provides a unique opportunity to demonstrate that precipitation variability has a strong influence on the seasonality of *ET* components in a grassland ecosystem. The response of *T/ET* to

other environmental drivers was modulated by the growing season precipitation patterns. For example, in a rainy year (2019), *T/ET* and T_{air} showed higher correlation, while in a dry year (2017) the variation of *T/ET* is mostly explained by θ_{45} (Fig. 3.9). In addition, in wet year *T/ET* showed higher correlation to *GCC* than in dry year. Therefore, future *ET* partitioning studies should consider not only the total precipitation, but also the timing, size, and frequency of rain events, especially during dry years.

Further comparative studies using techniques with spatial and temporal representativeness similar to the *EC* technique are still needed. In addition to the *uWUE*, several *ET* partitioning approaches based on *EC* measurements have been developed (Scott and Biederman, 2017; Nelson et al., 2018; Perez-Priego et al., 2018) and can be used to confirm our findings about the effect of rainfall variability on *ET* components in grasslands. Even so, considering that *T/ET* derived from the *uWUE* approach was able to capture the effects of rainfall variability and fire, our results indicate that this simple approach could be an invaluable tool to better understand ecosystem responses to climate variability and change and management practices. Given the various combinations of fire and grazing regimes and the variability of precipitation at KPBS, *T/ET* derived from the *uWUE* approach could be useful to quantify the effects of the interactions between these management practices and water availability. The long-term quantification of *T/ET* using the *uWUE* approach may be used to monitor the woody and shrub plant encroachment in grasslands, since *T/ET* has been shown to be more sensitive than *ET* to capture changes in the canopy structure (Wang et al., 2018).

3.5 Conclusions

In this study, we used the *EC* technique and *uWUE* approach for partitioning *ET* in a tallgrass prairie under growing seasons with contrasting rainfall regimes. The lowest *T/ET* average value (0.50) was observed in the dry growing season, while the largest *T/ET* averages (0.62 and 0.65) were observed in the wet growing seasons. A stronger relationship between *GCC* and *T/ET* occurred during wet growing seasons, but this relationship was weakened for growing seasons with drought periods. Air temperature was the main environmental driver of *T/ET* during the wet growing seasons. On the other hand, the soil water content at 0.45 m was the main environmental driver of *T/ET* during a dry growing season.

These results demonstrate that the precipitation variability not only has a direct impact on the *ET* components but also modulates the response of those components to other environmental drivers. Since *ET* partitioning studies at the ecosystem scale are still scarce, our results can improve *T/ET* and water use efficiency estimates in long-term modelling studies. This will help to better understand how *ET* in ecosystems will respond to global warming and increased CO_2 concentration during wet and dry growing seasons. Furthermore, our results revealed that the use of *GCC* as a predictor of *T/ET* should be used with caution during growing seasons that experience drought periods.

References

Anderson, M. C., Hain, C., Otkin, J., Zhan, X., Mo, K., Svoboda, M., Wardlow, B., 2013. An intercomparison of drought indicators based on thermal remote sensing and NLDAS-2 simulations with US Drought Monitor classifications. Journal of Hydrometeorology, 14(4), 1035-1056. https://doi.org/10.1175/JHM-D-12-0140.1

Bai, Y., Li, X., Zhou, S., Yang, X., Yu, K., Wang, M., Liu, S., Wang, P., Wu, X., Wang, X., Zhang, C., Shi, F., Wang, Y., Wu, Y., 2019. Quantifying plant transpiration and canopy conductance using eddy flux data: An underlying water use efficiency method. Agricultural and Forest Meteorology, 271, 375-384. https://doi.org/10.1016/j.agrformet.2019.02.035

Beer, C., Ciais, P., Reichstein, M., Baldocchi, D., Law, B. E., Papale, D., Soussana, J. F., Ammann, C., Buchmann, N., Frank, D., Gianelle, D., Janssens, I. A., Knhol, A., Köstner, B., Moors, E., Roupsard, O., Verbeeck, T., Vesala, T., Williams, C. A., Wohlfahrt, G., 2009. Temporal and among-site variability of inherent water use efficiency at the ecosystem level. Global Biogeochemical Cycles, 23(2). https://doi.org/10.1029/2008GB003233

Berg, A., Sheffield, J., 2019. Evapotranspiration partitioning in CMIP5 models: uncertainties and future projections. Journal of Climate, 32(10), 2653-2671. https://doi.org/10.1175/JCLI-D-18-0583.1
Blair, J. M., O'neal, P. R. 2021. KFH01 Konza prairie fire history. Environmental Data Initiative. http://dx.doi.org/10.6073/pasta/213f54ba6ce198ee51f5931fe66faad1

Bremer, D. J., Ham, J. M., 2010. Net carbon fluxes over burned and unburned native tallgrass prairie. Rangeland Ecology & Management, 63(1), 72-81. https://doi.org/10.2111/REM-D-09-00010.1

Briggs, J. M., Blair, J. M., Horne, E. A., 2016. Ecohydrological and climate change studies at the Konza Prairie Biological Station. Transactions of the Kansas Academy of Science (1903-), 119(1), 5-11.

Cavanaugh, M. L., Kurc, S. A., Scott, R. L., 2011. Evapotranspiration partitioning in semiarid shrubland ecosystems: a two-site evaluation of soil moisture control on transpiration. Ecohydrology, 4(5), 671-681. https://doi.org/10.1002/eco.157

Chen, J., Shao, C., Jiang, S., Qu, L., Zhao, F., Dong, G., 2019. Effects of changes in precipitation on energy and water balance in a Eurasian meadow steppe. Ecological Processes, 8(1), 1-15. https://doi.org/10.1186/s13717-019-0170-z

Chou, C., Chiang, J. C., Lan, C. W., Chung, C. H., Liao, Y. C., Lee, C. J., 2013. Increase in the range between wet and dry season precipitation. Nature Geoscience, 6(4), 263-267. https://doi.org/10.1038/ngeo1744

Collins, S. L., Calabrese, L. B., 2012. Effects of fire, grazing and topographic variation on vegetation structure in tallgrass prairie. Journal of Vegetation Science, 23(3), 563-575. https://doi.org/10.1111/j.1654-1103.2011.01369.x

Craine, J. M., Nippert, J. B., 2014. Cessation of burning dries soils long term in a tallgrass prairie. Ecosystems, 17(1), 54-65. https://doi.org/10.1007/s10021-013-9706-8

Cui, J., Tian, L., Wei, Z., Huntingford, C., Wang, P., Cai, Z., Ma, N., Wang, L., 2020. Quantifying the controls on evapotranspiration partitioning in the highest alpine meadow ecosystem. Water Resources Research, 56(4), e2019WR024815. https://doi.org/10.1029/2019WR024815

Donat, M. G., Lowry, A. L., Alexander, L. V., O'Gorman, P. A., Maher, N., 2016. More extreme precipitation in the world's dry and wet regions. Nature Climate Change, 6(5), 508-513. https://doi.org/10.1038/nclimate2941

Evett, S. R., Warrick, A. W., Matthias, A. D., 1995. Wall material and capping effects on microlysimeter temperatures and evaporation. Soil Science Society of America Journal, 59(2), 329-336. https://doi.org/10.2136/sssaj1995.03615995005900020009x

Evett, S. R., Schwartz, R. C., Howell, T. A., Baumhardt, R. L., Copeland, K. S., 2012. Can weighing lysimeter ET represent surrounding field ET well enough to test flux station measurements of daily and sub-daily ET?. Advances in Water Resources, 50, 79-90. https://doi.org/10.1016/j.advwatres.2012.07.023

Fan, S. M., Wofsy, S. C., Bakwin, P. S., Jacob, D. J., Fitzjarrald, D. R., 1990. Atmosphere-biosphere exchange of CO_2 and O_3 in the central Amazon forest. Journal of Geophysical Research: Atmospheres, 95(D10), 16851-16864. https://doi.org/10.1029/JD095iD10p16851

Fay, P. A., Carlisle, J. D., Knapp, A. K., Blair, J. M., Collins, S. L., 2000. Altering rainfall timing and quantity in a mesic grassland ecosystem: design and performance of rainfall manipulation shelters. Ecosystems, 3(3), 308-319. https://doi.org/10.1007/s100210000028

Feldman, S. R., Bisaro, V., Lewis, J. P., 2004. Photosynthetic and growth responses to fire of the subtropical-temperate grass, Spartina argentinensis Parodi. Flora-

Morphology, Distribution, Functional Ecology of Plants, 199(6), 491-499. https://doi.org/10.1078/0367-2530-00177

Felton, A. J., Slette, I. J., Smith, M. D., Knapp, A. K., 2020. Precipitation amount and event size interact to reduce ecosystem functioning during dry years in a mesic grassland. Global Change Biology, 26(2), 658-668. https://doi.org/10.1111/gcb.14789

Fischer, M. L., Torn, M. S., Billesbach, D. P., Doyle, G., Northup, B., Biraud, S. C., 2012. Carbon, water, and heat flux responses to experimental burning and drought in a tallgrass prairie. Agricultural and Forest Meteorology, 166, 169-174. https://doi.org/10.1016/j.agrformet.2012.07.011

Fisher, J. B., et al., 2017. The future of evapotranspiration: Global requirements for ecosystem functioning, carbon and climate feedbacks, agricultural management, and water resources. Water Resources Research, 53(4), 2618-2626. https://doi.org/10.1002/2016WR020175

Florentin, A., Agam, N., 2017. Estimating non-rainfall-water-inputs-derived latent heat flux with turbulence-based methods. Agricultural and Forest Meteorology, 247, 533-540. https://doi.org/10.1016/j.agrformet.2017.08.035

Gilliam, F. S., Seastedt, T. R., Knapp, A. K., 1987. Canopy rainfall interception and throughfall in burned and unburned tallgrass prairie. The Southwestern Naturalist, 267-271. https://doi.org/10.2307/3671570

Groisman, P. Y., Knight, R. W., Karl, T. R., 2012. Changes in intense precipitation over the central United States. Journal of Hydrometeorology, 13(1), 47-66. https://doi.org/10.1175/JHM-D-1

Han, D., Wang, G., Liu, T., Xue, B. L., Kuczera, G., Xu, X., 2018. Hydroclimatic response of evapotranspiration partitioning to prolonged droughts in semiarid grassland. Journal of Hydrology, 563, 766-777. https://doi.org/10.1016/j.jhydrol.2018.06.048

Heskel, M. A., Atkin, O. K., Turnbull, M. H., Griffin, K. L., 2013. Bringing the Kok effect to light: a review on the integration of daytime respiration and net ecosystem exchange. Ecosphere, 4(8), 1-14. https://doi.org/10.1890/ES13-00120.1

Hirschi, M., Michel, D., Lehner, I., Seneviratne, S. I., 2017. A site-level comparison of lysimeter and eddy covariance flux measurements of evapotranspiration. Hydrology and Earth System Sciences, 21(3), 1809-1825. https://doi.org/10.5194/hess-21-1809-2017

Hu, H., Chen, L., Liu, H., Ali Khan, M. Y., Tie, Q., Zhang, X., Tian, F., 2018. Comparison of the vegetation effect on ET partitioning based on eddy covariance method at five different sites of northern China. Remote Sensing, 10(11), 1755. https://doi.org/10.3390/rs10111755

Johnson, L. C., Matchett, J. R., 2001. Fire and grazing regulate belowground processes in tallgrass prairie. Ecology, 82(12), 3377-3389. https://doi.org/10.1890/0012-9658(2001)082[3377:FAGRBP]2.0.CO;2

Jones, S. K., Collins, S. L., Blair, J. M., Smith, M. D., Knapp, A. K., 2016. Altered rainfall patterns increase forb abundance and richness in native tallgrass prairie. Scientific Reports, 6(1), 1-10. https://doi.org/10.1038/srep20120

Kaimal, J. C., Finnigan, J. J., 1994. Atmospheric boundary layer flows: their structure and measurement. Oxford university press.

Kirchmeier-Young, M. C., Zhang, X., 2020. Human influence has intensified extreme precipitation in North America. Proceedings of the National Academy of Sciences, 117(24), 13308-13313. https://doi.org/10.1073/pnas.1921628117

Kljun, N., Calanca, P., Rotach, M. W., Schmid, H. P., 2015. A simple two-dimensional parameterisation for Flux Footprint Prediction (FFP). Geoscientific Model Development, 8(11), 3695-3713. https://doi.org/10.5194/gmd-8-3695-2015

Knapp, A. K., 1985. Effect of fire and drought on the ecophysiology of Andropogon gerardii and Panicum virgatum in a tallgrass prairie. Ecology, 66(4), 1309-1320. https://doi.org/10.2307/1939184

Knapp, A. K., Seastedt, T. R., 1986. Detritus accumulation limits productivity of tallgrass prairie. BioScience, 36(10), 662-668. https://doi.org/10.2307/1310387

Knapp, A. K., Beier, C., Briske, D. D., Classen, A. T., Luo, Y., Reichstein, M., Smith, M. D., Smith, S. D., Bell, J. E., Fay, P. A., Heisler, J. L., Leavit, S. W., Sherry, R., Smith, B., Weng, E., 2008. Consequences of more extreme precipitation regimes for terrestrial ecosystems. Bioscience, 58(9), 811-821. https://doi.org/10.1641/B580908

Kool, D., Agam, N., Lazarovitch, N., Heitman, J. L., Sauer, T. J., Ben-Gal, A., 2014. A review of approaches for evapotranspiration partitioning. Agricultural and Forest Meteorology, 184, 56-70. https://doi.org/10.1016/j.agrformet.2013.09.003

Li, Z., Chen, Y., Wang, Y., Fang, G., 2016. Dynamic changes in terrestrial net primary production and their effects on evapotranspiration. Hydrology and Earth System Sciences, 20(6), 2169-2178. https://doi.org/10.5194/hess-20-2169-2016

Lian, X., Piao, S., Huntingford, C., Li, Y., Zeng, Z., Wang, X., Ciais, P., McVicar, T. R., Peng, S., Ottlé, C., Yang, H., Yang, Y., Zhang, Y., Wang, T., 2018. Partitioning global land evapotranspiration using CMIP5 models constrained by observations. Nature Climate Change, 8(7), 640-646. https://doi.org/10.1038/s41558-018-0207-9

Liu, C., Allan, R. P., 2013. Observed and simulated precipitation responses in wet and dry regions 1850–2100. Environmental Research Letters, 8(3), 034002. https://doi.org/10.1088/1748-9326/8/3/034002

Loescher, H., Ayres, E., Duffy, P., Luo, H., Brunke, M., 2014. Spatial variation in soil properties among North American ecosystems and guidelines for sampling designs. Plos One, *9*(1), e83216. https://doi.org/10.1371/journal.pone.0083216

Mauder, M., Foken, T., 2004. Documentation and Instruction Manual of the Eddy Covariance Software Package TK2. Universität Bayreuth, Abteilung Mikrometeorologie: Arbeitsergebnisse 26, ISSN 1614-8924, 44 pp.

Maxwell, R. M., Condon, L. E., 2016. Connections between groundwater flow and transpiration partitioning. Science, 353(6297), 377-380. https://doi.org/%2010.1126/science.aaf7891

Metzger, S., Ayres, E., Durden, D., Florian, C., Lee, R., Lunch, C., Luo, H., Pingintha-Durden, N., Roberti, J. A., SanClements, M., Sturtevant, C., Xu, K., Zulueta, R. C., 2019. From NEON Field Sites to Data Portal: A Community Resource for Surface–Atmosphere Research Comes Online. Bulletin of the American Meteorological Society, 100(11), 2305-2325. https://doi.org/10.1175/BAMS-D-17-0307.1

Migliavacca, M., Galvagno, M., Cremonese, E., Rossini, M., Meroni, M., Sonnentag, O., Cogliati, S., Manca, G., Diotri, F., Busetto, L., Cescatti, A., Colombo, R., Fava, F., di Cella, U. M., Pari, E., Siniscalco, C., Richardson, A. D., 2011. Using digital repeat photography and eddy covariance data to model grassland phenology and photosynthetic CO2 uptake. Agricultural and Forest Meteorology, 151(10), 1325-1337. https://doi.org/10.1016/j.agrformet.2011.05.012

Moncrieff, J. B., Massheder, J. M., De Bruin, H., Elbers, J., Friborg, T., Heusinkveld, B., Kabat, P., Scott, S., Soeggard, H., Verhoef, A., 1997. A system to measure surface fluxes of momentum, sensible heat, water vapour and carbon dioxide. Journal of Hydrology, 188, 589-611. https://doi.org/10.1016/S0022-1694(96)03194-0

Moncrieff, J., Clement, R., Finnigan, J., Meyers, T., 2004. Averaging, detrending, and filtering of eddy covariance time series. In Handbook of Micrometeorology (pp. 7-31). Springer, Dordrecht.

Moorhead, J. E., Marek, G. W., Colaizzi, P. D., Gowda, P. H., Evett, S. R., Brauer, D. K., Marek, T. H., Porter, D. O., 2017. Evaluation of sensible heat flux and evapotranspiration estimates using a surface layer scintillometer and a large weighing lysimeter. Sensors, 17(10), 2350. https://doi.org/10.3390/s17102350

Moran, M. S., Scott, R. L., Hamerlynck, E. P., Green, K. N., Emmerich, W. E., & Collins, C. D. H. (2009). Soil evaporation response to Lehmann lovegrass (*Eragrostis lehmanniana*) invasion in a semiarid watershed. Agricultural and Forest Meteorology, 149(12), 2133-2142. https://doi.org/10.1016/j.agrformet.2009.03.018

Neftel, A., Spirig, C., Ammann, C., 2008. Application and test of a simple tool for operational footprint evaluations. Environmental Pollution, 152(3), 644-652. https://doi.org/10.1016/j.envpol.2007.06.062

Nelson, J. A., Carvalhais, N., Cuntz, M., Delpierre, N., Knauer, J., Ogée, J., Migliavacca, Reichstein, M, Jung, M., 2018. Coupling water and carbon fluxes to constrain estimates of transpiration: The TEA algorithm. Journal of Geophysical Research: Biogeosciences, 123(12), 3617-3632. https://doi.org/10.1029/2018JG004727

Nelson, J. A., et al., 2020. Ecosystem transpiration and evaporation: Insights from three water flux partitioning methods across FLUXNET sites. Global Change Biology, 26(12), 6916-6930. https://doi.org/10.1111/gcb.15314

NEON - National Ecological Observatory Network., 2020. Data Products NEON.DP1.00023.001, NEON.DP1.00033.001, NEON.DP1.00040.001, NEON.DP1.00094.001, NEON.DP1.00096.001, NEON.DP1.00098.001, NEON.IP0.00200.001. Provisional data downloaded from http://data.neonscience.org on February 10, 2020. Battelle, Boulder, CO, USA.

Nippert, J., 2020. APT01 Daily precipitation amounts measured at multiple sites across konza prairie ver 14. Environmental Data Initiative. https://doi.org/10.6073/pasta/55558b15424e960b0e5011d6f2004f88 (Accessed 2020-07-01).

Nippert, J. B., Fay, P. A., Knapp, A. K., 2007. Photosynthetic traits in C_3 and C_4 grassland species in mesocosm and field environments. Environmental and Experimental Botany, 60(3), 412-420. https://doi.org/10.1016/j.envexpbot.2006.12.012

Nippert, J. B., Wieme, R. A., Ocheltree, T. W., Craine, J. M., 2012. Root characteristics of C_4 grasses limit reliance on deep soil water in tallgrass prairie. Plant and Soil, 355(1), 385-394. https://doi.org/10.1007/s11104-011-1112-4

Niu, Z., He, H., Zhu, G., Ren, X., Zhang, L., Zhang, K., Yu, G., Ge, R., Li, P., Zeng, N., Zhu, X., 2019. An increasing trend in the ratio of transpiration to total terrestrial evapotranspiration in China from 1982 to 2015 caused by greening and warming. Agricultural and Forest Meteorology, 279, 107701. https://doi.org/10.1016/j.agrformet.2019.107701

O'Connor, R. C., Taylor, J. H., Nippert, J. B., 2020. Browsing and fire decreases dominance of a resprouting shrub in woody encroached grassland. Ecology, 101(2), e02935. https://doi.org/10.1002/ecy.2935

Oikawa, P. Y., Sturtevant, C., Knox, S. H., Verfaillie, J., Huang, Y. W., Baldocchi, D. D., 2017. Revisiting the partitioning of net ecosystem exchange of CO_2 into photosynthesis and respiration with simultaneous flux measurements of $^{13}CO_2$ and CO_2, soil respiration and a biophysical model, CANVEG. Agricultural and Forest Meteorology, 234, 149-163. https://doi.org/10.1016/j.agrformet.2016.12.016

Papale, D. et al., 2006. Towards a standardized processing of Net Ecosystem Exchange measured with eddy covariance technique: algorithms and uncertainty estimation. Biogeosciences, 3(4), 571-583. https://doi.org/10.5194/bg-3-571-2006

Patrignani, A., Knapp, M., Redmond, C., Santos, E., 2020. Technical overview of the Kansas Mesonet. Journal of Atmospheric and Oceanic Technology, 37(12), 2167-2183. https://doi.org/10.1175/JTECH-D-19-0214.1

Perez-Priego, O., Katul, G., Reichstein, M., El-Madany, T. S., Ahrens, B., Carrara, A., Scanlon, T. M., Migliavacca, M., 2018. Partitioning eddy covariance water flux components using physiological and micrometeorological approaches. Journal of Geophysical Research: Biogeosciences, 123(10), 3353-3370. https://doi.org/10.1029/2018JG004637

Prajapati, P., Santos, E. A., 2018. Estimating methane emissions from beef cattle in a feedlot using the eddy covariance technique and footprint analysis. Agricultural and Forest Meteorology, 258, 18-28. https://doi.org/10.1016/j.agrformet.2017.08.004

Rajan, N., Maas, S. J., Cui, S., 2015. Extreme drought effects on summer evapotranspiration and energy balance of a grassland in the Southern Great Plains. Ecohydrology, 8(7), 1194-1204. https://doi.org/10.1002/eco.1574

Reichstein, M., et al., 2005. On the separation of net ecosystem exchange into assimilation and ecosystem respiration: review and improved algorithm. Global Change Biology, 11(9), 1424-1439. https://doi.org/10.1111/j.1365-2486.2005.001002.x

Richardson, A. D., Jenkins, J. P., Braswell, B. H., Hollinger, D. Y., Ollinger, S. V., Smith, M. L., 2007. Use of digital webcam images to track spring green-up in a deciduous broadleaf forest. Oecologia, 152(2), 323-334. https://doi.org/10.1007/s00442-006-0657-z

Richardson, A. D., 2019. Tracking seasonal rhythms of plants in diverse ecosystems with digital camera imagery. New Phytologist, 222(4), 1742-1750. https://doi.org/10.1111/nph.15591

Rigden, A. J., Salvucci, G. D., Entekhabi, D., Short Gianotti, D. J., 2018. Partitioning evapotranspiration over the continental United States using weather station data. Geophysical Research Letters, 45(18), 9605-9613. https://doi.org/10.1029/2018GL079121

Schlesinger, W. H., Jasechko, S., 2014. Transpiration in the global water cycle. Agricultural and Forest Meteorology, 189, 115-117. https://doi.org/10.1016/j.agrformet.2014.01.011

Scott, R. L., Biederman, J. A., 2017. Partitioning evapotranspiration using long-term carbon dioxide and water vapor fluxes. Geophysical Research Letters, 44(13), 6833-6840. https://doi.org/10.1002/2017GL074324

Scott, R. L., Knowles, J. F., Nelson, J. A., Gentine, P., Li, X., Barron-Gafford, G., Bryant, R., Biederman, J. A., 2021. Water availability impacts on evapotranspiration partitioning. Agricultural and Forest Meteorology, 297, 108251. https://doi.org/10.1016/j.agrformet.2020.108251

Seyednasrollah, B., Young, A. M., Hufkens, K., Milliman, T., Friedl, M. A., Frolking, S., Richardson, A. D., 2019. Tracking vegetation phenology across diverse biomes using Version 2.0 of the PhenoCam Dataset. Scientific data, 6(1), 1-11. https://doi.org/10.1038/s41597-019-0229-9

Skaggs, T. H., Anderson, R. G., Alfieri, J. G., Scanlon, T. M., Kustas, W. P., 2018. Fluxpart: Open source software for partitioning carbon dioxide and water vapor fluxes. Agricultural and Forest Meteorology, 253, 218-224. https://doi.org/10.1016/j.agrformet.2018.02.019

Song, L., Liu, S., Kustas, W. P., Nieto, H., Sun, L., Xu, Z., Skaggs, T. H., Yang, Y., Ma, M., Xu, T., Tang, X, Li, Q., 2018. Monitoring and validating spatially and temporally continuous daily evaporation and transpiration at river basin scale. Remote Sensing of Environment, 219, 72-88. https://doi.org/10.1016/j.rse.2018.10.002

Sonnentag, O., Hufkens, K., Teshera-Sterne, C., Young, A. M., Friedl, M., Braswell, B. H., Milliman, T., O'Keefe, J., Richardson, A. D., 2012. Digital repeat photography for phenological research in forest ecosystems. Agricultural and Forest Meteorology, 152, 159-177. https://doi.org/10.1016/j.agrformet.2011.09.009

Stoy, P. C., et al., 2019. Reviews and syntheses: Turning the challenges of partitioning ecosystem evaporation and transpiration into opportunities. *Biogeosciences*, *16*(19), 3747-3775. https://doi.org/10.5194/bg-16-3747-2019

Sun, J. Y., Sun, X. Y., Hu, Z. Y., Wang, G. X., 2020. Exploring the influence of environmental factors in partitioning evapotranspiration along an elevation gradient on Mount Gongga, eastern edge of the Qinghai-Tibet Platea, China. Journal of Mountain Science, 17(2), 384-396. https://doi.org/10.1007/s11629-019-5687-1

Sun, X., Wilcox, B. P., Zou, C. B., 2019. Evapotranspiration partitioning in dryland ecosystems: A global meta-analysis of in situ studies. Journal of Hydrology, 576, 123-136. https://doi.org/10.1016/j.jhydrol.2019.06.022

Sun, X., Wilcox, B. P., Zou, C. B., Stebler, E., West, J. B., Wyatt, B., 2021. Isotopic partitioning of evapotranspiration in a mesic grassland during two wetting–drying episodes. Agricultural and Forest Meteorology, 301, 108321. https://doi.org/10.1016/j.agrformet.2021.108321

Tong, Y., Wang, P., Li, X. Y., Wang, L., Wu, X., Shi, F., Bai, Y., Li, E., Wang, J., Wang, Y., 2019. Seasonality of the transpiration fraction and its controls across typical ecosystems within the Heihe River Basin. Journal of Geophysical Research: Atmospheres, 124(3), 1277-1291. https://doi.org/10.1029/2018JD029680

Towne, E. G., 2002. Vascular plants of Konza Prairie Biological Station: an annotated checklist of species in a Kansas tallgrass prairie. SIDA, Contributions to Botany, 269-294.

Towne, E. G., Craine, J. M., 2014. Ecological consequences of shifting the timing of burning tallgrass prairie. PLoS One, 9(7), e103423. https://doi.org/10.1371/journal.pone.0103423

Vickers, D., Mahrt, L., 1997. Quality control and flux sampling problems for tower and aircraft data. Journal of Atmospheric and Oceanic Technology, 14(3), 512-526. https://doi.org/10.1175/1520-0426(1997)014%3C0512:QCAFSP%3E2.0.CO;2

Wagle, P., Gowda, P. H., Northup, B. K., Starks, P. J., Neel, J. P., 2019. Response of tallgrass prairie to management in the US Southern Great Plains: Site descriptions, management practices, and eddy covariance instrumentation for a long-term experiment. Remote Sensing, 11(17), 1988. https://doi.org/10.3390/rs11171988

Wagle, P., Xiao, X., Torn, M. S., Cook, D. R., Matamala, R., Fischer, M. L., Jin, C., Dong, J., Biradar, C., 2014. Sensitivity of vegetation indices and gross primary production of tallgrass prairie to severe drought. Remote Sensing of Environment, 152, 1-14. https://doi.org/10.1016/j.rse.2014.05.010

Wagle, P., Skaggs, T. H., Gowda, P. H., Northup, B. K., Neel, J. P., 2020. Flux variance similarity-based partitioning of evapotranspiration over a rainfed alfalfa field using high frequency eddy covariance data. Agricultural and Forest Meteorology, 285, 107907. https://doi.org/10.1016/j.agrformet.2020.107907

Wang, L., Liu, H., Bernhofer, C., 2016. Grazing intensity effects on the partitioning of evapotranspiration in the semiarid typical steppe ecosystems in Inner Mongolia. International Journal of Climatology, 36(12), 4130-4140. https://doi.org/10.1002/joc.4622

Wang, L., Good, S. P., Caylor, K. K., 2014. Global synthesis of vegetation control on evapotranspiration partitioning. Geophysical Research Letters, 41(19), 6753-6757. https://doi.org/10.1002/2014GL

Wang, D., Wang, L., 2017. Dynamics of evapotranspiration partitioning for apple trees of different ages in a semiarid region of northwest China. Agricultural Water Management, 191, 1-15. https://doi.org/10.1016/j.agwat.2017.05.010

Wang, P., Li, X. Y., Wang, L., Wu, X., Hu, X., Fan, Y., Tong, Y., 2018. Divergent evapotranspiration partition dynamics between shrubs and grasses in a shrub-encroached steppe ecosystem. New Phytologist, 219(4), 1325-1337. https://doi.org/10.1111/nph.15237

Wei, Z., Lee, X., Wen, X., Xiao, W., 2018. Evapotranspiration partitioning for three agro-ecosystems with contrasting moisture conditions: a comparison of an isotope method and a two-source model calculation. Agricultural and Forest Meteorology, 252, 296-310. https://doi.org/10.1016/j.agrformet.2018.01.019

Williams, D. G., Cable, W., Hultine, K., Hoedjes, J. C. B., Yepez, E. A., Simonneaux, V., Er-Raki, S., Boulet, G., de Bruin, H. A. R., Chehbouni, A., Hartogensis, Timouk, F., 2004. Evapotranspiration components determined by stable isotope, sap flow and eddy covariance techniques. Agricultural and Forest Meteorology, 125(3-4), 241-258. https://doi.org/10.1016/j.agrformet.2004.04.008

Wohlfahrt, G., Galvagno, M., 2017. Revisiting the choice of the driving temperature for eddy covariance CO_2 flux partitioning. Agricultural and Forest Meteorology, 237, 135-142. https://doi.org/10.1016/j.agrformet.2017.02.012

Wutzler, T., Lucas-Moffat, A., Migliavacca, M., Knauer, J., Sickel, K., Šigut, L., Menzer, O., Reichstein, M., 2018. Basic and extensible post-processing of eddy covariance flux data with REddyProc. Biogeosciences, 15(16), 5015-5030. https://doi.org/10.5194/bg-15-5015-2018

Xu, Z., Zhu, Z., Liu, S., Song, L., Wang, X., Zhou, S., Yang, X., Xu, T., 2021. Evapotranspiration partitioning for multiple ecosystems within a dryland watershed: Seasonal variations and controlling factors. Journal of Hydrology, 598, 126483. https://doi.org/10.1016/j.jhydrol.2021.126483

Yan, D., Scott, R. L., Moore, D. J. P., Biederman, J. A., Smith, W. K., 2019. Understanding the relationship between vegetation greenness and productivity across dryland ecosystems through the integration of PhenoCam, satellite, and eddy covariance data. Remote sensing of environment, 223, 50-62. https://doi.org/10.1016/j.rse.2018.12.029

Yang, Y., Guan, H., Batelaan, O., McVicar, T. R., Long, D., Piao, S., Liang, W., Liu, B., Jin, Z., Simmons, C. T., 2016. Contrasting responses of water use efficiency to drought across global terrestrial ecosystems. Scientific Reports, 6(1), 1-8. https://doi.org/10.1038/srep23284

Yue, P., Zhang, Q., Zhang, L., Li, H., Yang, Y., Zeng, J., Wang, S., 2019. Long-term variations in energy partitioning and evapotranspiration in a semiarid grassland in the Loess Plateau of China. Agricultural and Forest Meteorology, 278, 107671. https://doi.org/10.1016/j.agrformet.2019.107671

Zhang, Y., Peña-Arancibia, J. L., McVicar, T. R., Chiew, F. H., Vaze, J., Liu, C., Lu, X., Zheng, H., Wang, Y., Liu, Y. Y., Miralles, D. G., Pan, M., 2016. Multi-decadal trends in global terrestrial evapotranspiration and its components. Scientific Reports, 6(1), 1-12. https://doi.org/10.1038/srep19124

Zhang, R., Zhao, X., Zuo, X., Qu, H., Degen, A. A., Luo, Y., Ma, X., Chen, M., Liu, L., Chen, J., 2019. Impacts of Precipitation on Ecosystem Carbon Fluxes in Desert-Grasslands in Inner Mongolia, China. Journal of Geophysical Research: Atmospheres, 124(3), 1266-1276. https://doi.org/10.1029/2018JD028419

Zhou, S., Yu, B., Huang, Y., Wang, G., 2014. The effect of vapor pressure deficit on water use efficiency at the subdaily time scale. Geophysical Research Letters, 41(14), 5005-5013. https://doi.org/10.1002/2014GL060741

Zhou, S., Yu, B., Zhang, Y., Huang, Y., Wang, G., 2016. Partitioning evapotranspiration based on the concept of underlying water use efficiency. Water Resources Research, 52(2), 1160-1175. https://doi.org/10.1002/2015WR017766

Zhou, S., Yu, B., Zhang, Y., Huang, Y., Wang, G., 2018. Water use efficiency and evapotranspiration partitioning for three typical ecosystems in the Heihe River Basin,

northwestern China. Agricultural and Forest Meteorology, 253, 261-273. https://doi.org/10.1016/j.agrformet.2018.02.002

Zou, C. B., Caterina, G. L., Will, R. E., Stebler, E., Turton, D., 2015. Canopy interception for a tallgrass prairie under juniper encroachment. PLoS One, 10(11), e0141422. https://doi.org/10.1371/journal.pone.0141422

4 LEAF REGROWTH LEADS TO LARGER CHANGES IN CO_2 ASSIMILATION THAN WATER USE IN A GRAZED TALLGRASS PRAIRIE

Abstract

The effect of cattle grazing on water and carbon cycling in grasslands is not fully understood. The goal of this study was to evaluate how grazing and leaf regrowth affect carbon and water cycles in a tallgrass prairie. Eddy covariance measurements were carried out from 2003 to 2005 growing seasons (from May to September) in Manhattan, Kansas, U.S., in grazed (*GR*) and ungrazed (*UG*) tallgrass prairie paddocks. Net ecosystem CO_2 exchange (*NEE*) was partitioned into gross primary productivity (*GPP*) and ecosystem respiration (R_{eco}) using the relationship between the air temperature and nighttime *NEE* data. Evapotranspiration (*ET*) was partitioned into transpiration (*T*) and evaporation (*E*) using an approach based on the concept of underlying water use efficiency. Our results revealed that grazing reduced green leaf area index (*GLAI*) and aboveground biomass (*AGB*). Grazing also reduced *GPP*, *NEE* and *T* in the middle of the growing seasons but enhanced these flux components at the end of the growing seasons compared to the *UG* paddock. Grazing reduced *NEE* by 11.9% and enhanced *ET* by 3.3% compared to the *UG* paddock. The reduction in *NEE* at *UG* was associated with an increase in R_{eco} (9.4%). In turn, changes in *ET* in response to grazing were driven more by the increase in *E* (26.6%) than by the decrease in *T* (5.9%). Despite the reduction in *AGB* and *GLAI* caused by grazing, similar cumulative *GPP* values at both paddocks suggest that there are compensatory mechanisms maintained similar CO_2 assimilation at *UG* and *GR*. Our findings suggest that the grazing regime adopted in this tallgrass prairie impacts the carbon cycle more strongly than the water cycle, given the higher reduction in *NEE* compared to the slight increase in *ET* on *GR* compared to *UG*. These results can be useful to outline strategies to improve management practices aimed at improving the efficiency of rangelands.

Keywords: Grasslands; grazing; gross primary productivity; ecosystem respiration; evapotranspiration partitioning.

4.1 Introduction

Rangelands are highly dynamic agroecosystems that cover a substantial proportion of the Earth surface and provide a myriad of goods and services to a considerable proportion of the world population. For example, rangelands maintain soil health by cycling nutrients and preventing soil erosion, provide habitat for wild species of plants and animals, are large reservoirs of carbon and produce forage for livestock (White et al., 2000). In the North America Great Plains, cattle grazing in native tallgrass prairie is a vital component of beef cattle production. The tallgrass prairie of the Flint Hills in Kansas is one of the remaining native grasslands in the United States (Grudzinski and Daniels, 2018). The productivity of this agroecosystem is highly dependent on water variability and grazing (da Rocha et al., 2022; Owensby et al., 2020).

Previous studies have shown that grazing impacts net ecosystem CO_2 exchange (*NEE*) and evapotranspiration (*ET*) in the tallgrass prairie (Owensby et al., 2006; Owensby and Auen, 2020; Bremer et al., 2001; Brunsell et al., 2008). Grazing affects *NEE* and *ET* by changing canopy structure, soil properties and microclimate conditions (Han et al., 2016; Wang et al., 2015a; Lai and Kumar, 2020; Vaieretti et al., 20180). Reductions in the leaf area index (*LAI*) and aboveground biomass (*AGB*) due to grazing result in reduction of leaf photosynthetic area and ground cover, and in an increase of soil temperature (Chen et al., 2015; Li et al., 2015; Han et al., 2016). However, the responses of carbon and water fluxes in rangelands to grazing are complex and vary with the grazing intensity and climatic conditions (Chimner and Welker, 2011; Wang et al., 2016; Yan et al., 2017). For instance, it has been reported that heavy grazing causes a larger reduction in gross primary productivity (*GPP*) than in ecosystem respiration (R_{eco}), leading to an overall lower CO_2 uptake by grazing systems (Wang et al., 2017; Rong et al., 2017). Conversely, previous studies have shown that light or moderate grazing enhances *GPP*, increasing the grazed system carbon sequestration compared to ungrazed grasslands (Chimner and Welker, 2011; Zhang et al., 2015; Zhu et al., 2015; Rong et al., 2017). Nevertheless, ecosystem carbon flux responses are climate dependent and vary under drought conditions (Chimner and Welker, 2011; Ingrisch et al., 2018).

Despite of the fact that grazing is expected to have different impacts on plant and soil processes, very few studies have investigated the effects of grazing on *NEE* and *ET* primary components (Li et al., 2015; Wang et al., 2015b; Zhang et al., 2019).

Water and carbon cycles are coupled through transpiration (*T*) and *GPP* (Gentine et al., 2019). Hence, understanding the relationship between plant water and carbon fluxes in grazing systems is crucial to improve Earth-system models, and to predict how water and carbon cycles in rangelands will respond to global warming and increased CO_2 concentrations (Li et al., 2015; Niu et al., 2020; Quan et al., 2018).

Previous studies have shown that the contribution of *T* to *ET* (*T/ET*) is strongly affected by *LAI* in grasslands (Wei et al., 2017; Cui et al., 2020; Scott et al., 2021). However, the *LAI* reduction resulting from grazing has been shown to have variable effects on *T/ET* and *ET* depending on the ecosystem and water availability (Wang et al., 2016; Li et al., 2016; Zhang et al., 2019; Frank et al., 2003). Owensby et al. (2006) found that despite the lower *LAI*, a grazed tallgrass prairie had higher *NEE* magnitude compared to an ungrazed tallgrass prairie during the end of the growing season.

We hypothesize that although grazing reduces the overall *LAI* in the tallgrass prairie, grazed areas have more active leaf regrowth than the ungrazed prairie, which will enhance photosynthetic activity and plant water use. We also expect that the reduction in *LAI* and *AGB* in rangelands will also result in an increase of R_{eco} and soil evaporation. To test these hypotheses, we used eddy covariance (*EC*) CO_2 and H_2O flux data collected at grazed and ungrazed tallgrass prairie paddocks. The *EC* flux data was combined with existing flux partitioning approaches to infer soil and canopy primary components of *NEE* and *ET*. Additionally, the effect of cattle grazing on vegetation was quantified by collecting green *LAI* and *AGB* over the course of three growing seasons.

4.2 Material and methods

4.2.1 Site description

The field measurements were conducted from 2003 to 2005 growing seasons (May – September) in a tallgrass prairie on the Rannells Flint Hills Prairie Preserve in Manhattan, Kansas, U.S. (39º08’28” N, 96º31’31’’W, elevation 324 m). The vegetation at the site is a mixture of C_3 and C_4 species which includes grasses and forbs, with the following warm-season C_4 grasses predominating: *Andropogon gerardi*, *Sorghastrum nutans* and *Andropogon scoparius* (Owensby et al., 2006). The climate of the region is mid-continental with an average annual air temperature of 13 ºC and monthly mean

ranging from -3 ºC (January) to 13 ºC (July) (O'Connor et al., 2020; Towne and Craine, 2014). The long-term annual average precipitation (1981 – 2010) in the region is 906.8 mm, with 64% recorded between May and September (Owensby and Auen, 2020). The soil at the site is comprised of fine, mixed, mesic, Udic Argiustoolls with an average bulk density of 1.1 g cm^{-3} in the upper 10 cm (Owensby et al., 2006).

4.2.2 Experimental settings and vegetation sampling

Fluxes were measured in ungrazed (*UG*, 28 ha) and grazed (*GR*, 31 ha) paddocks. Steers were introduced into *GR* in early May, with an average weight of ~250 kg $steer^{-1}$ and removed from the paddock in late July with a mean weight of ~340 kg $steer^{-1}$. The stocking rate at *GR* was 0.81 ha $steer^{-1}$. Biomass samples were collected every two weeks following burning (April) until mid-July, and every four weeks until early October from four 0.25m^{-2} subplots within the flux source area. The samples were dried for 72 h at 55 ºC in an oven. Green leaf area was measured using an area meter (LI-3100, Li-Cor). Green *LAI* (*GLAI*) was calculated by the ratio between the total green leaf area and the subplot area (0.25 m^{-2}) where the leaves were collected. More details about the experimental site are given by Owensby et al. (2006).

4.2.3 Flux measurements

Two eddy covariance (*EC*) systems installed 3.0 m above the ground were used to measure *ET* and CO_2 fluxes at *GR* and *UG* systems. Sonic temperature and wind velocity components were obtained using a 3D sonic anemometer (CSAT3, Campbell Scientific, Inc., Logan, UT, USA). Carbon dioxide and water vapor concentrations were acquired using an infrared gas analyzer (LI-7500, Li-Cor, Lincoln, NE). Wind and concentration data were recorded at 20 Hz. Half-hourly latent heat flux (*LE*) and *NEE* were calculated using the EdiRe software (Clement, 1999). The flux data processing included coordination rotation and air density corrections (Webb et al., 1980). The ReddyProc tool was used for friction velocity (u^*) screening, gap filling and *NEE* partitioning into *GPP* and R_{eco} (Wutzler et al., 2018). The daytime R_{eco} was estimated using the relationship between air temperature and nighttime *NEE*, and *GPP* was obtained by subtracting R_{eco} from *NEE* (Reichstein et al., 2005). In addition, incoming

solar radiation, air temperature, relative humidity and precipitation were collected by an automatic meteorological station located on the site.

4.2.4 Evapotranspiration partitioning

The *ET* was partitioned into *T* and evaporation (*E*) using a statistical approach, based on the concept of underlying water use efficiency (*uWUE*), in which *T/ET* ratio is given by (Zhou et al., 2014; Zhou et al., 2016):

$$\frac{T}{ET} = \frac{uWUE_a}{uWUE_p} \quad (1)$$

where $uWUE_a$ and $uWUE_p$ are the apparent and potential *uWUE*, respectively. $uWUE_p$ is assumed constant during the growing season and represents conditions in which *T* approaches *ET* (*i.e., T/ET* ≅ 1). Growing season $uWUE_p$ values for *GR* and *UG* were estimated using the 95th percentile regression between normalized *GPP* ($GPP \cdot VPD^{0.5}$) and *ET* (Zhou et al., 2016), where *VPD* is the vapor pressure deficit.

Conversely, values of $uWUE_a$ are dependent on the contribution of *E* to *ET* and were estimated as the linear regression slope between $GPP \cdot VPD^{0.5}$ and *ET* on a weekly time scale (Zhou et al., 2016). Both regression analyses were performed forcing the regression line through the origin and using daytime (incoming solar radiation > 20 W m^{-2}) flux data. *T* was calculated by multiplying *ET* by *T/ET*, while *E* was obtained by the difference between *ET* and *T*. The weekly cumulative water vapor and carbon fluxes at *GR* and *UG* were compared using the Student's t-test ($p < 0.05$).

4.3 Results and discussion

4.3.1 Precipitation, air temperature and vegetation temporal dynamics

Average air temperature values were similar throughout the 2003 (22.5 ºC), 2004 (21.9 ºC) and 2005 (23.3 ºC) growing seasons, showing the typical seasonal variation for the region (Fig. 4.1). The precipitation totals in the 2003, 2004 and 2005 growing seasons were 476.5, 704.7 and 622.9 mm, respectively. The long-term total (1981 - 2010) precipitation for the same period (May to September) in the region is

579.1 mm (Owensby and Auen, 2020). The 2003 and 2005 growing seasons showed similar seasonal rainfall distribution with a drought period in the middle of the growing seasons (Fig. 4.1a and 4.1c). Conversely, rain events were more frequent throughout the 2004 growing season (Fig. 4.1b).

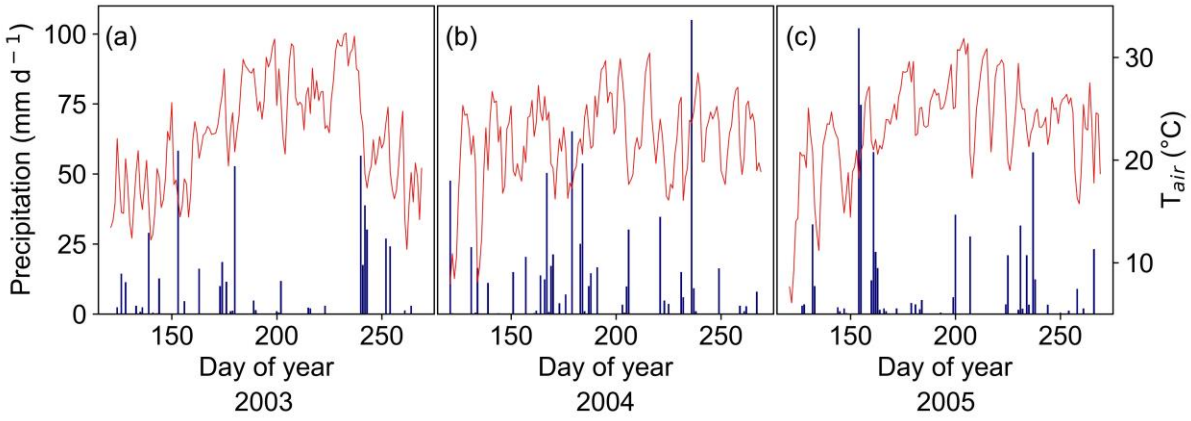

Figure 4.1 - Total precipitation (*P*, blue bars) and daily average of air temperature (T_{air}, red lines) in the 2003, 2004 and 2005 growing seasons.

The *AGB* and *GLAI* values are shown in Fig. 4.2. On average, the maximum *AGB* at *GR* (351.3 g m^{-2}) was 23% lower than the one at *UG* (453.3 g m^{-2}). Similarly, the maximum average *GLAI* at *GR* (2.7) was 25% lower than that at *UG* (3.6) (Fig. 4.2d-f).

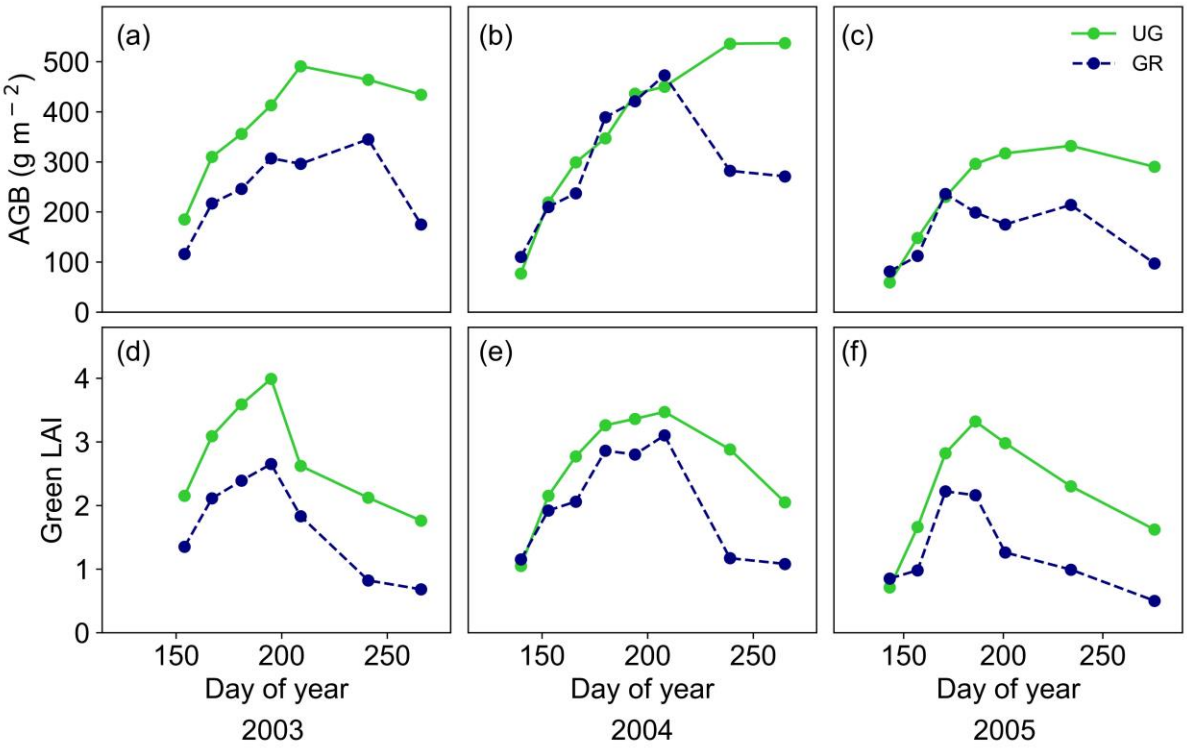

Figure 4.2 - Aboveground biomass (*AGB*) and green leaf area index (*GLAI*) in the 2003, 2004 and 2005 growing seasons at the ungrazed (*UG*) and grazed (*GR*) paddocks.

4.3.2 Seasonal carbon and water fluxes

Carbon fluxes showed similar temporal dynamics at *UG* and *GR* over the growing seasons (Fig. 4.3). The *GPP* values were often similar at *UG* and *GR* (Fig. 4.3a-c). R_{eco} was generally higher at *GR* than at *UG* in the 2003 and 2005 growing seasons (Fig. 4.3d-f). The seasonal patterns of *GPP* and R_{eco} resulted in an overall larger *NEE* at *UG* over the growing seasons, except at the end of the growing seasons (Fig. 4.3g-i). The carbon fluxes, *AGB* and *GLAI* maximum values were observed around the same time in the middle of the 2004 and 2005 growing seasons (Fig. 4.2 and Fig. 4.3). However, drought conditions in the middle of the 2003 growing season (Fig. 4.1c) reduced *GPP* and *NEE* during the *AGB* and *GLAI* peaks (Fig. 4.3a and 4.3g).

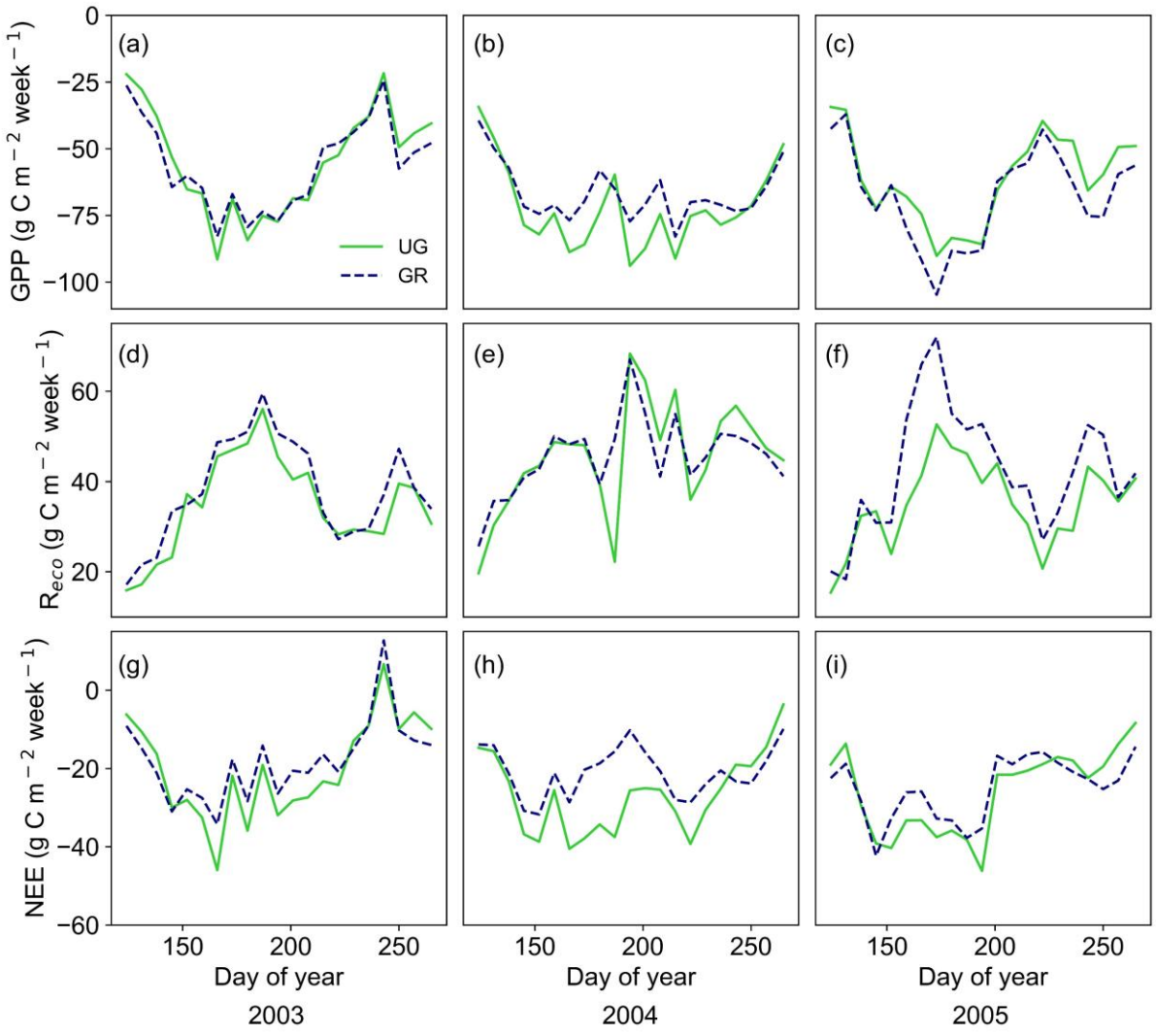

Figure 4.3 - Weekly cumulative values of a-c) gross primary productivity (*GPP*), d-f) ecosystem respiration (R_{eco}) and g-h) net ecosystem exchange (*NEE*) for the 2003, 2004 and 2005 growing seasons at the ungrazed (*UG*) and grazed (*GR*) paddocks.

The similar *GPP* at both paddocks show that the decrease in *NEE* magnitude at *GR* cannot be attributed to the reduction in *GPP*, but to the increase in R_{eco}. The effect of grazing on R_{eco} has been ecosystem dependent and variable with water availability. For example, Chimner and Welker (2011) found that while light and heavy grazing reduced R_{eco} in a wet growing season, R_{eco} was not affected by grazing in a dry growing season in a mixed-grass prairie in Wyoming, U.S. Conversely, Zhao et al. (2016) reported that grazing reduced R_{eco} in alpine steppe and alpine meadow grasslands, while R_{eco} increased due to grazing in swamp meadow on the central Tibetan Plateau, China.

The higher R_{eco} in grazed grasslands has been attributed to the increase in soil temperature and animal waste decomposition (Zhu et al., 2015; Zhang et al., 2015). However, in some grasslands, the decrease in R_{eco} has been attributed to the reduction in *AGB* and soil water content (Zhu et al., 2015; Wang et al., 2015a). Previous studies also showed that plant and soil respirations are affected differently by grazing in different grassland ecosystems (Hou et al., 2016). Future research should evaluate soil and plant respiration components separately to improve the current understanding of grazing effects on R_{eco} in rangelands.

The seasonal variation of *ET* and *T/ET* at *UG* and *GR* is shown in Fig. 4.4. The weekly cumulative *ET* peaks were recorded between late June (DOY 173) and mid-July (DOY 194) at both paddocks (Fig. 4.4a-c). In turn, *T/ET* peaked between early August (DOY 222) and mid-September (DOY 257) at GR and UG, reaching values close to and equal to 1.0 (Fig. 4.4d-f). The differences between *T/ET* at *UG* and *GR* were more evident than that observed for *ET*, especially in the middle of the growing seasons (Fig. 4.4d-f).

Interestingly, large rainfall events (Fig. 4.1) increased *ET* but reduced *T/ET* (Fig. 4.4), due to the increase in *E* in response to high soil moisture near the surface (Wang et al., 2016; Wagle et al., 2020). Sun et al. (2021) observed for a tallgrass prairie in Oklahoma, U.S., that the top 10-cm soil layer is the dominant source of *E*, but as the surface dries, *T* increases due to water uptake by plant roots from deeper soil layers. These *T/ET* responses to wetting-drying periods were observed in our study, especially during the middle of the 2004 and 2005 growing seasons (Fig. 4.4e-f), which were characterized by large rainfall events (Fig. 4.1b-c).

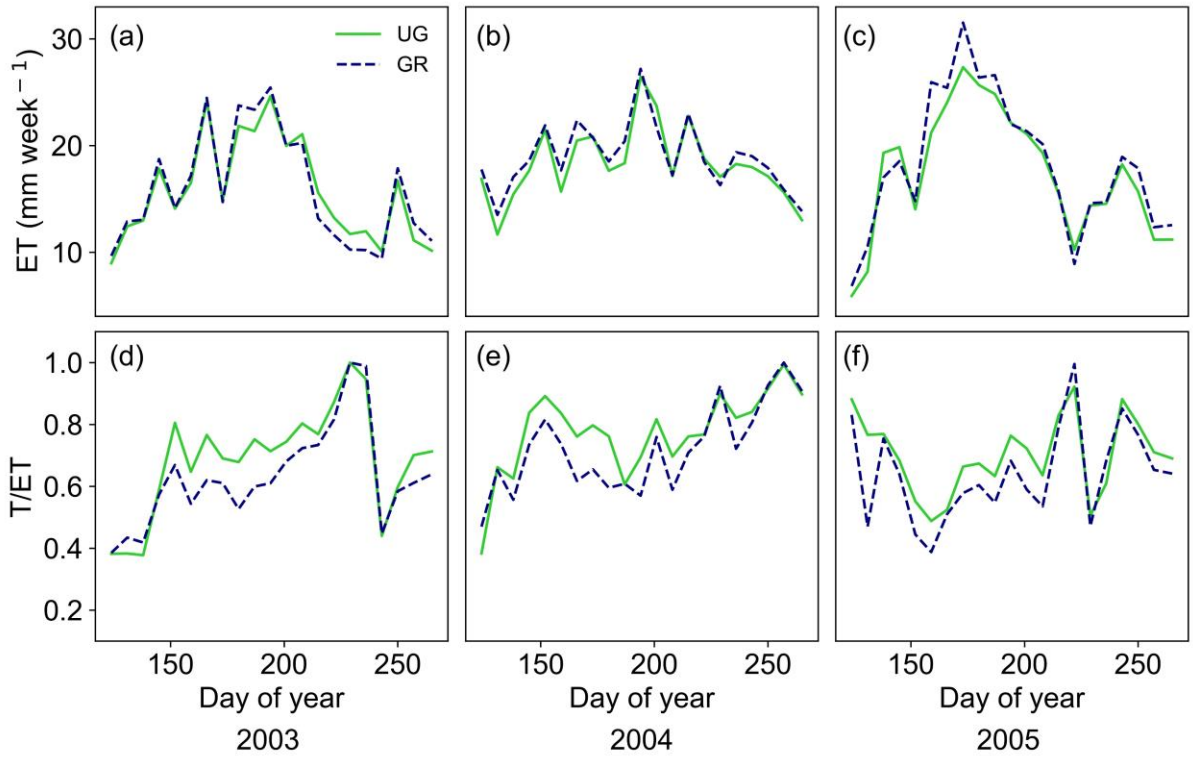

Figure 4.4 - Seasonal variation of weekly cumulative values of a-c) evapotranspiration (ET) and d-f) the ratio between transpiration to evapotranspiration (*T/ET*) in the 2003, 2004 and 2005 growing seasons at the ungrazed (UG) and grazed (*GR*) paddocks.

4.3.3 Cumulative carbon and water fluxes

Both *GR* and *UG* paddocks were a carbon sink during the three growing seasons (Table 1). On average, the growing season cumulative *GPP* at *GR* was slightly higher (1.1%) than that at *UG*, while the cumulative R_{eco} at *GR* surpassed that for *UG* by 9.4%. This resulted in an 11.9% reduction in *NEE* at *GR* compared to *UG* (Table 1). According to a t-test ($p < 0.05$), *NEE* and R_{eco} differed statistically between *GR* and *UG*, but the *GPP* was not significantly different at the two paddocks.

Table 4.1 - Cumulative gross primary productivity (GPP), ecosystem respiration (R_{eco}), net ecosystem exchange (*NEE*), evapotranspiration (*ET*), transpiration (*T*) and evaporation (*E*) over the 2003, 2004 and 2005 growing seasons at the ungrazed and grazed paddocks.

Ungrazed				
	Year of Growing Season			
Variables	2003	2004	2005	Average
GPP (g C m^{-2})	-1166.7	-1527.5	-1300.1	-1331.4
R_{eco} (g C m^{-2})	738.9	961.0	750.0	816.6
NEE (g C m^{-2})	-427.8	-566.5	-550.1	-514.8
ET (mm)	334.2	387.6	367.3	363.0
T (mm)	231.0	300.6	250.7	260.8
E (mm)	103.2	87.0	116.7	102.3
T/ET	0.70	0.77	0.67	0.71
Grazed				
	Year of Growing Season			
Variables	2003	2004	2005	Average
GPP (g C m^{-2})	-1189.5	-1411.7	-1437.8	-1346.3
R_{eco} (g C m^{-2})	806.1	968.3	904.8	893.1
NEE (g C m^{-2})	-383.4	-443.5	-533.0	-453.3
ET (mm)	337.0	402.3	385.9	375.1
T (mm)	208.4	288.1	240.1	245.5
E (mm)	128.6	114.2	145.8	129.5
T/ET	0.62	0.71	0.60	0.64

On average, the cumulative *ET* for *GR* increased by 3.3% compared to the values at *UG*, while the *T/ET* for *UG* was 7.0% higher than the one recorded for *GR* (Table 1). Compared with *UG*, the cumulative *T* for *GR* was reduced by 5.9%, while *E* was enhanced by 26.6% (Table 1). These results indicate that the increase in *ET* and reduction in *T/ET* observed for *GR* were driven more by an increase in *E*. The t-test ($p < 0.05$) indicated that *ET*, *T, E* and *T/ET* at *GR* and *UG* were statistically different. Our results agree with those reported for alpine meadows in Tibetan Plateau, in which

larger *E* in a grazed system drove an increase in *ET* by 12% (Zhang et al., 2019). Similarly, grazing did not affect total *T* in a temperate grassland in Japan, with major changes in *ET* being a result of an increase in *E* (Li et al., 2015).

Conversely, Frank et al. (2003) reported that grazing reduced the 3-year average *ET* by 7% in a semiarid prairie in North Dakota, U.S., and attributed these results to the low soil moisture that limited regrowth in the grazed site. Wang et al. (2012) observed that grazing reduced the 2-year average *ET* by 32% in a semiarid grassland in Inner Mongolia, China. They credited the reduction in *ET* to a reduction in soil moisture and in surface available energy in the grazed grassland. Bremmer et al. (2001) observed higher *ET* values coinciding with large rainfall events in a grazed tallgrass in Kansas, U.S. Hence, the occurrence of large rainfall events, especially during 2004 and 2005, contributed to the increase in *E* and could explain the slightly higher *ET* at *GR* in our study.

Nevertheless, while grazing decreased the average *T/ET* during the three growing seasons in our study, previous studies have shown that *T/ET* in grazed grasslands is modulated by the water availability and variable among grasslands (Wang et al., 2016; Li et al., 2015). For instance, Wang et al. (2016) demonstrated that the reduction in *LAI* by heavy grazing reduced *T/ET* by 17% during a normal precipitation year in a semiarid typical steppe in Inner Mongolia, China. Conversely, during a dry year, Wang et al. (2016) found that grazing enhanced *T/ET* by 4% due to a decrease in rainfall interception by the canopy. In contrast, Li et al. (2015) did not observe statistically significant differences in *ET* and *T/ET* between grazed and ungrazed temperate grasslands in Japan. Yet, they pointed out that the higher *LAI* in ungrazed grasslands than in grazing systems increase shading, which can reduce the *T* contribution from adjacent leaves. In a tallgrass prairie, rainfall canopy interception is a key component of *E* (Gilliam et al., 1987), which can lead to a reduction in *T/ET* in ungrazed paddocks after the occurrence of light rains.

4.3.4 Leaf regrowth, above ground biomass and canopy fluxes

Despite the reduction in *AGB* and *GLAI* caused by grazing (Fig. 4.2), similar cumulative *GPP* values at both paddocks suggest that there are compensatory mechanisms maintained similar CO_2 assimilation at *UG* and *GR*. The regrowth of new leaves, which have greater stomatal conductance and photosynthetic capacity,

associated with the higher penetration of solar radiation inside the canopy are the probable reasons for the higher carbon assimilation efficiency in grazed systems (Owensby et al., 2006; Zhang et al., 2021; Wang et al., 2011; Otieno et al., 2011). In addition, leaf regrowth contributed to maintaining *T/ET* at *GR* similar levels than the ones at *UG* in the end of the growing season (Fig. 4.4d-f). Comparable results were reported for a temperate grassland in Japan (Wagle et al., 2020) and alfalfa in Oklahoma, U.S. (Wang et al., 2015b), in which leaf regrowth after cuts enhanced *T/ET*.

This compensatory effect of leaf regrowth on carbon assimilation and plant water is noticeable by analyzing the hourly *GPP* and *T* at different growth stages (Fig. 4.5). From the beginning to the middle of the growing season, the *GPP* and *T* at *GR* decreased compared to *UG* (Fig. 4.5a and 4.5d), but the opposite occurred in the end of the growing season (Fig. 4.5c and 4.5f). The lower *GPP* and similar *T* at *UG* compared to *GR* in the end of growing season could be explained by the presence of older leaves, while the plant regrowth at *GR* in response to grazing increases leaf photosynthetic capacity even at the end of growing season (Owensby et al., 2006).

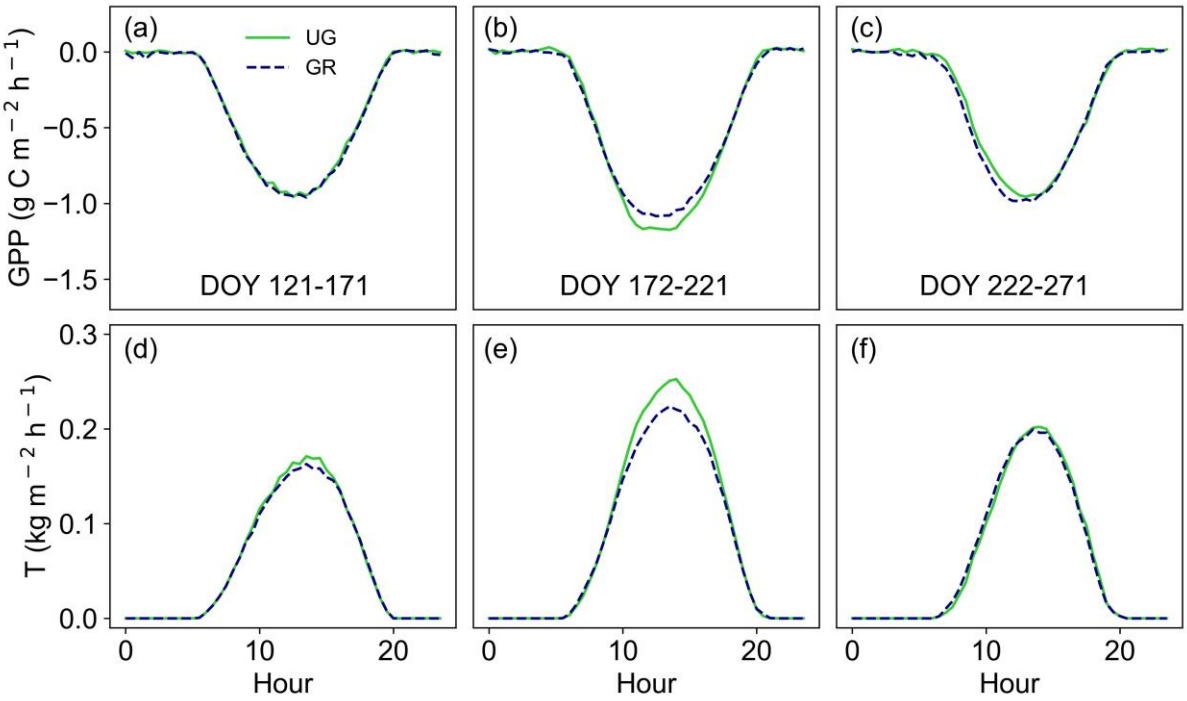

Figure 4.5 - Ensemble average of a-c) gross primary productivity (*GPP*) and d-f) transpiration (*T*) for 2003, 2004 and 2005 in the beginning (Day of year - DOY 121-171), middle (DOY 172-221) and end of growing seasons (DOY 222-271) at the ungrazed (*UG*) and grazed (*GR*) paddocks.

The differences between the *UG* and *GR* systems are more evident when fluxes are normalized by *GLAI* (Fig. 4.6) and *AGB* (Fig. 4.7). The normalized fluxes revealed that the carbon assimilation and water vapor losses per unit of *GLAI* were similar between *GR* and *UG* from the beginning to the middle of the growing seasons (Fig. 4.6). After this period, the normalized fluxes per unit of *GLAI* became much larger at *GR* as compared to *UG* (Fig. 4.6). Similar seasonal patterns were observed when fluxes were normalized by the *AGB*; however, carbon and water vapor fluxes per unit of *AGB* were more variable in the beginning of the growing seasons (Fig. 4.7). According to t-test ($p < 0.05$), *ET*, *T* and *GPP* per unit of *GLAI* and *AGB* differed statistically between *GR* and *UG*.

The rapid increase in carbon assimilation and plant water use at *GR* compared to *UG* from the middle of the growing season coincided with the removal of cattle in late July. This effect can be attributed to the delayed senescence at *GR* compared to *UG*, as well the regrowth after the animals were removed (Bremmer et al., 2001).

Parsons et al. (1988) evaluated the effect of rotational and continuous grazing in ryegrass. The authors observed that rotational grazing resulted in higher gross photosynthesis during the regrowth period, *i.e.,* when the animals were removed from the paddock. These results show unequivocally the impact of new leaves on photosynthetic efficiency and plant water use. This effect should be considered when evaluating and modeling the impact of grazing on grasslands.

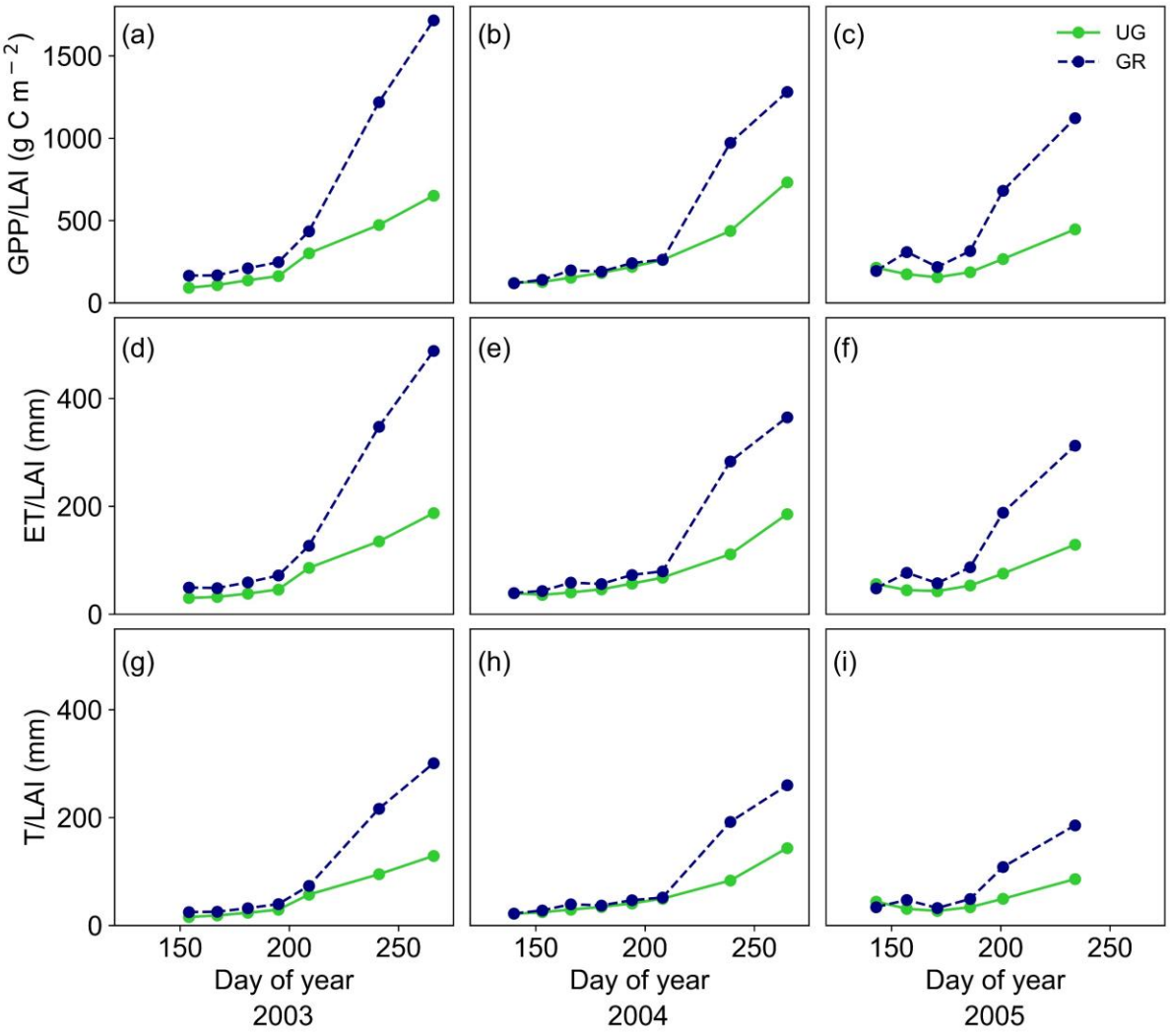

Figure 4.6 - Cumulative gross primary productivity (*GPP*), evapotranspiration (*ET*) and transpiration (*T*) normalized by the green leaf area index (*GLAI*) during three growing seasons (2003, 2004 and 2005) at the ungrazed (*UG*) and grazed (GR) paddocks.

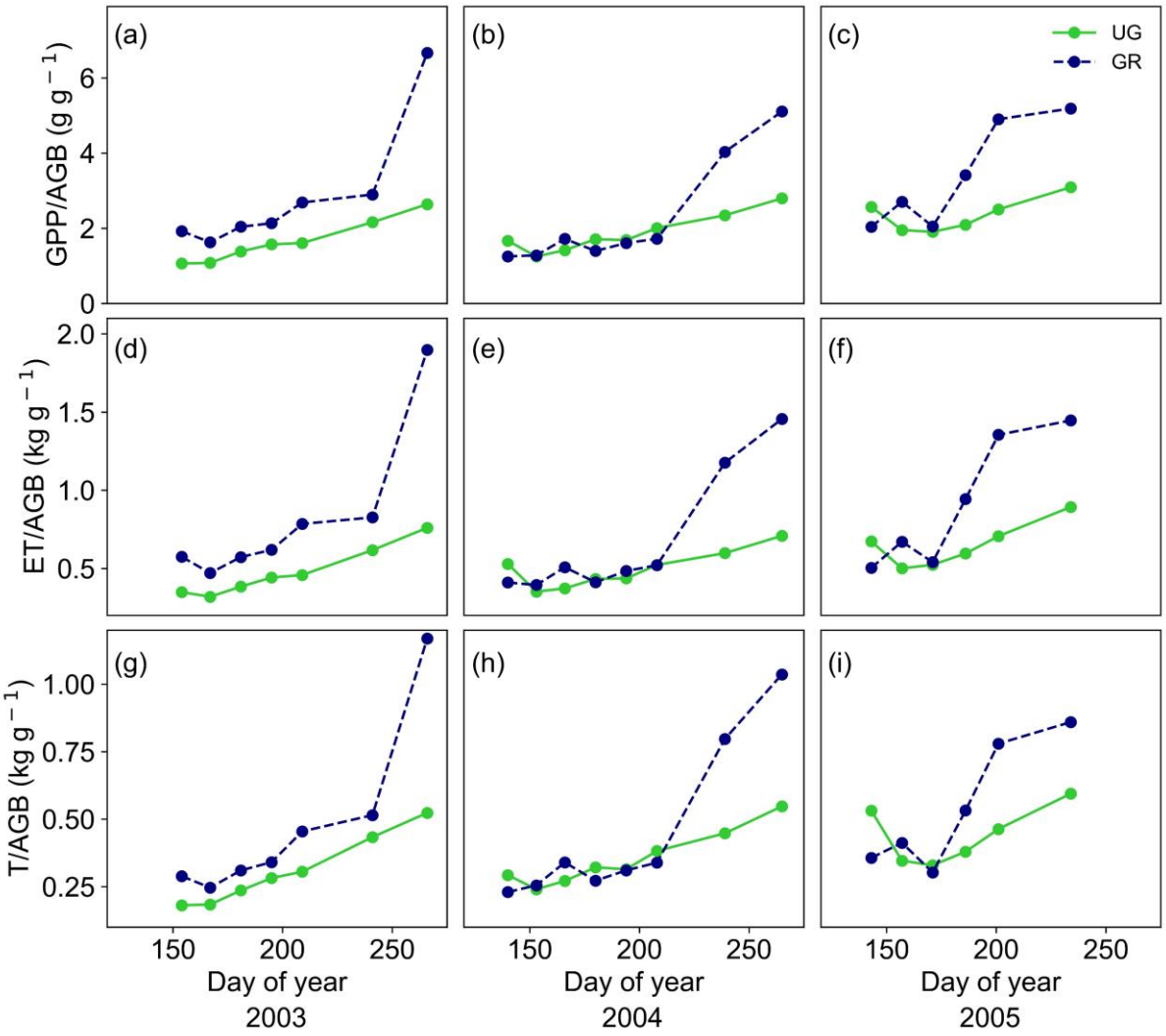

Figure 4.7 - Cumulative gross primary productivity (*GPP*), evapotranspiration (*ET*) and transpiration (*T*) normalized by aboveground biomass (*AGB*) during three growing seasons (2003, 2004 and 2005) at the ungrazed (*UG*) and grazed (*GR*) paddocks.

4.4 Conclusions

Grazing reduced *NEE* by 11.9% and enhanced *ET* by 3.3% in comparison with an ungrazed paddock. The reduction in *NEE* on the grazed paddock was associated with an increase in R_{eco} (9.4%). In turn, changes in *ET* in response to grazing were driven more by the increase in *E* (26.6%) than by the decrease in *T* (5.9%). Despite the reduction in *AGB* and *GLAI* caused by grazing, similar cumulative *GPP* values at both paddocks suggest that there are compensatory mechanisms maintained similar CO_2 assimilation at *UG* and *GR*. Our findings indicate that the grazing regime adopted

in this tallgrass prairie impacts the carbon cycle more strongly than the water cycle, given the higher reduction in *NEE* compared to the slight increase in *ET* on grazed paddock compared to ungrazed paddock. These results can be useful to outline strategies to improve management practices aimed at improving the efficiency of rangelands. Considering the high rainfall variability in the region, further long-term studies are needed to investigate how the tallgrass prairie responds to different grazing regimes during dry and wet growing seasons. In addition, considering the contrasting responses of R_{eco} to grazing reported in the literature, partitioning this component into soil and plant components is critical to improving models and predicting the responses of tallgrass prairies to climate change.

References

Bremer, D. J., Auen, L. M., Ham, J. M., Owensby, C. E., 2001. Evapotranspiration in a prairie ecosystem: effects of grazing by cattle. Agronomy Journal, 93(2), 338-348. https://doi.org/10.2134/agronj2001.932338x

Brunsell, N. A., Ham, J. M., Owensby, C. E., 2008. Assessing the multi-resolution information content of remotely sensed variables and elevation for evapotranspiration in a tall-grass prairie environment. Remote Sensing of Environment, 112(6), 2977-2987. https://doi.org/10.1016/j.rse.2008.02.002

Chen, J., Shi, W., Cao, J., 2015. Effects of grazing on ecosystem CO_2 exchange in a meadow grassland on the Tibetan Plateau during the growing season. Environmental Management, 55(2), 347-359. https://doi.org/10.1007/s00267-014-0390-z

Chimner, R. A., Welker, J. M., 2011. Influence of grazing and precipitation on ecosystem carbon cycling in a mixed-grass prairie. Pastoralism: Research, Policy and Practice, 1(1), 1-15. https://doi.org/10.1186/2041-7136-1-20

Clement, R., 1999. EdiRe data software. Edinburgh, Scotland: The University of Edinburgh.

Cui, J., Tian, L., Wei, Z., Huntingford, C., Wang, P., Cai, Z., Ma, N., Wang, L., 2020. Quantifying the controls on evapotranspiration partitioning in the highest alpine meadow ecosystem. Water Resources Research, 56(4), e2019WR024815. https://doi.org/10.1029/2019WR024815

da Rocha, A. E. Q., Santos, E. A., Patrignani, A., 2022. Partitioning evapotranspiration in a tallgrass prairie using micrometeorological and water use efficiency approaches under contrasting rainfall regimes. Journal of Hydrology, 127624. https://doi.org/10.1016/j.jhydrol.2022.127624

Frank, A. B., 2003. Evapotranspiration from northern semiarid grasslands. Agronomy Journal, 95(6), 1504-1509. https://doi.org/10.2134/agronj2003.1504

Gentine, P., Green, J. K., Guérin, M., Humphrey, V., Seneviratne, S. I., Zhang, Y., Zhou, S., 2019. Coupling between the terrestrial carbon and water cycles—a review. Environmental Research Letters, 14(8), 083003. https://doi.org/10.1088/1748-9326/ab22d6

Gilliam, F. S., Seastedt, T. R., Knapp, A. K., 1987. Canopy rainfall interception and throughfall in burned and unburned tallgrass prairie. The Southwestern Naturalist, 267-271. https://doi.org/10.2307/3671570

Grudzinski, B. P., Daniels, M. D., 2018. Bison and cattle grazing impacts on grassland stream morphology in the flint hills of Kansas. Rangeland Ecology & Management, 71(6), 783-791. https://doi.org/10.1016/j.rama.2018.06.007

Han, J., Li, L., Chu, H., Miao, Y., Chen, S., Chen, J., 2016. The effects of grazing and watering on ecosystem CO_2 fluxes vary by community phenology. Environmental Research, 144, 64-71. https://doi.org/10.1016/j.envres.2015.09.002

Hou, L., Liu, Y., Du, J., Wang, M., Wang, H., Mao, P., 2016. Grazing effects on ecosystem CO_2 fluxes differ among temperate steppe types in Eurasia. Scientific Reports, 6(1), 1-8. https://doi.org/10.1038/srep29028

Ingrisch, J., Karlowsky, S., Anadon-Rosell, A., Hasibeder, R., König, A., Augusti, A., Gleixner, G., Bahn, M., 2018. Land use alters the drought responses of productivity and CO_2 fluxes in mountain grassland. Ecosystems, 21(4), 689-703. https://doi.org/10.1007/s10021-017-0178-0

Lai, L., Kumar, S., 2020. A global meta-analysis of livestock grazing impacts on soil properties. PloS One, 15(8), e0236638. https://doi.org/10.1371/journal.pone.0236638

Li, Y., Fan, J., Hu, Z., Shao, Q., Zhang, L., Yu, H., 2015. Influence of land use patterns on evapotranspiration and its components in a temperate grassland ecosystem. Advances in Meteorology, 2015, https://doi.org/10.1155/2015/452603

Niu, Z., He, H., Zhu, G., Ren, X., Zhang, L., Zhang, K., 2020. A spatial-temporal continuous dataset of the transpiration to evapotranspiration ratio in China from 1981–2015. Scientific data, 7(1), 1-13. https://doi.org/10.1038/s41597-020-00693-x

O'Connor, R. C., Taylor, J. H., Nippert, J. B., 2020. Browsing and fire decreases dominance of a resprouting shrub in woody encroached grassland. Ecology, 101(2), e02935. https://doi.org/10.1002/ecy.2935.

Otieno, D. O., K'Otuto, G. O., Jákli, B., Schröttle, P., Maina, J. N., Jung, E., Onyango, J. C., 2011. Spatial heterogeneity in ecosystem structure and productivity in a moist Kenyan savanna. Plant Ecology, 212(5), 769-783. https://doi.org/10.1007/s11258-010-9863-1

Owensby, C. E., Auen, L. M., 2020. Stocking rate impacts on tallgrass prairie landscape carbon fluxes. Crop, Forage & Turfgrass Management, 6(1), e20048. https://doi.org/10.1002/cft2.20048

Owensby, C. E., Ham, J. M., Auen, L. M., 2006. Fluxes of CO_2 from grazed and ungrazed tallgrass prairie. Rangeland Ecology & Management, 59(2), 111-127. https://doi.org/10.2111/05-116R2.1

Parsons, A. J., Johnson, I. R., Williams, J. H. H., 1988. Leaf age structure and canopy photosynthesis in rotationally and continuously grazed swards. Grass and Forage Science, 43(1), 1-14. https://doi.org/10.1111/j.1365-2494.1988.tb02136.x

Quan, Q., Zhang, F., Tian, D., Zhou, Q., Wang, L., Niu, S., 2018. Transpiration dominates ecosystem water-use efficiency in response to warming in an alpine meadow. Journal of Geophysical Research: Biogeosciences, 123(2), 453-462. https://doi.org/10.1002/2017JG004362

Reichstein, M., et al., 2005. On the separation of net ecosystem exchange into assimilation and ecosystem respiration: review and improved algorithm. Global Change Biology, 11(9), 1424-1439. https://doi.org/10.1111/j.1365-2486.2005.001002.x

Rong, Y., Johnson, D. A., Wang, Z., Zhu, L., 2017. Grazing effects on ecosystem CO_2 fluxes regulated by interannual climate fluctuation in a temperate grassland steppe in northern China. Agriculture, Ecosystems & Environment, 237, 194-202. https://doi.org/10.1016/j.agee.2016.12.036

Scott, R. L., Knowles, J. F., Nelson, J. A., Gentine, P., Li, X., Barron-Gafford, G., Bryant, R., Biederman, J. A., 2021. Water availability impacts on evapotranspiration partitioning. Agricultural and Forest Meteorology, 297, 108251. https://doi.org/10.1016/j.agrformet.2020.108251

Sun, X., Wilcox, B. P., Zou, C. B., Stebler, E., West, J. B., Wyatt, B., 2021. Isotopic partitioning of evapotranspiration in a mesic grassland during two wetting–drying episodes. Agricultural and Forest Meteorology, 301, 108321. https://doi.org/10.1016/j.agrformet.2021.108321

Towne, E. G., Craine, J. M., 2014. Ecological consequences of shifting the timing of burning tallgrass prairie. PLoS One, 9(7), e103423. https://doi.org/10.1371/journal.pone.0103423

Vaieretti, M. V., Iamamoto, S., Harguindeguy, N. P., Cingolani, A. M., 2018. Livestock grazing affects microclimate conditions for decomposition process through changes in vegetation structure in mountain grasslands. Acta Oecologica, 91, 101-107. https://doi.org/10.1016/j.actao.2018.07.002

Wang, Y. F., Cui, X. Y., Hao, Y. B., Mei, X. R., Yu, G. R., Huang, X. Z., Kang, X. M., Zhou, X. Q., 2011. The fluxes of CO_2 from grazed and fenced temperate steppe during two drought years on the Inner Mongolia Plateau, China. Science of the Total Environment, 410, 182-190. https://doi.org/10.1016/j.scitotenv.2011.09.067

Wang, L., Liu, H., Ketzer, B., Horn, R., Bernhofer, C., 2012. Effect of grazing intensity on evapotranspiration in the semiarid grasslands of Inner Mongolia, China. Journal of Arid Environments, 83, 15-24. https://doi.org/10.1016/j.jaridenv.2012.04.005

Wang, D., Wu, G. L., Liu, Y., Yang, Z., Hao, H. M., 2015a. Effects of grazing exclusion on CO_2 fluxes in a steppe grassland on the Loess Plateau (China). Ecological Engineering, 83, 169-175. https://doi.org/10.1016/j.ecoleng.2015.06.017

Wang, P., Yamanaka, T., Li, X. Y., Wei, Z., 2015b. Partitioning evapotranspiration in a temperate grassland ecosystem: Numerical modeling with isotopic tracers. Agricultural and Forest Meteorology, 208, 16-31. https://doi.org/10.1016/j.agrformet.2015.04.006

Wang, L., Liu, H., Bernhofer, C., 2016. Grazing intensity effects on the partitioning of evapotranspiration in the semiarid typical steppe ecosystems in Inner Mongolia. International Journal of Climatology, 36(12), 4130-4140. https://doi.org/10.1002/joc.4622

Wang, L., Liu, H., Bernhofer, C., 2017. Response of carbon dioxide exchange to grazing intensity over typical steppes in a semi-arid area of Inner Mongolia. Theoretical and Applied Climatology, 128(3-4), 719-730. https://doi.org/10.1007/s00704-016-1736-7

Wagle, P., Skaggs, T. H., Gowda, P. H., Northup, B. K., Neel, J. P., 2020. Flux variance similarity-based partitioning of evapotranspiration over a rainfed alfalfa field using high frequency eddy covariance data. Agricultural and Forest Meteorology, 285, 107907. https://doi.org/10.1016/j.agrformet.2020.107907

Webb, E. K., Pearman, G. I., Leuning, R., 1980. Correction of flux measurements for density effects due to heat and water vapour transfer. Quarterly Journal of the Royal Meteorological Society, 106(447), 85-100. https://doi.org/10.1002/qj.49710644707

Wei, Z., Yoshimura, K., Wang, L., Miralles, D. G., Jasechko, S., Lee, X., 2017. Revisiting the contribution of transpiration to global terrestrial evapotranspiration. Geophysical Research Letters, 44(6), 2792-2801. https://doi.org/10.1002/2016GL072235

White, R. P., Murray, S., Rohweder, M., Prince, S. D., Thompson, K. M. 2000. Grassland Ecosystems (p. 81). Washington, DC, USA: World Resources Institute.

Wutzler, T., Lucas-Moffat, A., Migliavacca, M., Knauer, J., Sickel, K., Šigut, L., Menzer, O., Reichstein, M., 2018. Basic and extensible post-processing of eddy covariance flux data with REddyProc. Biogeosciences, 15(16), 5015-5030. https://doi.org/10.5194/bg-15-5015-2018

Yan, R. R. et al., 2017. Response of ecosystem CO_2 fluxes to grazing intensities–a five-year experiment in the Hulunber meadow steppe of China. Scientific Reports, 7(1), 1-12. https://doi.org/10.1038/s41598-017-09855-1

Zhang, T., Xu, M., Zhang, Y., Zhao, T., An, T., Li, Y., Sun, Y., Chen, N., Zhao, T., Zhu, J., Yu, G, 2019. Grazing-induced increases in soil moisture maintain higher productivity during droughts in alpine meadows on the Tibetan Plateau. Agricultural and Forest Meteorology, 269, 249-256. https://doi.org/10.1016/j.agrformet.2019.02.022

Zhang, T., Zhang, Y., Xu, M., Zhu, J., Wimberly, M. C., Yu, G., Niu, S., Xi, S., Zhang, X., Wang, J., 2015. Light-intensity grazing improves alpine meadow productivity and adaption to climate change on the Tibetan Plateau. Scientific Reports, 5(1), 1-12. https://doi.org/10.1038/srep15949

Zhang, Z., Gong, J., Li, X., Ding, Y., Wang, B., Shi, J., Min, L., Yang, B., 2021. Underlying mechanism on source-sink carbon balance of grazed perennial grass during regrowth: Insights into optimal grazing regimes of restoration of degraded grasslands in a temperate steppe. Journal of Environmental Management, 277, 111439. https://doi.org/10.1016/j.jenvman.2020.111439

Zhao, J., Li, X., Li, R., Tian, L., Zhang, T., 2016. Effect of grazing exclusion on ecosystem respiration among three different alpine grasslands on the central Tibetan Plateau. Ecological Engineering, 94, 599-607. https://doi.org/10.1016/j.ecoleng.2016.06.112

Zhou, S., Yu, B., Huang, Y., Wang, G., 2014. The effect of vapor pressure deficit on water use efficiency at the subdaily time scale. Geophysical Research Letters, 41(14), 5005-5013. https://doi.org/10.1002/2014GL060741

Zhou, S., Yu, B., Zhang, Y., Huang, Y., Wang, G., 2016. Partitioning evapotranspiration based on the concept of underlying water use efficiency. Water Resources Research, 52(2), 1160-1175. https://doi.org/10.1002/2015WR017766

Zhu, L., Johnson, D. A., Wang, W., Ma, L., Rong, Y., 2015. Grazing effects on carbon fluxes in a Northern China grassland. Journal of Arid Environments, 114, 41-48. https://doi.org/10.1016/j.jaridenv.2014.11.004

5 GENERAL CONCLUSIONS

In this work, we evaluated how rainfall variability and grazing affects the evapotranspiration (*ET*), net ecosystem exchange (*NEE*) and their components in a tallgrass prairie. In addition, it was investigated the spatial representativeness of eddy covariance measurements using a flux footprint model and the main causes that contribute to the lack of energy balance closure (*EBC*). Our findings demonstrate that:

- The spatial representativeness of eddy covariance measurements at the KONZ site were influenced by stability atmospheric conditions and wind direction. However, the flux footprint model revealed that most of the fluxes (84.9%) originated from a single watershed, so the *EBC* was not affect by surface heterogeneity.

- Stable atmospheric conditions resulted in poor *EBC* over the growing seasons. The inclusion of soil heat storage improved the regressions slopes more than energy balance ratio (*EBR)*. *EBR* improved with the increase of *TKE*, but the increase in *u** did not result in an improvement in *EBR.* The correlation coefficients between wind velocity and scalars indicated that *EBR* at KONZ site is influenced by low-frequency processes.

- The lowest relative contribution of transpiration (*T*) to *ET* (*T/ET*) was observed during a dry growing season, while highest *T/ET* occurred in wet growing seasons. During wet growing seasons, *T/ET* was mainly controlled by air temperature, while subsurface soil water content was the main driver of *T/ET* during a dry growing season. Our results demonstrate that the precipitation variability not only has a direct impact on the *ET* components but also modulates the response of those components to other environmental drivers.

- The relationships between the green chromatic coordinate (*GCC*) and *T/ET* were strongest during wet growing seasons. During growing seasons that experienced drought periods, the relationships between *GCC* and *T/ET* were reduced. These results suggest that the use of *GCC* as a predictor of *T/ET*

should be used with caution during growing seasons that experience drought periods.

- Gross primary productivity (*GPP*) was not affected by cattle grazing, but the increase in ecosystem respiration (R_{eco}) reduced net ecosystem exchange (*NEE*) at a grazed plot. On the other hand, despite the reduction in *T* and *T/ET*, grazing slightly enhanced *ET* due to increased evaporation (*E*). These results show that the grazing regime adopted in this tallgrass prairie impacts the carbon cycle more strongly than the water cycle.

- Our findings can be used to improve *T/ET* and water use efficiency estimates in long-term modeling studies and optimize management practices aimed at reducing greenhouse gas emissions and improving water use efficiency. Furthermore, our results will help to better understand how *ET* and *NEE* in tallgrass prairie will respond to global warming and increased CO_2 concentration during wet and dry growing seasons.

- Futures studies should focus on validating *ET* partitioning estimated by the underlying water use efficiency approach. In addition, the responses of *ET* and *NEE* components to rainfall variability need to be evaluated considering different combinations of fire frequency and grazing intensity. Soil and plant respiration measurements could help better understand the mechanisms that lead to increased R_{eco} in grazed grasslands.